論文 / 著書情報
Article / Book Information

題目(和文)	A Study on Interfacial Properties of Weak Amphoteric Charged Membranes （両性弱電解質膜の界面物性に関する研究）
Title(English)	A Study on Interfacial Properties of Weak Amphoteric Charged Membranes
著者(和文)	松本英俊
Author(English)	Hidetoshi Matsumoto
出典(和文)	学位:博士(工学), 学位授与機関:東京工業大学, 報告番号:甲第5213号, 授与年月日:2002年6月30日, 学位の種別:課程博士, 審査員:
Citation(English)	Degree:Doctor of Engineering, Conferring organization: Tokyo Institute of Technology, Report number:甲第5213号, Conferred date:2002/6/30, Degree Type:Course doctor, Examiner:
学位種別(和文)	博士論文
Type(English)	Doctoral Thesis

A Study on Interfacial Properties of Weak Amphoteric Charged Membranes

A Doctoral Dissertation

by

Hidetoshi Matsumoto

Department of Organic and Polymeric Materials

Graduate School of Science and Engineering

Tokyo Institute of Technology

Doctor of Engineering

Tokyo, Japan

June, 2002

Contents

Chapter 1

General Introduction

Interface between membrane phase and external solution plays a significant role in membrane phenomena for both artificial and biological membranes. To know the interaction mechanism between membrane surfaces and solute molecules such as inorganic ions, organic molecules, and biological macromolecules (e.g., protein and DNA), will be to understand the principle of the membrane phenomena such as molecular recognition and separation. Multiple interactions, nonspecific (e.g., electrostatic interaction, hydrogen bonding, van der Waals force, and hydrophobic interaction) or specific (e.g., biological interactions), can work between membrane and solute molecules [1, 2]. Therefore, the elucidation of correlation between interfacial physicochemical properties of membrane and interaction mechanisms at the membrane interface is essential for both fundamental studies on artificial and biological membranes, and tailor-made design of the high-functional membranes, which can control a specific interaction at the interface [3]. Interfacial charge property, which is represented as zeta potential or surface charge density, is a key parameter in membrane science; because surface charge on a membrane has a significant influence on the separation properties [4, 5] and fouling tendency [6, 7]. Electrokinetic measurements are a powerful and convenient method to provide information about *in situ* charge state of membrane surfaces [8]. Furthermore, these measurements have higher sensitivity than the conventional surface analysis method such as scanning electron microscopy/energy dispersive X-ray analysis (SEM/EDX), Fourier transform infrared spectroscopy/attenuated total reflection method (FT-IR/ATR), and X-ray photoelectron spectroscopy (XPS) [9], and an advantage for the characterization of inside pores of membranes. Recently, electrokinetic measurements have been extensively used for characterization of membrane surfaces from the recognition that *in situ* interfacial charge property is essential for improvement in membrane performance [8].

Artificial membranes are widely used for separation process in industrial and biomedical applications such as filtration processes (e.g., nanofiltration, ultrafiltration, and hyperfiltration) and dialysis processes (e.g., elctrodialysis, diffusiondialysis, piezodialysis, and hemodialysis). These are now

recognized as an energy-saving and easy operation process. The main obstacles of membrane separation technologies are low selectivity and membrane fouling when conventional membrane materials are used in new applications and separation tasks [10]. Modification of the conventional membrane surfaces is a useful alternative for solving these problems. Surface modification with hydrophilic polymers is promising area of not only biomedical research but also membrane technology [3, 10-12]. Various hydrophilic polymers, including poly(ethylene glycol) (PEG), poly(2-hydroxyethylene methacrylate) (poly(HEMA)), poly(acrylamide) (PAAm), poly(vinyl alcohol) (PVA), poly(vinyl pyrrolidone) (PVP), and polysaccharides, have protein and cell resistance characteristics [3, 11, 12]. Among these polymers, PEG appears to the best one for providing “protein friendly” surfaces [13-15] due to the hydrated, neutral, highly mobile, and flexible chains [11]. Therefore, it is very interesting that the surface modification using PEG can be applied to porous membranes for the purpose of creating an antifouling or antithrombotic membranes. Koyama has recently prepared a PEG derivative with pendant amino groups (PEG-A) by addition of aminoethanethiol to the double bond pendants of copoly(allyl glycidyl ether/ethylene oxide) (copoly(AGE/EO)) [16]. This polyelectrolyte has both the advantages from the polyether backbone structure, such as hydrophilicity, biocompatibility, and nonspecific adsorption resistance [11, 13-15], and functionality from the pendant charge groups. In this study, we synthesize three kinds of PEG derivatives with pendant ionizable groups (Figure 1-1) by addition of mercaptans to the double bond pendants of copoly(AGE/EO), and then used these polyelectrolytes for the surface modification of porous membranes.

Amphoteric (or *zwitterionic*) molecules are mainly seen *in vivo* such amino acids, proteins, and cell membrane surfaces. During recent decades, increasing attention has been focused on artificial amphoteric materials in polymer science, colloid science, electrochemistry, and biomedical science (e.g., polyampholyte [17-19], latex [20-22], ionic liquid, [23], polypeptide [24], and phospholipid polymers [25]). In the field of artificial membrane, weak amphoteric charged membranes also have attracted attentions. These membranes contain both weak acidic groups (negatively charged) groups and weak basic (positively charged) groups. The membranes are expected as next-generation charged membrane for the following features: controllability of the charge property by changing the pH of outer solution and potentiality as an antifouling material that prevents adsorption of organic molecules and biological

macromolecules on the surface [26-38]. These properties can be applied to antifouling membranes for separation of ionic drugs and proteins, medical devices, and drug delivery systems [33-38]. Recently, Saito et al. showed weak amphoteric polymer membrane, N-succinyl chitosan/poly(vinyl alcohol) (PVA) blend membrane, showed unique salt transport behavior in piezodialysis [28-30]. Jimbo et al. also studied preparation and electrokinetic characterization of weak amphoteric charged poly(acrylonitrile) (PAN) porous membranes, and their transport phenomena of ionic drugs both theoretically and experimentally [33-38]. There, however, have been few studies on interactions of organic molecules and proteins with amphoteric charged membrane surfaces.

In this study, we propose two types of novel amphoteric charged membranes by surface modification of porous membranes using polyelectrolytes. They are the amphoteric ion-pair side chain (ASC) type, where polyampholytes having ion pairs on their side chain are grafted onto the pore surface, and the mixed grafted chain (MGC) type, where anionic and cationic polyelectrolytes are grafted onto the pore surface. The concept of these amphoteric charged membranes is schematically illustrated in Figure 1-2. The amphoteric ion pair, which consists of an amino group and a carboxyl group, forms the complex where a proton is mediated between the amino group and the carboxyl group (Figure 1-3). This complex is called a dipolar ion structure and appears as amphoteric charge states over a wide range of pH, as typical in amino acids [39]. We take note of this character obtained only in the ASC-type membrane but not in the MGC-type one. The objectives of this study are (1) to propose novel architecture for amphoteric charged membranes by surface modification using PEG derivatives with pendant ionizable groups and characterize their interfacial properties, and (2) to elucidate the interaction mechanism of organic molecules and proteins with the weak amphoteric charged membrane surfaces based on interfacial properties of membranes. This thesis consists of the following eight chapters:

Chapter 1 is “General Introduction”.

Chapter 2 is “Surface Characterization of Porous Membranes by Streaming Potential Measurements: Theoretical and Experimental Aspects”, which describes the theoretical backgrounds, experimental details, and analytical modeling of the results for the surface characterization of porous membranes by streaming potential measurements.

Chapter 3 is “Membrane Materials”, where characteristics of membrane materials used in this

study are shown. Two types of porous membranes are characterized by hydraulic permeability measurements and SEM observations. Three kinds of PEG derivatives with pendant ionizable groups are prepared and then characterized by nuclear magnetic resonance (NMR) and gel permeation chromatography (GPC) measurements.

Chapter 4 is “Preparation and Characterization of Weak Amphoteric Charged Membranes I: Surface Modification of Cellulose Acetate Porous Membranes”, where novel weak amphoteric charged membranes having amphoteric ion pairs are prepared by two approaches of the graft copolymerization of PEG derivatives with pendant cysteine residues (PEG-Cys) onto cellulose acetate (CA) porous membranes and then characterized by streaming potential measurements. The pH dependence of their interfacial charge properties is theoretically examined using a site dissociation model (SDM) based on the dissociation behavior of ionizable groups on the pore surface.

Chapter 5 is “Preparation and Characterization of Weak Amphoteric Charged Membranes II: Surface Modification of Polyethylene Porous Membranes”, which describes preparation and characterization of two types of novel amphoteric charged membranes. These membranes are prepared by radiation-induced graft copolymerization of PEG derivatives with pendant ionizable groups onto high-density polyethylene (PE) porous membranes and then characterized by the streaming potential and dynamic contact angle (DCA) measurements. The pH dependence of their interfacial charge properties is theoretically examined using a SDM.

Chapter 6 is “Interactions of Organic Molecules with Weak Amphoteric Charged Membranes”, where adsorption experiments is carried out using four kinds of model organic molecules (i.e., highly hydrophobic and having an anionic, a cationic, and a polar group) in order to demonstrate their interaction characteristics with the membranes. The adsorbed amount of organic molecules onto the weak amphoteric charged membranes prepared in chapter 5 is investigated by fluorescence spectroscopy.

Chapter 7 is “Interactions of Proteins with Weak Amphoteric Charged Membranes”, where the pH dependence of the protein adsorption onto the weak amphoteric charged membranes prepared in chapter 5 is investigated by fluorescence spectroscopy. Effect of electrostatic interaction on the protein adsorption is examined based on the interfacial charge properties of both the membranes and protein.

Chapter 8 is “Conclusions”.

References

1. Jozefonvicz, J.; Jozefonvicz, M. *J. Biomater. Sci. Polymer Edn.* **1990**, *1*, 147.
2. Black, F. E.; Hartshorne, M.; Davies, M. C.; Roberts, C. J.; Tendler, S. J. B.; Williams, P. M.; Shakesheff, K. M.; Cannizzaro, S. M.; Kim, I.; Langer, R. *Langmuir* **1999**, *15*, 3157.
3. Tsuruta, T. *Adv. Polym. Sci.* **1996**, *126*, 1.
4. Wang, D. I. C.; Sinskey, A. J.; Sonoyama, T. *Biotechnol. Bioeng.* **1969**, *11*, 987.
5. Dukhin, S. S.; Derjaguin, B. W., In *Surface and Colloid Science*, Vol. 7; Matijevic Ed., Wiley: New York, 1974; p118 and 127.
6. Larsson, K. *Desalination* **1980**, *35*, 105.
7. Breslau, B. R.; Testa, A. J.; Milnes, B. A.; Medjanis, G., In *Ultrafiltration Membranes and Applications*; Cooper, A. R. Ed.; Plenum Press: New York, 1980; p109-128.
8. Jimbo, T. Doctoral Dissertation, Tokyo Institute of Technology, Tokyo, 1999.
9. Ikeda, K.; Hachisuka, H.; Nakamura, T.; Kimura, S.; Ueyama, K. *J. Chem. Eng. Jpn.* **1999**, *32*, 581.
10. Mulder, M. *Basic Principles of Membrane Technology*, 2nd edn.; Kluwer Academic: Dordrecht, 1996.
11. Harris, J. M. Ed. *Poly(Ethylene Glycol) Chemistry: Biotechnical and Biomedical Applications*; Plenum Press: New York, 1992.
12. Park, K. D.; Okano, T.; Nojiri, C.; Kim, S. W. *J. Biomed. Mater. Res.* **1988**, *22*, 977.
13. Prime, K. L.; Whitesides, G. M. *J. Am. Chem. Soc.* **1993**, *115*, 10714.
14. Andrade, J. D.; Hlady, V.; Jeon, S. I. In *Hydrophilic Polymers*; Glass, J. E. Ed.; American Chemical Society: Washington DC, 1996.
15. Yang, Z.; Galloway, J. A.; Yu, H. *Langmuir* **1999**, *15*, 8405.
16. Koyama, Y.; Umehara, M.; Mizuno, A.; Itaba, M.; Yasukouchi, T.; Natsume, K.; Suginaka, A.; Watanabe, K. *Bioconjugate Chem.* **1996**, *7*, 298.
17. Higgs, P. G.; Joanny, J.-F. *J. Chem. Phys.* **1991**, *94*, 1543.
18. Kathmann, E. E. L.; White, L. A.; McCornick, C. L. *Macromolecules* **1997**, *30*, 5297.
19. Viklund, C.; Irgum, K. *Macromolecules* **2000**, *33*, 2539.
20. Shirahama, H.; Ohno, H.; Suzawa, T. *Colloids Surfaces* **1991**, *60*, 1.
21. Kashiwabara, M.; Fujimoto, K.; Kawaguchi, H. *Colloid Polym. Sci.* **1995**, *273*, 339.

22. Fang, S.-J.; Fujimoto, K.; Kondo, S.; Shiraki, K.; Kawaguchi, H. *Colloid Polym. Sci.* **2000**, *278*, 864.

23. Yoshizawa, M.; Hirao, M.; Ito-Akita, K.; Ohno, H. *J. Mater. Chem.* **2001**, *11*, 1057.

24. Gaal, D.; Hudecz, F. *Eur. J. Cancer* **1998**, *34*, 155.

25. Ueda, T.; Ishihara, K.; Nakabayashi, N. *J. Biomed. Mater. Res.* **1995**, *29*, 381.

26. Elmidaoui, A.; Boutevin, B.; Belcadi S.; Gavach, C. *J. Polym. Sci B: Polym. Phys.* **1991**, *29*, 705.

27. Chen, J.; Tanioka, A.; Minoura, N. *Polymer* **1994**, *35*, 2853.

28. Saito, K.; Tanioka, A. *Polymer* **1996**, *37*, 2299.

29. Saito, K.; Tanioka, A. *Polymer* **1996**, *37*, 5117.

30. Saito, K.; Ishizuka, S.; Higa, M.; Tanioka, A. *Polymer* **1996**, *37*, 2493.

31. Ramírez, P.; Mafé, S.; Tanioka, A.; Saito, K. *Polymer* **1997**, *38*, 4931.

32. Ramírez, P.; Alcaraz, A.; Mafé, S. *J. Electroanal. Chem.* **1997**, *436*, 119.

33. Jimbo, T.; Higa, M.; Minoura, N.; Tanioka, A. *Macromolecules* **1998**, *31*, 1277.

34. Jimbo, T.; Tanioka A.; Minoura, N. *Langmuir* **1998**, *14*, 7112.

35. Jimbo, T.; Tanioka A.; Minoura, N. *Colloids Surfaces A* **1999**, *159*, 459.

36. Jimbo, T.; Tanioka A.; Minoura, N. *Langmuir* **1999**, *15*, 1829.

37. Jimbo, T.; Ramírez, P.; Tanioka A.; Mafé, S.; Minoura, N. *J. Colloid Interface Sci.* **2000**, *225*, 447.

38. Uematsu, I.; Jimbo, T.; Tanioka, A. *J. Colloid Interface Sci.* **2002**, *245*, 319.

39. Stryer, L. *Biochemistry*, 3rd ed.; W. H. Freeman and Company: New York, 1988.

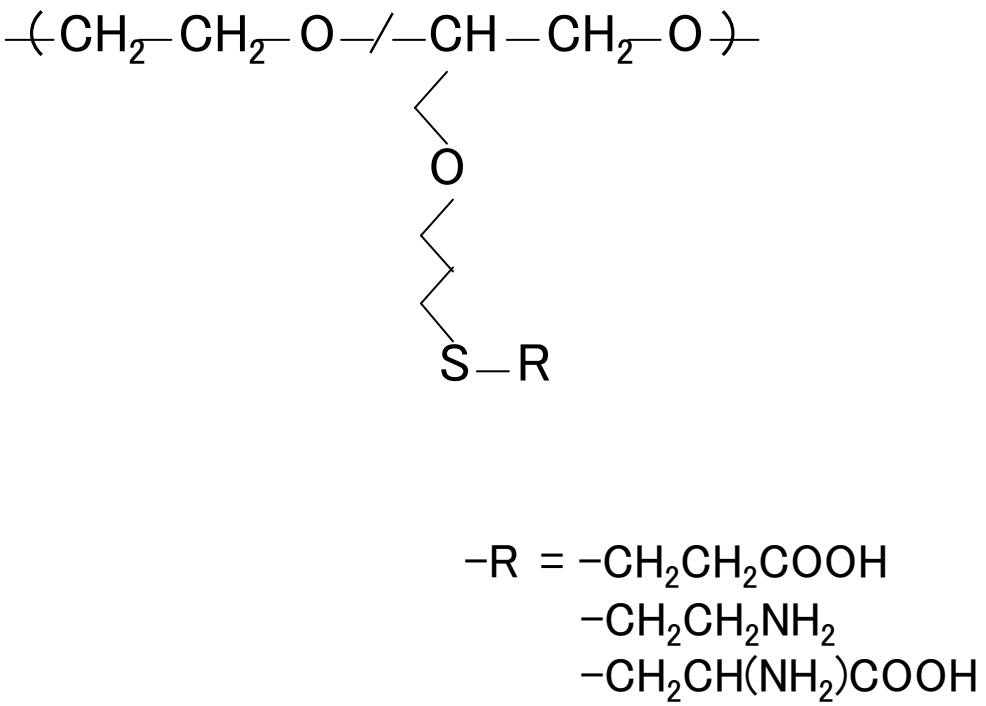

Figure 1-1. Chemical structure of poly(ethylene glycol) derivatives with pendant ionizable groups.

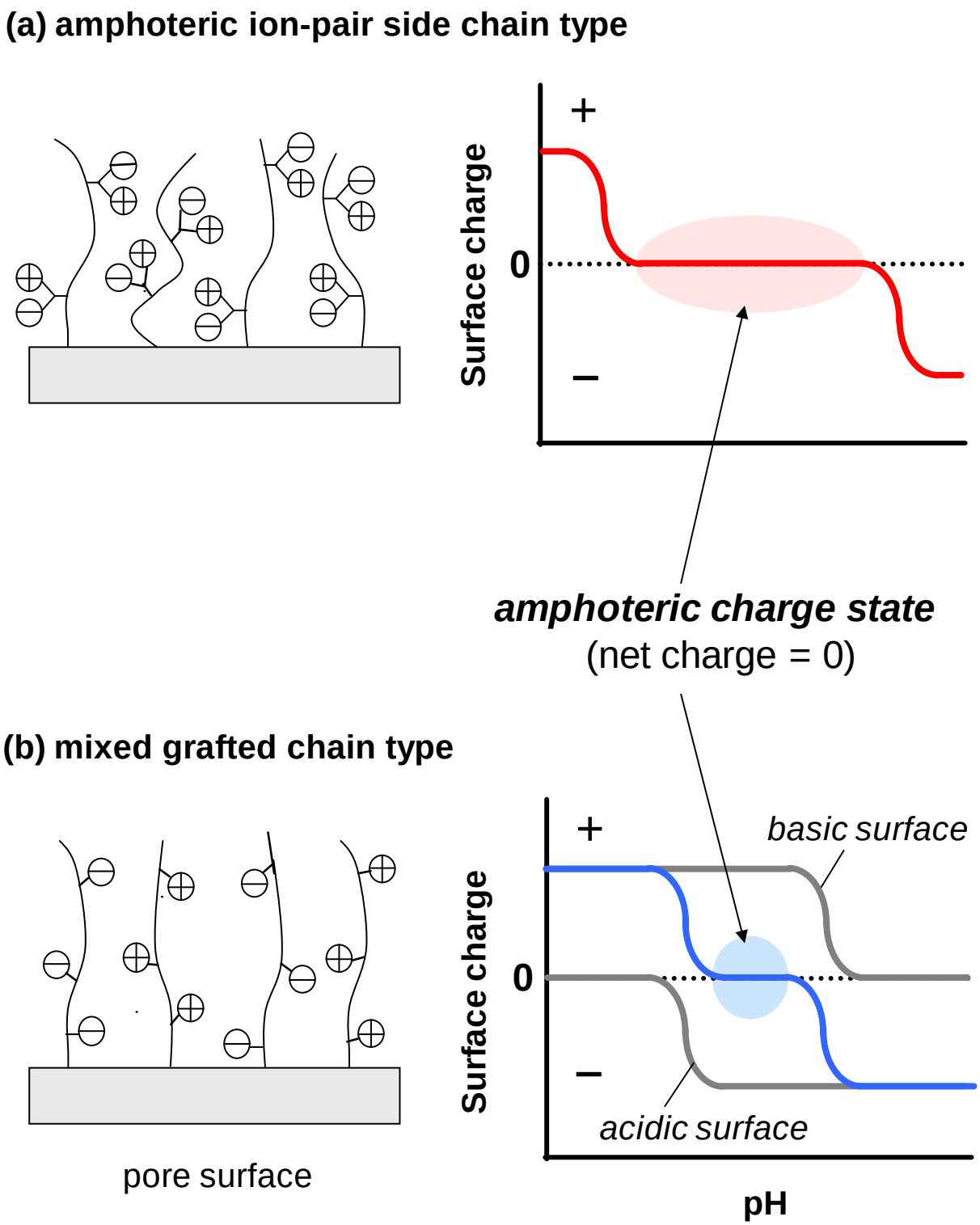

Figure 1-2. Concept of polyelectrolyte grafted-type weak amphoteric charged membranes.

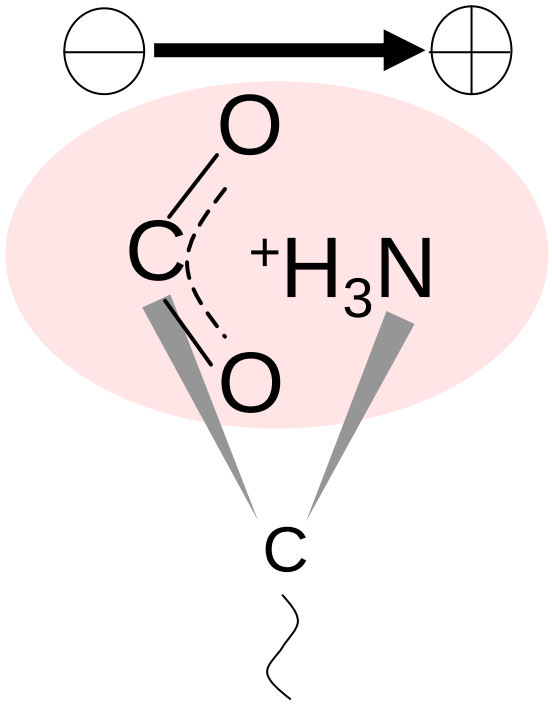

Figure 1-3. Dipolar ion structure of an amphoteric ion pair.

Chapter 2

Characterization of Porous Membranes by Streaming Potential Measurements: Theoretical and Experimental Aspects

2.1 Principle of streaming potential [1, 2]

Electrokinetics has obtained prominent positions in colloid science as additional means of electrical surface characterization. Moreover, there is important practical use. Characterization of solid interfacial charge has been extensively studied using electrokinetic phenomena such as electrophoresis, electro-osmosis, streaming potential, streaming current, colloidal vibration potential, and electrokinetic sonic amplitude. Jimbo has showed a comprehensive procedure to describe pore-surface charge from streaming potential measurements in modified porous membrane system [3]. In this study, we adapted the streaming potential measurements to characterize porous membrane system for experimental convenience.

The streaming potential, E_{str}, is the potential difference at zero current caused by the flow of liquid under a pressure gradient through a porous membrane. Consider a capillary-like pore with charged walls as the model of porous membrane (see Figure 2-1) through which liquid is forced under the influence of an applied pressure head ΔP. A parabolic Poiseuille-type of flow ensures as follows:

$$v(r) = \frac{\Delta P}{4\eta l}(a^2 - r^2) \tag{2.1}$$

where η is the viscosity, l is the length of the capillary-like pore, and a is pore radius.

With this flow, countercharge is entrained, so that an electric current arises, the streaming current, I_{str} given by:

$$I_{str} = \int_{volume} v(r)\ \rho(r) dV = 2\pi \int_0^a v(r)\rho(r) r dr \tag{2.2}$$

where $\rho(r)$ is the local volume density of charge.

We now consider the case of wide capillaries. For $\rho(r)$ then the one-dimensional variant of the Poisson's equation may be substituted as follows:

$$\rho(r) = -\varepsilon_0 \varepsilon_r \frac{d^2\psi}{dz^2} \tag{2.3}$$

where ε_0, ε_r, ψ, and z are the permittivity of vacuum, relative permittivity of liquid, electric potential, and the distance from the surface ($z = a - r$), respectively.

Since the electrical double layer is assumed to be confined to a thin region near the wall of the capillary, only values of r near to $r = a$ are of importance in determining the current (i.e., the bulk of the moving liquid carries no net charge). We substitute $r = a - z$ and, hence,

$$v \approx \frac{\Delta P \cdot a}{2\eta l}(a - r) = \frac{\Delta P \cdot az}{2\eta l}$$

and eq (2.2) reduces to

$$I_{s\ t\ \overline{r}} = -2\pi \int_a^0 (a - z) \frac{\Delta P \cdot az}{2\eta l} \rho(z) dz$$

$$\approx -\frac{\pi r^2 \Delta P}{\eta l} \int_a^0 z\rho(z) dz \tag{2.4}$$

Substituting for $\rho(r)$ from the Poisson's equation (2.3) and integrating by parts we have:

$$I_{str} = \frac{\pi r^2 \Delta P}{\eta l} \int_a^0 z\varepsilon_0 \varepsilon_r \frac{d^2\Psi}{dz^2} dz$$

$$= \frac{\pi r^2 \varepsilon_0 \varepsilon_r \Delta P}{\eta l} \left\{ \left(z \frac{d\Psi}{dz} \right)_{z=a}^{z=0} - \int_a^0 \frac{d\Psi}{dz} dz \right\}$$

$$= -\frac{\pi r^2 \varepsilon_0 \varepsilon_r \Delta P}{\eta l} \int_0^\zeta d\Phi = -\frac{\varepsilon_0 \varepsilon_r \zeta}{\eta l} \pi r^2 \Delta P \qquad (2.5)$$

where ζ is the zeta potential which is generated at the hydrodynamic slipping plane.

When the external circuit has a high resistance, a potential difference, the streaming potential E_{str}, is generated across the capillary. It causes conduction current in the reverse direction of the streaming current inside capillary. In the stationary state this counter current equals I_{str}:

$$\frac{\pi r^2 E_{str} \lambda}{l} + I_{str} = 0 \qquad (2.6)$$

where λ is the liquid conductivity.

From eqs (2.5) and (2.6),

$$E_{str} = \frac{\varepsilon_0 \varepsilon_r \zeta \Delta P}{\eta \lambda} \qquad \text{(Helmholtz－Smoluchowski equation)} \quad (2.7)$$

In this limiting case the measured signal is independent of the geometry of the capillary and, hence, the equation is generally applicable. In real porous membrane systems, streaming potential measurements require the consideration of hydrodynamics for other geometries and electrical double layer overlapping. However, when a is large enough to permit ignoring these effect, the fields closely follows the surface and equations (2.7) remain good approximations.

2.2 Instrumentation [3-5]

The experimental setup for streaming potential measurements as shown in Figure 2-2 was build

by ourselves, which is consisting of the following components:

- Measurement cell;
- Pressure generation and control unit;
- Tubing system and liquid reservoirs;
- Digital multimeter, conductivity meter, pH meter, and thermometer;
- Microcomputer for data collection.

The measurement cell was made of acrylic resin composed of two 64-cm^3 compartments. The membrane was set between two compartments. The area of the membrane exposed to the liquid flow was 1.8 cm^2. The Ag/AgCl electrodes were used to prevent the polarization of the electrodes in streaming potential measurements for the low applied pressure [6]. Hydrostatic pressure across the membrane was applied by changing the solution levels of both reservoirs. By varying the applied pressure (ΔP), the streaming potential (ΔE), which was generated by a flow of ions due to ΔP , was measured with a digital multimeter (HP 3458A, Hewlett-Packard, USA), and the data were recorded using a microcomputer. ΔE is positive if the higher potential is on the high-pressure side. Conductivity, pH, and temperature of the solution were measured in the low-pressure side of a liquid reservoir. Conductivity and pH of the solution were measured using a pH meter (HM-60V, TOA, Japan) with a pH combination glass electrode (GST-5211C, TOA, Japan) and a conductivity meter (CM-20S, TOA, Japan) with a conductivity cell (CG-511B, TOA, Japan), respectively. All measurements were performed in a stirred solution thermostated at 25 ± 0.1℃.

The zeta potential was obtained from the slope of a $\Delta E - \Delta P$ plot using the following Helmholtz－Smoluchowski equation as mentioned above (see eq (2.7)):

$$\zeta = \frac{\eta \lambda}{\varepsilon_0 \varepsilon_r} \frac{\Delta E}{\Delta P} \tag{2.8}$$

where η , λ , ε_0 , and ε_r are the solution viscosity, electrical conductivity of the solution, the

permittivity of vacuum (8.854×10^{-12} [$J^{-1}C^2m^{-1}$]), and relative permittivity of solvent, respectively. Here, we used our experimental value of the solution at 25℃ as λ, and the values of water at 25℃ in ref 7 as η and ε_r, which were 0.8902 [mPa s] and 78.3.

2.3 Surface charge density

The Gouy－Chapman treatment of the electrical double layer is based on solutions to the Poisson－Boltzmann equation which for a 1:1 electrolyte can be written as:

$$\frac{\rho}{\varepsilon}=\frac{d^2\Psi}{dx^2}=\frac{ec}{\varepsilon}\exp\left(-\frac{e\Psi}{kT}\right) \tag{2.9}$$

This equation represents electric field flux within a fluid volume, of charge density (ρ), adjacent to uniformly charged planar surface in terms of distance from the surface (x), bulk electrolyte concentration (c), temperature (T), the Boltzmann constant (k), permittivity of the medium (ε), the Coulombic charge (e), and electric potential (Ψ), assuming an equilibrium Boltzmann distribution of conterions within the volume. The theory treats ions in solution as point charges in a continuous dielectric medium.

Electroneutrality within the system requires that the surface charge density (σ_0) is compensated by the counterions in solution such that

$$\sigma_0=\int_0^\infty \rho\,dx=\frac{2\varepsilon kT\kappa}{e}\sinh\left(\frac{e\Psi_0}{2kT}\right) \tag{2.10}$$

where κ is the reciprocal of the electrical double-layer thickness and ψ_0 is the potential at the surface.

In this study, the apparent surface charge density of the pore surface, which is the charge density on hydrodynamic slipping plane (see Figure 2-3), was calculated from the zeta potential using eq (2.10):

$$\sigma_S=\frac{2\varepsilon kT\kappa}{e}\sinh\left(\frac{e\zeta}{2kT}\right) \tag{2.11}$$

2.4 Site dissociation model [8]

The pH dependence of apparent surface charge density was analyzed using a site dissociation model (SDM). Here, this model treats the apparent pore surface, i.e. the hydrodynamic slipping plane, as the two-dimensional array of acidic- and basic-sites. When the effect of specific adsorption of electrolyte ions is not considered, the equilibrium between charge groups and the solution at the interface is represented as:

$$AH \leftrightarrow A^- + H^+ \tag{2.12}$$

$$BH^+ \leftrightarrow B + H^+ \tag{2.13}$$

where AH and B are the acidic and basic groups, respectively. These equilibria have the following dissociation constants, K:

$$K_a = \frac{[A^-][H^+]_S}{[AH]} \tag{2.14}$$

$$K_b = \frac{[B][H^+]_S}{[BH^+]} \tag{2.15}$$

where subscripts a and b stand for the acidic site and basic site, respectively. $[H^+]_S$ is the hydronium ion concentration at the pore surface, which is based on the hypothesis that the ion concentration in the electrolyte solution follows the Boltzmann distribution outside the plane where the zeta potential is generated, and is written in the form

$$[H^+]_S = [H^+]_0 \exp\left(\frac{-e\zeta}{kT}\right) \tag{2.16}$$

where $[H^+]_0$ is the hydronium ion concentration in the bulk solution. The total site density of the pore surface, N, is denoted by

$$N_a = [A^-] + [AH] \tag{2.17}$$

$$N_b = [BH^+] + [B] \tag{2.18}$$

Therefore, the apparent surface charge density, σ_S, can be expressed by combining eqs (2.14) and (2.15) with (2.17) and (2.18). For a multiple charged pore surface, σ_S is given by

$$\begin{aligned} \sigma_S &= -e\sum_i [A^-]_i + e\sum_j [BH^+]_j \\ &= \sum_i \left[\frac{-eN_a}{1+10^{(pK_a - pH_S)}} \right] + \sum_j \left[\frac{eN_b}{1+10^{(pH_S - pK_b)}} \right] \end{aligned} \tag{2.19}$$

where pK_a and pK_b are the equilibrium acidic dissociation constants of the acidic and basic sites, respectively, and pH_S is the surface pH.

2.5 References

1. Hunter, R. J. *Zeta Potential in Colloid Science*; Academic Press: London, 1981.
2. Lyklema, J. *Fundamentals of Interface and Colloid Science: Volume II Solid-liquid Interface*; Academic Press: London, 1995.
3. Jimbo, T. Doctoral Dissertation, Tokyo Institute of Technology, Tokyo, 1999.
4. Matsumoto, H.; Koyama, Y.; Tanioka, A. *J. Colloid Interface Sci.* **2001**, *239*, 467.
5. Matsumoto, H.; Koyama, Y.; Tanioka, A. *Langmuir* **2001**, *17*, 3375.
6. Werner, C.; Körber, H.; Zimmermann, R.; Dukhin, S.; Jacobasch, H.-J. *J. Colloid Interface Sci.* **1998**, *208*, 329.
7. 日本化学会編, “化学便覧 基礎編 II 改訂 3 版” 丸善, 1984.
8. Healy, T. W.; White, L. R. *Adv. Colloid Interface Sci.* **1978**, *9*, 303.

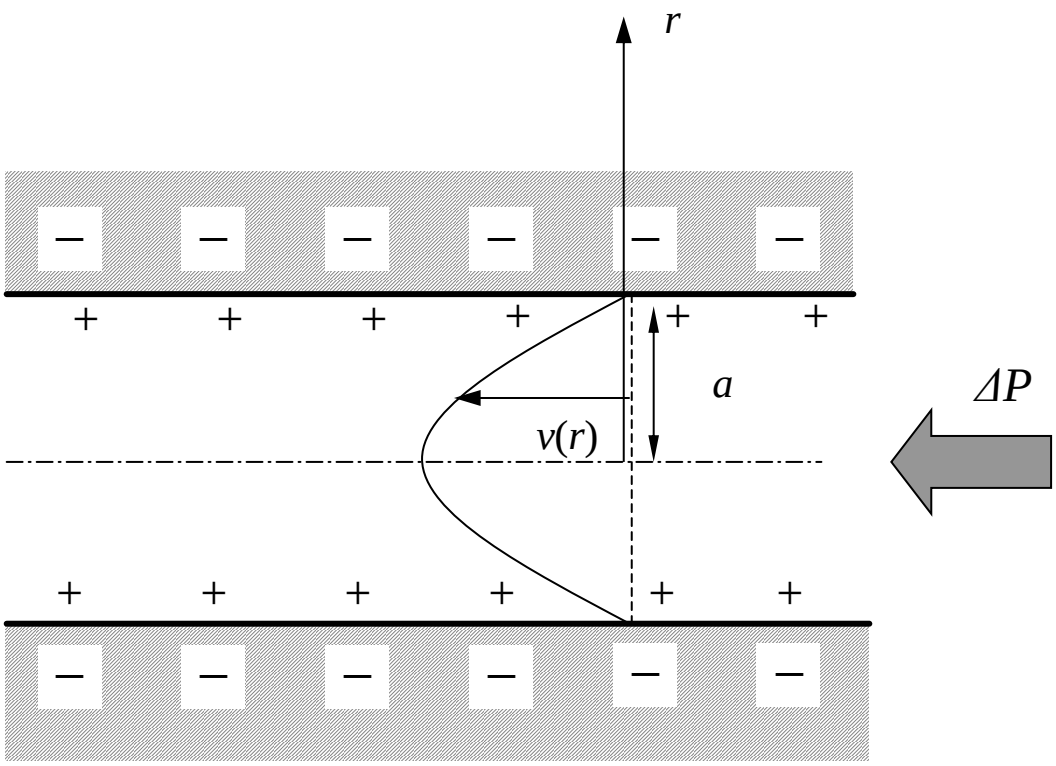

Figure 2-1. Origin of streaming current and streaming potential. For the sake of simplicity the countercharge is only represented by plus signs.

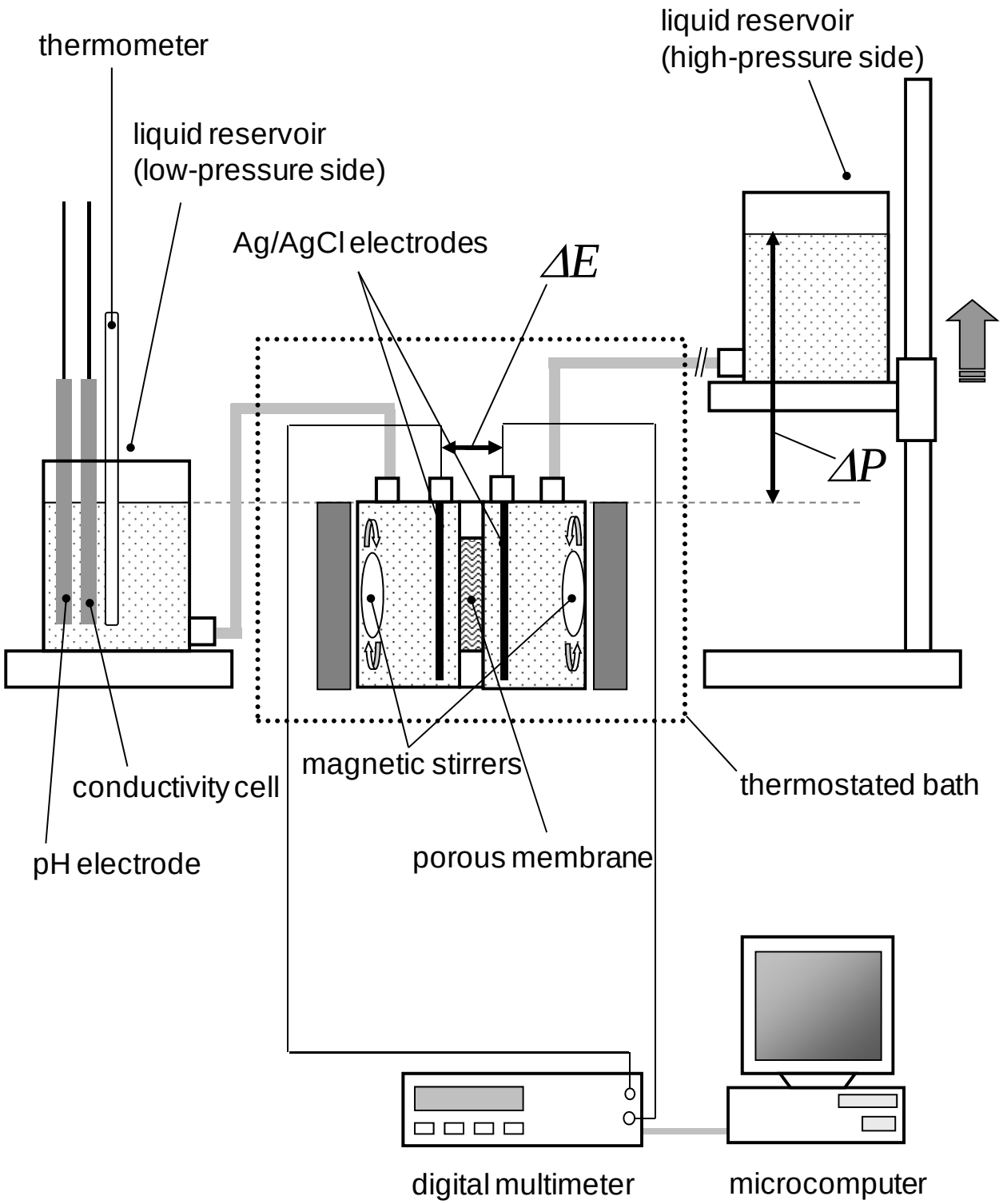

Figure 2-2. Apparatus for streaming potential measurements.

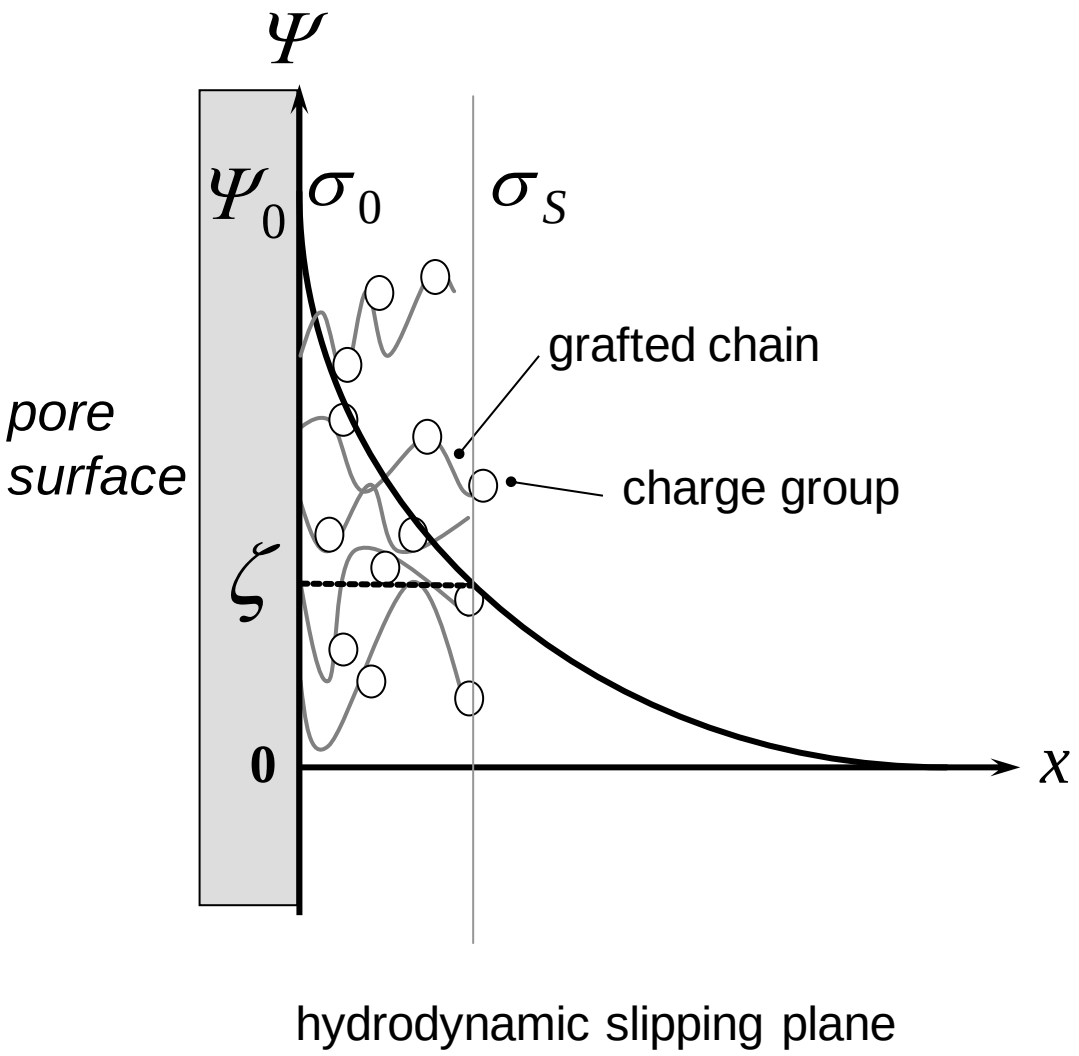

Figure 2-3. Schematic model of potential distribution at polyelectrolyte-grafted pore surface.

Chapter 3

Membrane Materials

3.1 Introduction

It is widely recognized that poly(ethylene glycol) (PEG) has biocompatibility and protein and cell resistance characteristics [1-5]. Many researchers, such as Harris et al., have reported surface modifications by PEG [6-12]. Thus, it is very interesting that the surface modification using PEG can be applied to a porous membrane for the purpose of creating an antifouling or antithrombotic membrane. Koyama has recently prepared a PEG derivative having pendant amino groups (PEG-A) by addition of aminoethanethiol to the double bond pendants of copoly(allyl glycidyl ether/ethylene oxide) (copoly(AGE/EO)) [13]. This polymer has only ether linkage along the main chain, and also a very narrow molecular weight distribution ($\overline{M}_w / \overline{M}_n$ = 1.06). The carbon-carbon double bond side chain of copoly(AGE/EO) may be susceptible to the addition reactions of other mercaptans having weak charge groups to afford PEG derivatives having pendant ionizable groups. Such ionic PEG derivatives have both the advantage from the polyether backbone structure and functionality from the pendant charge groups. Therefore, they are expected as functionalized PEG derivatives for applications to surface modification of membranes.

In this study, we used two kinds of typical artificial filtration membranes, which are cellulose acetate (CA) porous membranes and high-density polyethylene (PE) porous membranes, as substrate; and three kinds of ionic PEG derivatives, which are anionic, cationic, and amphoteric PEG derivatives, as the grafting polymer for surface modification of the porous membranes. This chapter gives the characteristics of membrane materials used in this study. Two types of porous membranes are characterized by hydraulic permeability measurements and scanning electron microscopy (SEM) observations. Three kinds of PEG derivatives with pendant ionizable groups are prepared and then characterized by nuclear magnetic resonance (NMR) and gel permeation chromatography (GPC) measurements.

3.2 Experimental

3.2.1 Materials

Cellulose acetate (CA) porous membranes (C020G047A) and high-density polyethylene (PE) porous membranes (Hipore® N720) were obtained from Toyo Roshi, Japan, and Asahi Kasei, Japan, respectively. Characteristics of these porous membranes are summarized in Table 3-1, and their surface SEM images are shown in Figure 3-1.

Copoly(allyl glycidyl ether/ethylene oxide) (copoly(AGE/EO) [13], AGE/EO=13.6/86.4 in molar ratio, $\overline{M}_n$ = 3260, $\overline{M}_w / \overline{M}_n$ = 1.05) was provided by NOF, Japan. L-Cysteine hydrochloride monohydrate, 2-aminoethanethiol hydrochloride, 3-mercaptopropionic acid, methanol, chloroform, diethyl ether, acetone, N,N-dimethylformamide dehydrated, acetic anhydride, triethylamine, and potassium chloride were purchased from Wako Pure Chemical, Japan. These reagents were of extra-pure grade. N,N-dimethylformamide dehydrated was distilled over calcium hydride under reduced pressure and stored with molecular sieves. The other reagents were used without further purification.

3.2.2 Preparation of PEG derivatives with pendant ionizable groups

The preparation of PEG derivatives with pendant ionizable groups is shown in Figure 3-2. We synthesized the PEG derivatives by adding highly reactive mercaptans having a weak charge group to the double bond side chains of copoly(AGE/EO). The PEG derivatives having amino groups (PEG-A), carboxyl groups (PEG-C), and the amphoteric ion pair, i.e. cysteine residues (PEG-Cys), were synthesized using 2-aminoehtanthiol, 3-mercaptopropionic acid, and L-cysteine, respectively.

3.2.2.1 Synthesis of PEG-A

Copoly(AGE/EO) (5.02 g) was dissolved in methanol (7 mL), and was added dropwise at room temperature to the solution of 2-aminoethanthiol hydrochloride (10.01 g) in methanol (12 mL). After standing at room temperature for 2 days, the reaction mixture was evaporated to remove the methanol. The residual syrup was dissolved in chloroform, neutralized by sodium hydroxide, and washed two times with water. After evaporated, it was washed two times by diethyl ether and purified by reprecipitation with acetone/diethyl ether. Removal of the solvent under reduced pressure gave a syrupy product (4.13 g).

3.2.2.2 Synthesis of PEG-C

Copoly(AGE/EO) (5.03 g) and the solution of 3-mercaptopropionic acid (5 mL) in methanol (7 mL) were mixed. After standing at room temperature for 2 days, the polymer was precipitated and then washed two times by diethyl ether. Removal of the solvent under reduced pressure gave a syrupy product (5.82 g).

3.2.2.3 Synthesis of PEG-Cys

Copoly(AGE/EO) (5.0 g) in methanol (20 mL) was added dropwise at room temperature to the L-cysteine hydrochloride monohydrate (15 g) in methanol solution (20 mL). After standing at room temperature for 2 days, the polymer was purified by repeated reprecipitation with methanol/diethyl ether. Removal of the solvent under reduced pressure gave a syrupy product in the theoretical yield.

3.2.2.4 Acetylation of PEG-A and PEG-Cys

PEG-A (50 mg) or PEG-Cys (50 mg) prepared above was dissolved in 200 μL of dry dimethylformamide, and then 200 μL of acetic anhydride and 200 μL of triethylamine were added to the solution. After the mixture stood for 90 min at room temperature, 200 μL of water was added. The solution was stirred for 30 min. Removal of the solvent under reduced pressure gave a pale yellow syrup.

3.2.3 Measurements

3.2.3.1 Hydraulic permeability measurements

The hydraulic permeability of the membranes was calculated from the flow rate of deionized water, which was eluted for 20 min under an applied constant hydrostatic pressure difference of 75.0 cm H_2O across the membrane. The area of the membrane exposed to the flow was 4.9 cm^2. All measurements were done at 25±0.1℃.

3.2.3.2 Scanning electron microscopy (SEM) observations

SEM observations of the surfaces of original CA and PE porous membranes were performed using a Hitachi S-800 field emission gun, scanning electron microscope (FE-SEM) without sample coating.

3.2.3.3 Nuclear magnetic resonance (NMR) measurements

The completion of the addition reaction of the double bond side chain of copoly(AGE/EO) with

each mercaptan was confirmed by NMR measurements. The ^{1}H NMR spectra of the prepared polymer were measured with a JEOL JNM-AL300 instrument in $CDCl_3$ (for copoly(AGE/EO)) or DMSO-d6 (for the other polymers) at 40℃. Tetramethylsilane was used as internal standard.

3.2.3.4 Gel permeation chromatography (GPC) Measurements

The molecular weight distribution of the polymers was estimated by GPC using a Tosoh Model CCPS apparatus equipped with a column TSK G3000HXL and a refractive index detector Model RI 8020. Tetrahydrofuran was used as an eluent at a flow rate of 1.0 mL/min. The molecular weight was calculated using standard PEGs.

3.3 Results and Discussion

The ionic PEG derivatives were synthesized by the addition of the corresponding mercaptan to the double bond side chains of copoly(AGE/EO). The reaction was completed in methanol at room temperature without a catalyst. The ^{1}H NMR spectra of all the PEG derivatives having pendant ionizable groups showed no residual double bond peak which had been observed near 5.2 and 5.8 ppm with copoly(AGE/EO), and the spectra indicated that PEG derivatives having pendant ionizable groups with a definite structure were obtained (Figure 3-3).

Gel permeation chromatograms of the polymers are shown in Figure 3-4. Here, the amino groups of PEG-A and PEG-Cys had been acetylated by acetic anhydride/triethylamine before analyzed [13] and then their molecular distribution was analyzed by GPC. The GPC spectrum of the acetylated PEG-A showed a narrow molecular weight distribution (M_w/M_n =1.12, Figure 3-4 (b)). The GPC spectra of PEG-C and the acetylated PEG-Cys were bimodal (Figure 3-4 (c), (d)); a small peak appeared at a high-molecular-weight region. It indicates radical coupling of the polymers occurred during the reaction, but the most part of the polymer remains almost monodisperse, and overall M_w/M_n were still very small (1.09 for PEG-C and 1.14 for the acetylated PEG-Cys).

3.4 Conclusions

In this chapter, characteristics of membrane materials used in this study were shown. Two types porous membranes were characterized by hydraulic permeability measurements and SEM observations.

Three kinds of PEG derivatives with pendant ionizable groups were prepared by addition of mercaptans to the double bond pendants of coply(AGE/EO). ^{1}H NMR spectra revealed the completion of the reactions, and GPC profiles of these products showed their narrow molecular weight distributions. These cationic, anionic, and amphoteric PEG derivatives are expected for surface modification of porous membranes, especially for the preparation of novel amphoteric charged membranes described in Chapter 1.

3.5 References

1. Harris, J. M., Ed. *Poly(Ethylene Glycol) Chemistry: Biotechnical and Biomedical Applications*; Plenum Press: New York, 1992.
2. Harris, J. M., Zalipsky, S., Eds. *Poly(Ethylene Glycol): Chemical and Biological Applications*; ACS Symposium Series, Vol. 680; American Chemical Society: Washington, DC, 1997.
3. Jeon, S. I.; Lee, J. H.; Andrade J. D.; De Gennes, P. G. *J. Colloid Interface Sci.* **1991**, *142*, 149.
4. Prime, K. L.; Whitesides, G. M., *J. Am. Chem. Soc.* **1993**, *115*, 10714.
5. Gingell, D.; Owens, N. *J. Biomed. Mater. Res.* **1994**, *28*, 491.
6. Bergström, K.; Holmberg, K.; Safranji, A.; Hoffman, A. S.; Edgell, M. J.; Kozlowski, A.; Hovanes, B. A.; Harris, J. M. *J. Biomed. Mater. Res.* **1992**, *26*, 779.
7. Van Alstine, J. M.; Burns, N. L.; Riggs, J. A.; Holmberg, K.; Harris, J. M. *Colloids Surfaces A* **1993**, *77*, 149.
8. Österberg, E.; Bergström, K.; Holmberg, K.; Riggs, J. A.; Van Alstine, J. M.; Schuman, T. P.; Burns, N. L.; Harris, J. M. *Colloids Surfaces A* **1993**, *77*, 159.
9. Burns, N. L.; Van Alstine, J. M.; Harris, J. M. *Langmuir* **1995**, *11*, 2768.
10. Österberg, E.; Bergström, K.; Holmberg, K.; Schuman, T. P.; Riggs, J. A.; Burns, N. L.; Emoto, K.; Van Alstine, J. M.; Harris, J. M. *J. Biomed. Mater. Res.* **1995**, *29*, 741.
11. Emoto, K.; Van Alstine, J. M.; Harris, J. M. *Langmuir* **1998**, *14*, 2722.
12. Burns, N. L.; Emoto, K.; Holmberg, K.; Van Alstine, J. M.; Harris, J. M. *Biomaterials* **1998**, *19*, 423.
13. Koyama, Y.; Umehara, M.; Mizuno A.; Itaba M.; Yasukouchi, T.; Natsume, K.; Suginaka, A. *Bioconjugate Chem*. **1996**, *7*, 298.

Table 3-1 Characteristics of porous membranes

Membrane	CA	PE
Average pore size (nm)	200	50
Porosity (%)	66	40
Thickness (μm)	130	25
Hydraulic permeability ($mL/m^2 \cdot h \cdot cmH_2O$)	386	72*

* Measured after immersion in MeOH.

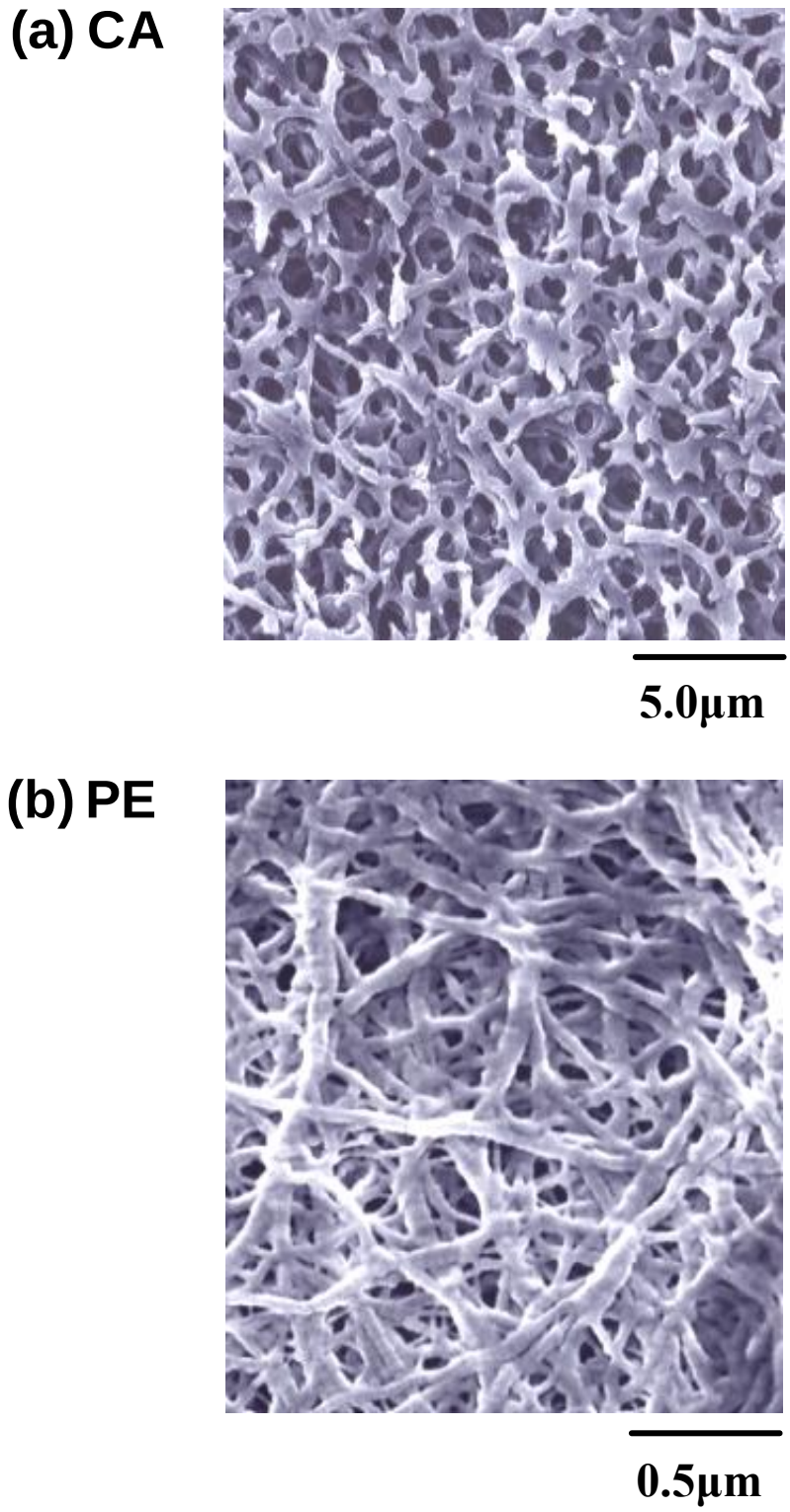

Figure 3-1. Surface SEM images of (a) CA porous membrane and (b) PE porous membrane.

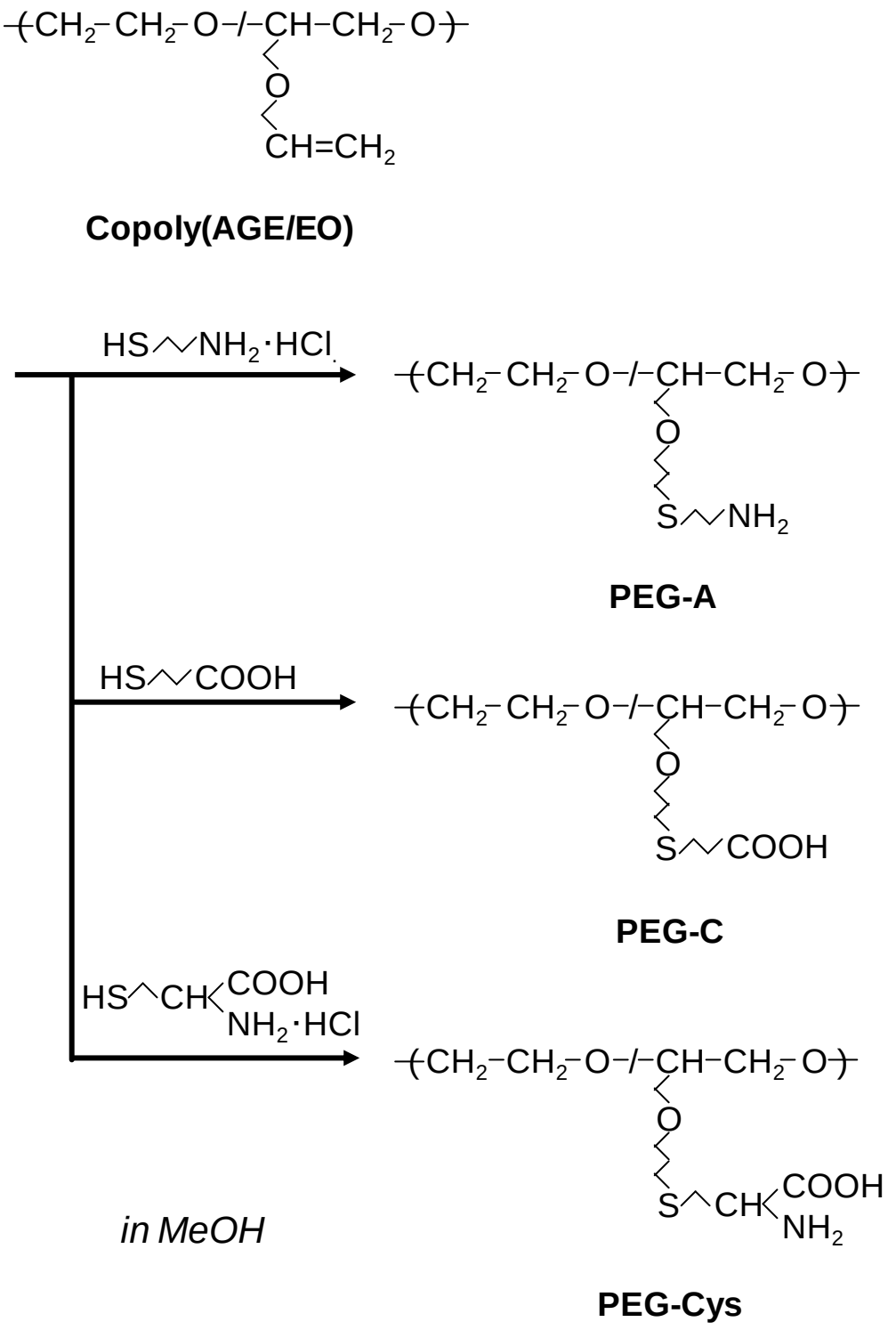

Figure 3-2. Synthesis of the PEG derivatives with pendant ionizable groups.

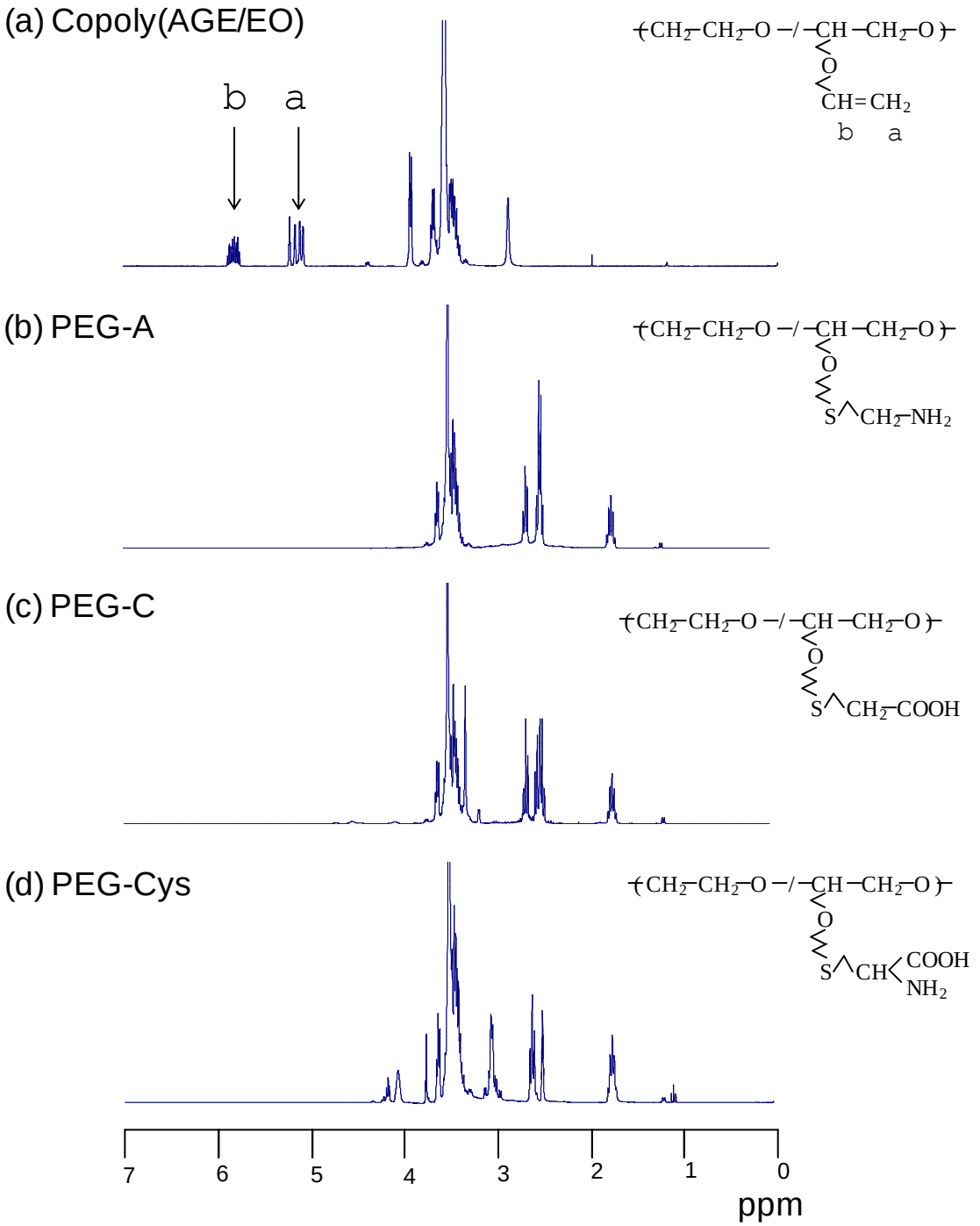

Figure 3-3. ^{1}H NMR spectra of (a) copoly(AGE/EO), (b) PEG-A, (c) PEG-C, and (d) PEG-Cys.

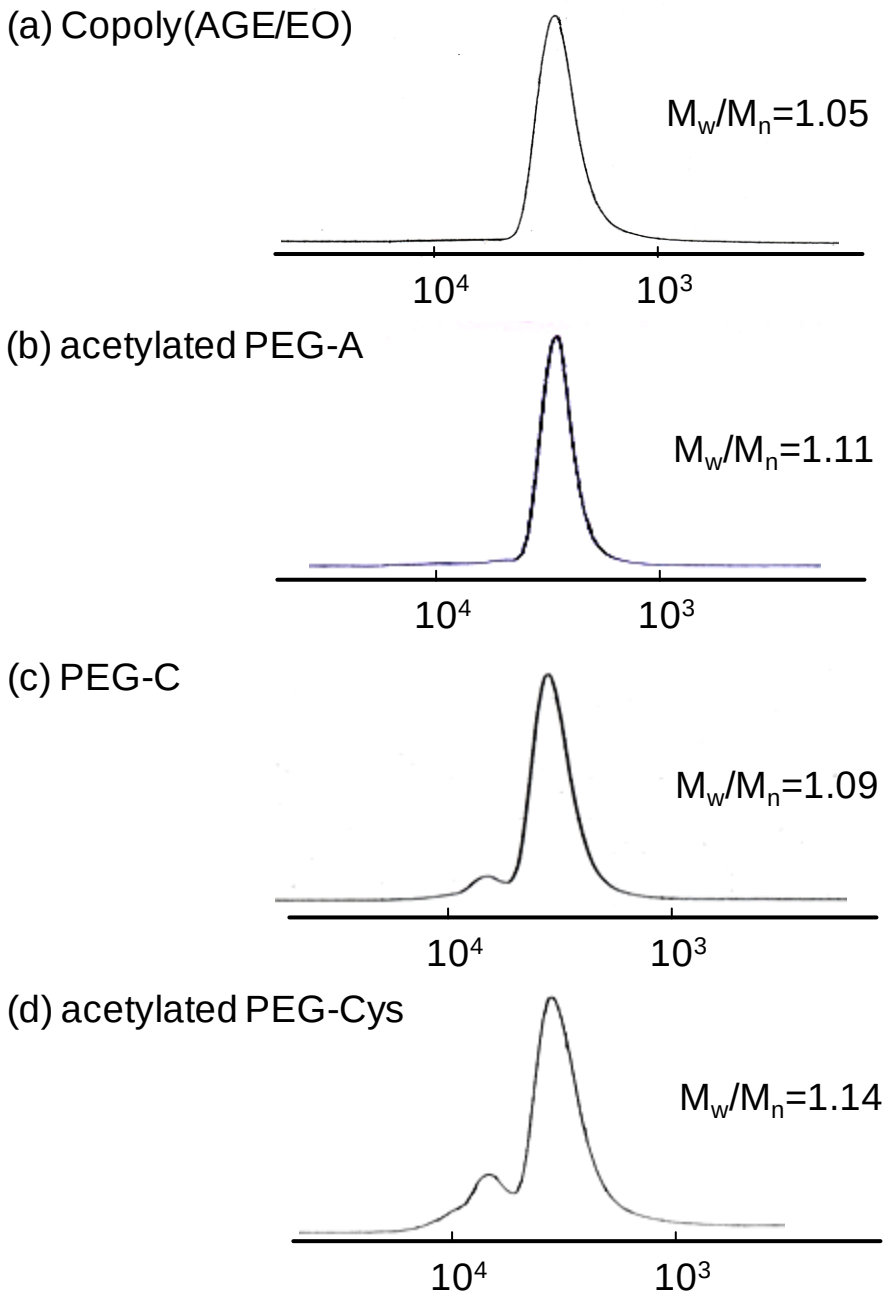

Figure 3-4. Gel permeation chromatograms of (a) copoly(AGE/EO), (b) the acetylated PEG-A, (c) PEG-C, and (d) the acetylated PEG-Cys.

Chapter 4

Preparation and Characterization of Weak Amphoteric Charged Membranes I: Surface Modification of Cellulose Acetate Porous Membranes

4.1 Introduction

Weak amphoteric charged porous membranes contain both weak acidic (negative charge) groups and weak basic (positive charge) groups on the pore surface [1-6]. The physicochemical properties of these membranes such as permselectivity and adsorption characteristics are influenced by the pore surface charge [7]. The interfacial charge structure of these membranes is so complicated that there have been few theoretical discussions on the correlation between their interfacial charge properties and their macroscopic properties [8]. Electrokinetic measurements have been theoretically established and widely utilized for the characterization of polymer surfaces [1-4, 7, 9, 10], particularly for the surfaces of porous polymeric membranes [2-4, 7]. While the zeta potential is the electrokinetic potential that is generated at the hydrodynamic slipping plane, strictly differ from the pore surface, it provides qualitative information related to complex surface changes [1-4, 9-11]. We deduced the zeta potential from the observed streaming potentials to estimate the charge property on the pore surface. These measurements are also sensitive to the pH dependence of the dissociation of the surface ioniazble groups [1-4, 9-11]. Healy and White have suggested that surface charge can be described in terms of a site dissociation model (SDM) for surface ionizable groups (see chapter 2) [12]. This model seems to be suitable for analyzing the charge properties on the pore surface such as surface charge density and dissociation constant of the charge group. We have adapted this semiquantitative methodology to characterize the amphoteric charged porous membranes.

In chapter 3, we prepared novel ionic PEG derivative with pendant cysteine residues. The polyampholyte (PEG-Cys), which has amphoteric ion pairs in the molecule, is a unique material for

introducing amphoteric charge groups on a porous membrane at the following point. Since a pair of an amino group and a carboxyl group in the cysteine residue forms a dipolar ion structure [13], it can be expected that the PEG-Cys grafted membrane exhibits an amphoteric charge state over a wider range of pH than the membrane on which amino groups and carboxyl groups are differently introduced. In this chapter, first, novel weak amphoteric charged membranes were prepared by grafting the polyampholyte (PEG-Cys) onto the pore surface of a cellulose acetate (CA) porous membrane. Second, the interfacial charge properties of these amphoteric charged membranes were characterized by the zeta potential obtained from streaming potential measurements. The pH dependence of the apparent surface charge density derived from the zeta potential was examined based on a SDM.

4.2 Experimental

4.2.1 Materials

Copoly(allyl glycidyl ether/ethylene oxide) (copoly(AGE/EO) [14], AGE/EO=13.6/86.4 in molar ratio, $\overline{M}_n$ = 3260, $\overline{M}_w / \overline{M}_n$ = 1.05) was provided by NOF Corporation, Japan. L-Cysteine hydrochloride monohydrate, 2-aminoethanethiol hydrochloride, cerium (IV) ammonium nitrate, nitric acid, and potassium chloride were purchased from Wako Pure Chemical, Japan. These reagents were of extra-pure grade. Hydrochloric acid and potassium hydroxide were from Wako Pure Chemical, Japan. These reagents were of analytical grade. All reagents were used without further purification.

The PEG derivative with pendant cysteine residues (PEG-Cys, see chapter 3) was used as grafting polymer.

Cellulose acetate (CA) porous membranes (see chapter 3) were used as substrate in this study.

4.2.2 Membrane preparation

CA porous membranes were used as the substrates on which the PEG derivatives were graft polymerized. Two approaches to creating free radicals by ceric ion (Ce^{4+}) and gamma-ray irradiation were investigated. A schematic illustration of grafting PEG derivatives onto CA membranes is shown in Figure 4-1.

4.2.2.1 Ceric ion method

Copoly(AGE/EO) (15 g) was dissolved in distilled water (100 mL), in which CA porous membranes were immersed. Cerium (IV) ammonium nitrate (16.5 g) and nitric acid (228 μg) were dissolved in distilled water (30 mL) and then added dropwise in five portions at room temperature under a N_2 atmosphere to the membrane in the copoly(AGE/EO) solution. After 20 min, membranes were removed and washed thoroughly with distilled water. L-Cysteine hydrochloride monohydrate (25 g) was dissolved in methanol (100 mL), and the membranes were immersed. After 2 days standing at room temperature, these membranes were rinsed with deionized water to remove the nonreacted amino acid sufficiently. 2-Aminoethanethiol hydrochloride was also used instead of L-cysteine hydrochloride for comparison between a positively charged membrane and an amphoteric charged membrane. The PEG-Cys-grafted CA membranes and the PEG-A-grafted CA membranes were prepared here.

4.2.2.2 Gamma-ray method

The CA porous membranes were immersed in 12 wt% PEG-Cys aqueous solution. Each membrane was pulled up and then placed between two glass plates. The plates were sealed with cellophane tape. The plates were then irradiated by 1.17 eV and 1.33 eV of gamma-rays in a ^{60}Co general purpose irradiation device (Model RE-1012, TOSHIBA, Japan) at dose rates of 2.47 kGy/hr and total doses of 100 kGy. After the irradiation, the plates were unsealed and soaked in deionized water for 12 h. The membranes were removed from the plates and washed with deionized water to remove the nongrafted PEG-Cys sufficiently.

4.2.3 Measurements

4.2.3.1 X-ray fluorescence analysis (XRF)

Elementary analysis by XRF of freeze-dried membranes was carried out using a Philips PW2404 apparatus.

4.2.3.2 Potentiometric titration measurements

The potentiometric titration measurements were performed using a complex electrode (GST-5721C, TOA Electronics, Japan) and a pH meter (HM-60G, TOA Electronics, Japan). All procedures were carried out as previously described in ref 15. Membranes were titrated with 0.1 mol/L HCl or 0.1 mol/L KOH in 3 mol/L KCl solution (150 mL) under a nitrogen gas flow with stirring. To

clarify the end points of the titration, the contributions of excess H^+ and OH^- were subtracted by conducting blank titration [16]. All measurements were carried out at 25±0.1℃.

4.2.3.3 Hydraulic permeability measurements

The hydraulic permeability of the membranes was calculated from the flow rate of deionized water, which was eluted for 20 min under an applied constant hydrostatic pressure difference of 75.0 cm H_2O across the membrane. The area of the membrane exposed to the flow was 4.9 cm^2. All measurements were done at 25±0.1℃.

4.2.3.4 Streaming potential measurements

The device used for the streaming potential measurements was described in chapter 2. By varying the applied pressure (ΔP) ranging from 15 to 120 cmH_2O, the streaming potential (ΔE) which has been generated by a flow of ions due to ΔP, was measured with a digital multimeter (HP3458A, Hewlett-Packard, USA) and recorded using a microcomputer. The zeta potential was obtained from the slope of a $\Delta E - \Delta P$ plot using the Helmholtz－Smoluchowski equation as follows:

$$\frac{\Delta E}{\Delta P} = \frac{\varepsilon \zeta}{\eta \lambda} \tag{4.1}$$

where ε is the permittivity of the solution, η is the solution viscosity, and λ is the electrical conductivity of the solution. The apparent surface charge density of the pores was calculated from the zeta potential using the Gouy－Chapman equation:

$$\sigma_S = \frac{2\varepsilon kT\kappa}{z_+ e} \sinh\left(\frac{z_+ e\zeta}{2kT}\right) \tag{4.2}$$

where k is the Boltzmann constant, T is the temperature, κ is the reciprocal of the electrical double layer thickness, z_+ is the valence of the counterion, and e is the Coulombic charge. The outer solution was 1 mmol/L KCl throughout measurements. The pH of the outer solution was regulated from 2.5 to 10 by adding HCl or KOH. All measurements were carried out in a stirred solution thermostated at 25± 0.1℃. The measurements were carried out three times for each experimental point, and the mean value

(± standard deviation) of each experimental point is indicated.

4.3 Results and Discussion

4.3.1 Preparation of grafted membranes

Copoly(AGE/EO) was grafted onto CA membrane with Ce^{4+} system, and then reacted with the mercaptans. Positive and amphoteric charged membranes were prepared by addition reaction with aminoethanethiol and cysteine, respectively. Ionic PEG chain grafted CA membranes could also be obtained by the radiation graft copolymerization of the corresponding polymers. The effect of graft polymerization of PEG-Cys onto CA membranes was confirmed by potentiometric titration measurements. The net charge density was calculated by normalizing the sum of the equivalents at the endpoint of the titration curve on both the added alkali side and the added acid side with the weight of the dried membrane. The calculated values for four kinds of membranes are listed in Table 4-1. All grafted membranes exhibit a higher net charge density than the base CA membrane. This result revealed that ionic PEG chains were grafted onto the CA membranes. We also performed elementary analysis of unmodified and grafted membranes using XRF. The results verified the presence of a sulfur atom from PEG-Cys on the modified membranes.

4.3.2 Zeta potential measurements of unmodified and grafted CA membranes

The streaming potentials were measured at five pressures, as shown in Figure 4-2. Good linearity of the relationship between the streaming potential and the pressure difference for each membrane could lead to the calculation of the zeta potential using eq (4.1), which implies that no irregular change in the charge state of the grafted pore surface due to pressure-driven fluid flow can be observed. We, however, must consider the effects of pore diameter and surface roughness on the value of the zeta potential in the porous membrane system [2-4]. The pore size of unmodified CA membrane, 0.2 μm in average pore diameter, is large enough to permit ignoring the electrical conductance effect at the diffuse part of the double layer (the Debye screening length is 10 nm in 1 mmol/L KCl solution) [4]. All grafted membranes showed the same degree of hydraulic permeability, nearly 400 $mL/m^2 \cdot hr \cdot H_2O$, as the unmodified membrane shown in Table 4-1. This value is within the range where the effect of pore size is negligible as reported by Jimbo et al. [4]. Therefore, we did not take into account the surface

conductance and double-layer overlapping effects in unmodified and grafted CA membranes. However, because it is impossible to determine the real state of the pore surface (i.e., whether it is ideally smooth), the zeta potential obtained in this study must be regarded as an apparent value.

Figure 4-3 shows the pH dependence of the zeta potentials of unmodified and grafted CA membranes. The zeta potential of the unmodified CA membrane had a negative value and decreased with pH increase. This trend appears to be generated from the weak acidic groups on the pore surface of the CA membranes. In the case of the PEG-A grafted CA membrane, the zeta potential showed a positive value at low pH, approached that of the base membrane at higher pH, and finally agreed with it. For the PEG-Cys grafted membranes, particularly the membrane grafted by gamma-ray method, the zeta potential changed from a positive to a negative value, across the *plateau* which showed a constant potential in the range of pH 4－9. This behavior is characteristic of weak amphoteric charged membranes [2-4, 6] and the constant potential in the intermediate pH region would be evidence of the dipolar ion structure in the cysteine residues. Zeta potential/pH profiles for the amphoteric charged membranes, which have not amphoteric ion pairs as charged groups, never show the flat section [2-4].

4.3.3 Theoretical analysis according to a site dissociation model

To explain the experimental results mentioned above, we simulated the apparent surface charge density/pore surface pH profiles using a site dissociation model [1-4, 9-12]. When there is no specific adsorption of electrolyte ions, ionizable groups can contribute to a surface charge. Equilibrium between charge groups and the solution at the interface is represented as:

$$AH \leftrightarrow A^- + H^+ \tag{4.3}$$

$$BH^+ \leftrightarrow B + H^+ \tag{4.4}$$

where AH and B are acidic and basic groups, respectively. These equilibria have dissociation constants, K,

$$K_a = \frac{[A^-][H^+]_S}{[AH]} \tag{4.5}$$

$$K_b = \frac{[B][H^+]_S}{[BH^+]} \tag{4.6}$$

where subscripts *a* and *b* stand for acidic site and basic site, respectively. $[H^+]_S$ is the hydronium ion concentration at the pore surface, which is based on the hypothesis that the ion concentration in the electrolyte solution follows the Boltzmann distribution outside of the plane where the zeta potential is generated, and is written in the form

$$[H^+]_S = [H^+]_0 \exp\left(\frac{-e\zeta}{kT}\right) \tag{4.7}$$

where $[H^+]_0$ is the hydronium ion concentration in the bulk solution. The total site charge density of the pore surface, N, is denoted by

$$N_a = [A^-] + [AH] \tag{4.8}$$

$$N_b = [BH^+] + [B] \tag{4.9}$$

Therefore, the apparent surface charge density, σ_S, can be expressed by combining eqs (4.5) and (4.6) with (4.8) and (4.9), respectively. For a multiple charged pore surface, σ_S is given by

$$\begin{aligned}\sigma_S &= -e\sum_i [A^-]_i + e\sum_j [BH^+]_j \\ &= \sum_i \left[\frac{-eN_a}{1+10^{(pK_a - pH_S)}}\right] + \sum_j \left[\frac{eN_b}{1+10^{(pH_S - pK_b)}}\right]\end{aligned} \tag{4.10}$$

where pK_a and pK_b are the equilibrium acidic dissociation constants of the acidic and basic sites, respectively, and pH_S is the surface pH. The experimental value of the apparent surface charge density is plotted as a function of the surface pH in Figure 4-4. The gray solid line noted as calculated-1 in Figure

4-4 represents the calculation result according to a nonlinear regression method based on the SDM. In this calculation, 1.9 and 10.8 were used as pK_a and pK_b, respectively. These values are dissociation constants of Cys in ref 17. The calculated results could explain the tendency of pH dependence in the experimental value, but the difference between the experimental value and the calculated one appeared in the range of pH 4－9. We then thought that the effect of the charge groups on the base membrane should be also taken into consideration. The CA membrane has a negative potential, as shown in Figure 4-3. In Figure 4-5, the squares stand for the apparent surface charge density of the CA membranes. The dissociation constants of the CA membrane were obtained from the fitting parameter by calculation with the SDM based on the assumption that there are two types of acidic groups. They are 3.0 and 10.0. The fitting curve using these constants agreed with the experimental data exactly. Demisch and Pusch pointed out that CA membranes had a small amount of carboxyl groups besides hydroxyl groups [18]. Thus, these values from the fitting would be also reasonable for the chemical structure. The black solid line noted as calculated-2 in Figure 4-4 is the result calculated by the nonlinear regression method based on the SDM including the effect of the charge site on both the grafted polyampholyte chain and the substrate membrane. It was proven that the value calculated using this method could explain the experimental value well in all pH ranges in the experiment. A similar theoretical approach made possible an interpretation of the charge properties on the both PEG-A grafted CA membrane and PEG-Cys grafted CA membrane by the ceric ion method as shown in Figs 4-6 and 4-7, respectively. N_a and N_b on grafted polymer chain and pK_{a1}, pK_{a2}, N_{a1}, and N_{a2} on base membrane were determined by implementing a nonlinear parameter estimation program, UNCMIN [19], and are summarized in Table 4-2. We have to consider that the charge properties on these amphoteric charged membranes are related to macroscopic properties. The physical meaning of the apparent surface charge density obtained here must be more clarified through further considerations.

4.4 Conclusions

In this chapter, novel weak amphoteric charged membranes having cysteine residues were prepared by graft polymerization of the amphoteric PEG derivatives onto CA porous membranes. The zeta potential/pH profiles of these membranes showed the peculiarity of a polyampholyte having

amphoteric ion pairs. Since the original CA membrane has two types of charge groups, it is difficult to consider the total surface charge density on ionic PEG chain grafted CA membrane. We, however, can reach the conclusion that an analysis of the pore surface charge including the effect of not only amphoteric charge groups on the grafted polymer chains but also charge groups originated from the base membrane can be achieved by the SDM.

4.5 References

1. Burns, N. L.; Holmberg K.; Brink C. *J. Colloid Interface Sci*. **1996**, *178*, 116.
2. Jimbo, T.; Higa M.; Minoura, N.; Tanioka A. *Macromolecules* **1998**, *31*, 1277.
3. Jimbo, T.; Tanioka A.; Minoura, N. *Langmuir* **1998**, *14*, 7112.
4. Jimbo, T.; Tanioka A.; Minoura, N. *Colloids Surfaces A* **1999**, *159*, 459.
5. Jimbo, T.; Tanioka A.; Minoura, N. *Langmuir* **1999**, *15*, 1829.
6. Werner, C.; Jacobasch, H.-J.; Reichelt G. *J. Biomater. Sci. Polymer Edn.* **1995**, *7*, 61.
7. Caussreand C.; Nyström M.; Aimar P. *J. Membrane Sci.* **1994**, *88*, 211.
8. Ramírez, P.; Alcaraz, A.; Mafé, S. *J. Electroanal. Chem*. **1997**, *436*, 119.
9. Burns, N. L.; Van Alstine, J. M.; Harris, J. M. *Langmuir* **1995**, *7*, 2768.
10. Emoto, K.; Van Alstine, J. M.; Harris, J. M. *Langmuir* **1998**, *14*, 2722.
11. Hunter, R. J. *Zeta Potential in Colloid Science*; Academic Press: London, 1981; Chapter 7.
12. Healy, T. W.; White, L. R. *Adv. Colloid Interface Sci.* **1978**, *9*, 303.
13. Stryer, L. *Biochemistry,* 3rd ed.; W. H. Freeman and Company: New York, 1988.
14. Koyama, Y.; Umehara, M.; Mizuno A.; Itaba M.; Yasukouchi, T.; Natsume, K.; Suginaka, A. *Bioconjugate Chem*. **1996**, *7*, 298.
15. Saito, K.; Tanioka, A.; Miyasaka, K. *Polymer* **1996**, *37*, 2299.
16. Kawaguchi, S.; Nishikawa, Y.; Kitano, T.; Ito, K.; Minakata, A. *Macromolecules* **1990**, *23*, 2710.
17. Martell, A. E.; Smith, R. M. *Critical Stability Constants*; Plenum Press: New York, 1974; Vol. 1; 1975; Vol. 2. For the assignment of cysteine's pK, see also: Greenstein, J. P.; Winitz, M. *Chemistry of the Amino Acids*; John Willey & Sons: New York, 1961; Vol.1, p 494. Calvin, M. In *Glutathione*; Colowick, S.P., Ed.; Academic Press: New York, 1954; p.8.
18. Demisch, H.-U.; Pusch, W. *J. Electrochem. Soc.* **1976**, *123*, 370.
19. Kahaner, D.; Moler, C.; Nash, S. *Numerical Methods and Software*; Prentice Hall: Englewood Cliffs, NJ, 1989.

Table 4-1. Net charge density and hydraulic permeability of unmodified and grafted CA membranes

Membrane	Net charge density [a] ($\times 10^{-5}$ mol/g-dry memb.)	Hydraulic permeability [b] ($mL/m^2 \cdot h \cdot cmH_2O$)	Thickness [c] (μm)
PEG-A-g-CA	2.9	402	158
PEG-Cys-g-CA (1) [d]	3.1	410	158
PEG-Cys-g-CA (2) [d]	4.8	387	128
Unmodified CA	2.0	386	130

[a] The net charge density was obtained from potentiometric titration.

[b] The hydraulic permeability was measured at pH 5.6.

[c] The thickness was measured in the wet state.

[d] (1) Graft coplymerization by ceric ion method; (2) graft polymerization by gamma-ray method.

Table 4-2. Characteristic parameters for the unmodified and grafted CA membranes derived from the Site Dissociation Model

Membrane	Grafted polymer chain				Unmodified CA			
	pK_a	pK_b	$10^3 N_a$ (nm^{-2})	$10^3 N_b$ (nm^{-2})	pK_{a1}	pK_{a2}	$10^3 N_{a1}$ (nm^{-2})	$10^3 N_{a2}$ (nm^{-2})
PEG-A-g-CA	-	8.2 [b]	-	7.18	3.0	10.0	4.68	8.61
PEG-Cys-g-CA (1) [a]	1.9 [b]	10.8 [b]	0.32	0.32	3.0	10.0	4.31	7.37
PEG-Cys-g-CA (2) [a]	1.9 [b]	10.8 [b]	4.43	4.43	3.0	10.0	1.69	2.50
Unmodified CA	-	-	-	-	3.0	10.0	4.61	8.81

[a] (1) Graft coplymerization by ceric ion method; (2) graft polymerization by gamma-ray method.

[b] In ref 17

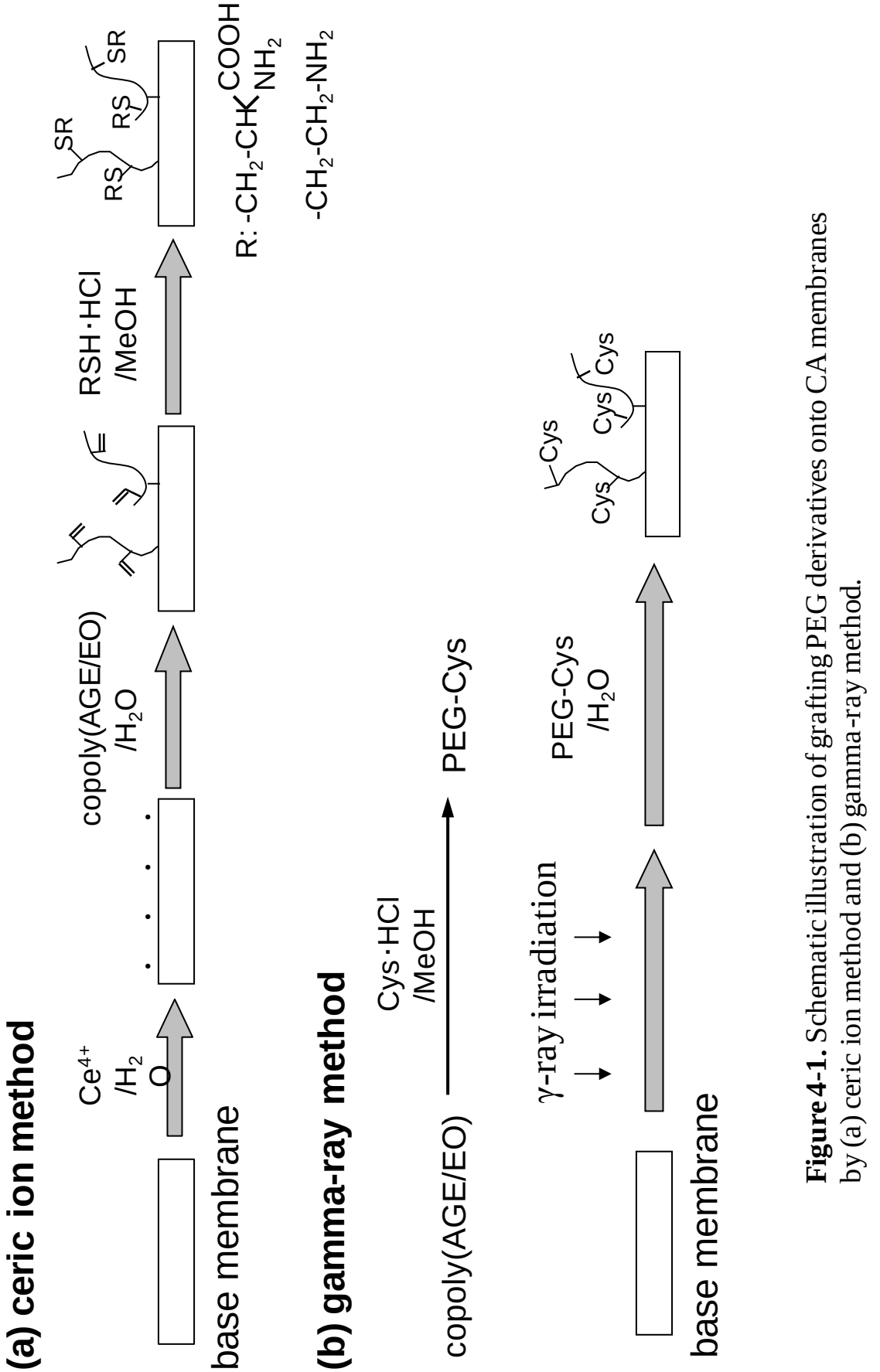

Figure 4-1. Schematic illustration of grafting PEG derivatives onto CA membranes by (a) ceric ion method and (b) gamma-ray method.

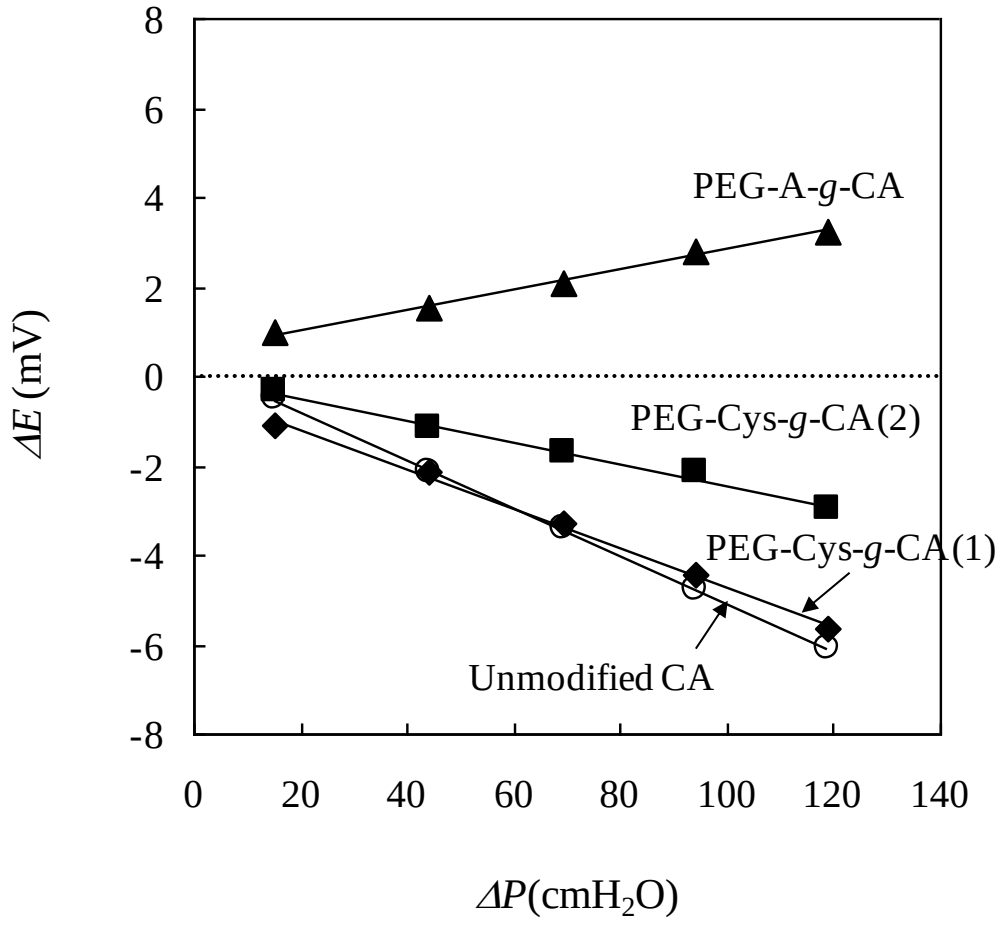

Figure 4-2. Steaming potential as a function of pressure difference for unmodified and grafted CA membranes (1 mM KCl, pH 5.6).

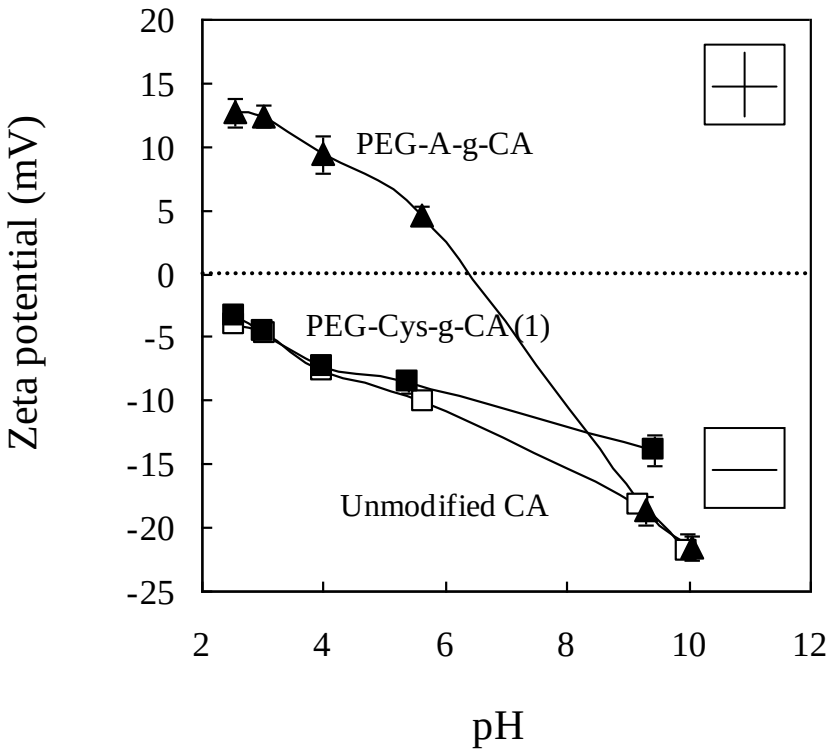

Figure 4-3a. The pH dependence of zeta potential for unmodified and grafted CA membranes (ceric ion method).

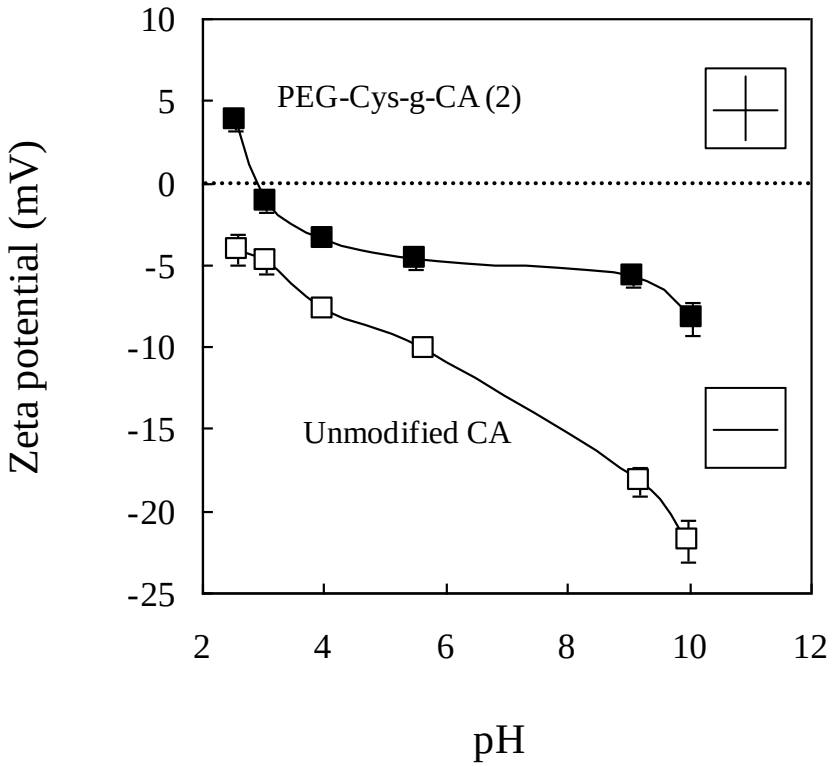

Figure 4-3b. The pH dependence of zeta potential for unmodified and grafted CA membranes (gamma-ray method).

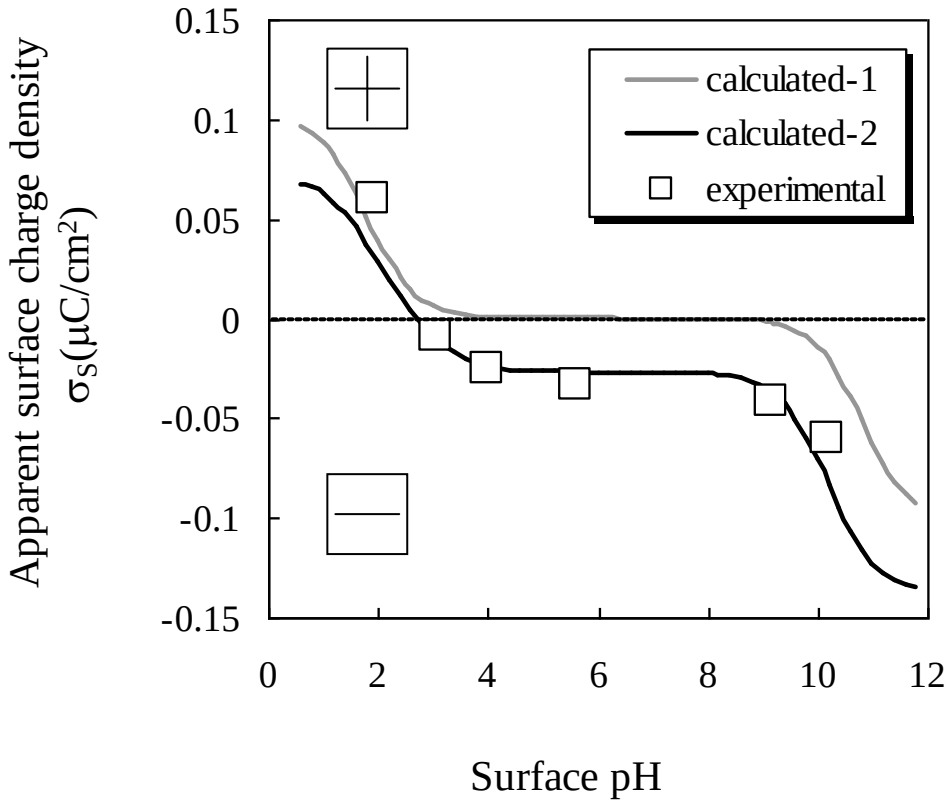

Figure 4-4. The pH dependence of the apparent surface charge density for the PEG-Cys grafted CA membrane by the gamma-ray method. The gray solid line corresponds to theoretical fits using the SDM based on the assumption that PEG-Cys has pairs of acidic and basic sites with pK_a = 1.9 and pK_b = 10.8. The black solid line corresponds to theoretical fits using the SDM based on the assumption that PEG-Cys has pairs of acidic and basic sites with pK_a = 1.9 and pK_b = 10.8, and the CA membrane has two kinds of acidic sites with pK_{a1} = 3.0 and pK_{a2} = 10.0.

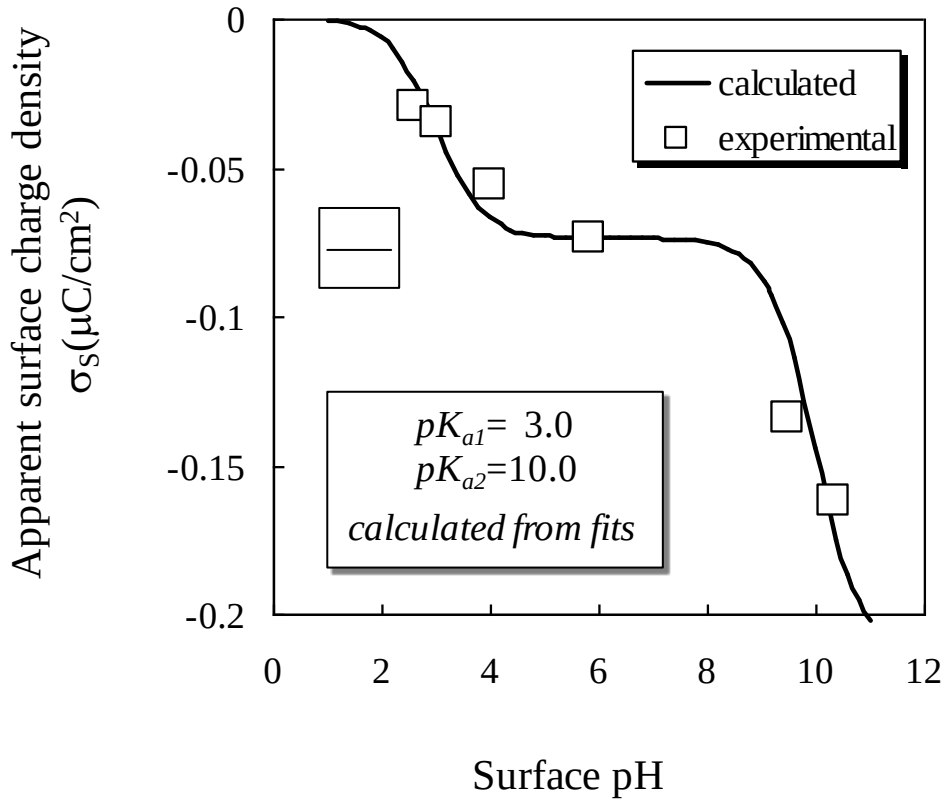

Figure 4-5. The pH dependence of the apparent surface charge density for the CA membrane. The drawn line corresponds to theoretical fits using the SDM based on the assumption that the CA membrane has two kinds of acidic sites. Dissociation constants, pK_{a1} and pK_{a2}, were deduced from the fitting.

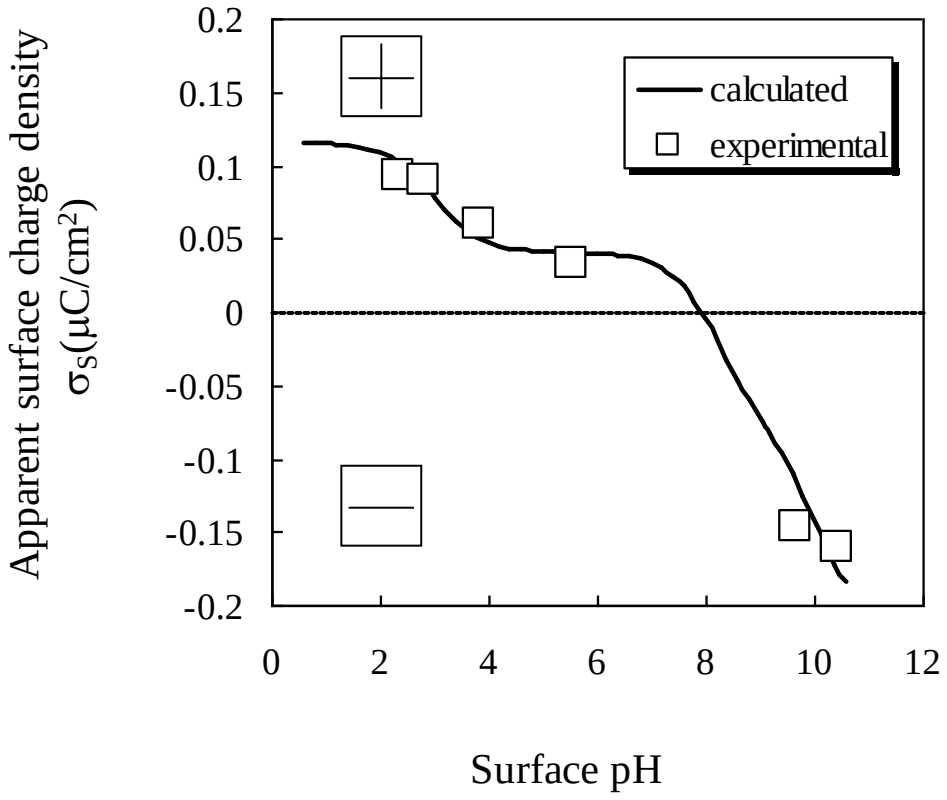

Figure 4-6. The pH dependence of the apparent surface charge density for the PEG-A grafted CA membrane. The drawn line corresponds to theoretical fits using the SDM based on the assumption that PEG-A has a single kind of basic site with pK_b = 8.2, and the CA membrane has two kinds of acidic sites with pK_{a1} = 3.0 and pK_{a2} = 10.0.

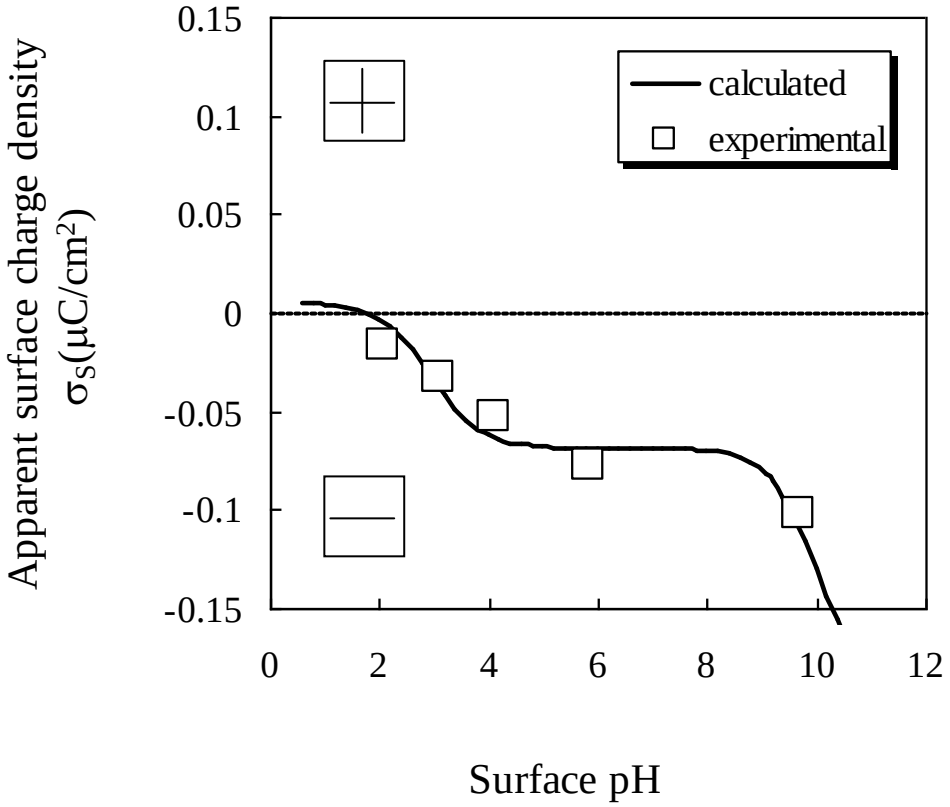

Figure 4-7. The pH dependence of the apparent surface charge density for the PEG-Cys grafted CA membrane by the ceric ion method. The drawn line corresponds to theoretical fits using the SDM based on the assumption that PEG-Cys has pairs of acidic and basic sites with pK_a = 1.9 and pK_b = 10.8, and the CA membrane has two kinds of acidic sites with pK_{a1} = 3.0 and pK_{a2} = 10.0.

Chapter 5

Preparation and Characterization of Weak Amphoteric Charged Membranes II: Surface Modification of Polyethylene Porous Membranes

5.1 Introduction

In previous chapters, we have prepared ionic PEG derivatives and then prepared the amphoteric charged membranes by the graft polymerization of the polyampholyte onto CA porous membranes. The streaming potential measurements revealed their unique pH dependence of interfacial charge properties. The charge characteristics of CA membranes, however, are so complicated that it is difficult to consider the total surface charge on the grafted CA membranes [1]. In this chapter, we prepared two kinds of amphoteric charged membranes, which were the amphoteric ion-pair side chain (ASC) type and the mixed grafted chain (MGC) type, by the radiation-induced graft copolymerization of amphoteric PEG derivatives and the mixture of cationic and anionic PEG derivatives onto high-density polyethylene (PE) porous membranes, respectively. The concept of these membranes has described in chapter 1. The amphoteric ion pair, which consists of an amino group and a carboxyl group, forms the complex where proton is mediated between the amino group and carboxyl group (see Figure 1-3). This complex is called a dipolar ion structure and appears as amphoteric charge states over a wide range of pH as typical in amino acids [2]. We took note of this character obtained only in the ASC-type membrane but not in the MGC-type one. The unmodified and grafted PE membranes were characterized by the zeta potential obtained from streaming potential measurements over the pH range of 2－12. The pH dependence of the apparent surface charge density derived from the zeta potential was compared to the calculated results using a site dissociation model (SDM).

5.2 Experimental

5.2.1 Materials

Potassium chloride was purchased from Wako Pure Chemical, Japan. These reagents were of extra-pure grade. The 0.1 mol/L hydrochloric acid and 0.1 mol/L potassium hydroxide were from Wako Pure Chemical, Japan. These reagents were of analytical grade. All reagents were used without further purification.

Three kinds of ionic PEG derivatives (see chapter 3) were used as grafting polymer: PEG-A (cationic), PEG-C (anionic), and PEG-Cys (amphoteric).

High-density polyethylene (PE) porous membranes (see chapter 3) were used as substrate.

5.2.2 Membrane preparation

Two types of amphoteric charged membranes, the ASC type and the MGC type, and two types of single charged membranes, the acidic type and the basic type, (Figure 5-1) were prepared by the radiation-induced graft copolymerization. PEG-Cys, the mixture of PEG-A and PEG-C (the mixture ratio of $-NH_2$ in PEG-A to –COOH in PEG-C was 1:1 in moles), PEG-C, and PEG-A were used as the grafting polymer for the ASC-type and the MGC-type amphoteric charged membranes, and the acidic-type and the basic-type single charged membranes, respectively. The PE porous membranes were used as the substrate on which the PEG derivatives were graft polymerized. A schematic illustration of grafting the PEG derivatives onto the PE porous membranes by gamma-ray irradiation is shown in Figure 5-2. The circular PE membranes samples (area = 17.35 cm^2) were extracted in methanol for 12 h, dried, and weighed before use. After soaking in methanol and deionized water, these membranes were immersed in 16 wt% polymer aqueous solution on a glass plate. This glass plate was covered with another one and then the plates were sealed with cellophane tape. The plates were irradiated by 1.17 eV and 1.33 eV gamma-rays in a ^{60}Co general-purpose irradiation device (Model RE-1012, TOSHIBA, Japan) at dose rates of 2.47 kGy/hr and total doses of 50 kGy. The grafted membranes were washed and then rinsed for 12 h with deionized water to sufficiently remove the nongrafted polymers. Thereafter these membranes were dried at 60℃ under vacuum for 12 h. The degree of graft copolymerization (DG) was calculated using the following equation:

$$DG = \frac{W_2 - W_1}{W_1} \tag{5.1}$$

where W_1 is the weight of the dried membrane before graft copolymerization and W_2 is that of the dried membrane after graft copolymerization.

5.2.3 Measurements

5.2.3.1 X-ray fluorescence analysis (XRF)

Elementary analysis by XRF of freeze-dried membranes was carried out using a Philips PW2404 apparatus.

5.2.3.2 Hydraulic permeability measurements

The hydraulic permeability of the membranes was calculated from the flow rate of deionized water, which was eluted for 20 min under an applied constant hydrostatic pressure difference of 75.0 cmH_2O across the membrane. The area of the membrane exposed to the flow was 4.9 cm^2. All measurements were done five times at 25 ± 0.1℃ and were reproducible to within ± 2 $mL/m^2 \cdot h \cdot cmH_2O$.

5.2.3.3 Streaming potential measurements

The experimental setup is the same as previously mentioned in chapter 2. By varying the applied pressure (ΔP) ranging from 15 to 120 cmH_2O, the streaming potential (ΔE), which had been generated by a flow of ions due to ΔP, was measured with a digital multimeter (HP3458A, Hewlett-Packard, USA) and recorded using a microcomputer. The zeta potential was obtained from the slope of a $\Delta E - \Delta P$ plot using the following Helmholtz－Smoluchowski equation:

$$\frac{\Delta E}{\Delta P} = \frac{\varepsilon \zeta}{\eta \lambda} \tag{5.2}$$

where η is the solution viscosity, ε and λ is the permittivity and electrical conductivity of the solution, respectively. The apparent surface charge density of the pores was calculated from the zeta potential using the Gouy－Chapman equation:

$$\sigma_S = \frac{2\varepsilon kT\kappa}{z_+ e}\sinh\left(\frac{z_+ e\zeta}{2kT}\right) \tag{5.3}$$

where k is the Boltzmann constant, T is the temperature, κ is the reciprocal of the electrical double layer thickness, z_+ is the valence of the counterion, and e is the Coulombic charge. The KCl concentration in the outer solution was 1, 10, or 100 mmol/L throughout the measurements. The pH of the outer solution was regulated from 2 to 12 by adding 0.1 mol/L HCl or 0.1 mol/L KOH. All measurements were carried out in a stirred solution thermostated at 25±0.1℃. The measurements were carried out five times for each experimental point, and the mean value (± standard deviation) of each experimental point is indicated.

5.2.3.4 Dynamic contact angle (DCA) measurements

The dynamic contact angle measurements were carried out on the freeze-dried membranes using an automatic dynamic contact angle meter (DCA-VZ, Kyowa Interface Science, Japan) employing the sessile drop technique with distilled water at pH 5.6. This instrument is equipped with automatic image acquisition and computation software for the time dependence of the contact angle. Dynamic contact angles were measured by reading automatically the angle between the tangent at the contact point and the horizontal line of the solid at 33-ms interval and recording the data using a microcomputer from 100 to 1600 ms after a drop. All measurements were carried out at least three times at 25±1℃ and were reproducible within 3 degree.

5.3 Results and Discussion

5.3.1 Preparation of grafted membranes

The degree of graft polymerization (DG), hydraulic permeability, and contact angle of the prepared membranes are listed in Table 6-1. Here, the PE membrane is so hydrophobic that the hydraulic permeability measurements could be carried out after immersion in MeOH. The ASC-type, MGC-type, and basic-type membranes had similar DG values of about 5 %, while the acidic-type membrane had a 2.7 % DG. The difference in DG between the acidic-type and the other types of membranes would be caused by the difference in the grafting efficiency during graft copolymerization. All of the grafted

membranes have a smaller hydraulic permeability than an unmodified PE membrane. Ionic PEG chain grafting also facilitated the wettability and reduced contact angles. These results indicated that the pore surfaces of the PE membranes were covered with the ionic PEG chains by graft copolymerization. We also conducted elementary analysis of unmodified and grafted membranes by XRF. The results verified the presence of a sulfur atom from ionic PEG derivatives on the grafted membranes.

5.3.2 Zeta potential measurements of unmodified and grafted PE membranes

The slope of the $\Delta E - \Delta P$ plot displayed good linearity for each membrane under various pH and concentration conditions. The zeta potential was calculated using eq (5.2). In dealing with a porous membrane, we need to consider the effects of pore diameter and surface roughness on the zeta potential [1,3]. The pore size of the unmodified PE membrane, an average 50 nm pore diameter, appears to be large enough to permit ignoring the electrical conductance effect in the diffuse part of the double layer (the Debye screening length is 10 nm long in 1 mmol/L KCl solution) [3]. Therefore, we did not take into account the surface conductance and double-layer overlapping effects in both the unmodified and grafted PE membranes. However, because it is impossible to determine the real state of the pore surface (i.e., whether it is ideally smooth), the zeta potential obtained in this study must be regarded as an apparent value.

Figure 5-3 shows the pH dependence of the zeta potential in 10 mmol/L KCl for unmodified PE membrane and prepared amphoteric charged membranes. In Figure 5-3a, the zeta potential of the unmodified PE membrane had a near zero value at low pH < 4 but decreased with pH increase and had a constant negative value (about –15 mV) at pH > 6. This negative value indicated that the PE membrane used in this study had some charge groups on the pore surface initially. The zeta potential of the unmodified PE membrane did not change before and after irradiation. Therefore, there was no possibility that charge groups generated on the pore surface during gamma-ray irradiation. Here, the unmodified and irradiated PE membranes are so hydrophobic that zeta potential measurements were carried out after immersion in MeOH and sufficient washing with deionized water. As can be seen from Figure 5-3b, the zeta potential for the ASC-type (PEG-Cys grafted) amphoteric charged membrane, changed from a positive to a negative value, across the *plateau*, which showed a constant potential in the range of pH 6－11. This behavior is characteristic of the ASC-type amphoteric charged membranes, and the constant

potential in the intermediate pH region would be the evidence of the dipolar ion structure in the cysteine residues [1]. In Figure 5-3c, the basic-type (PEG-A grafted) membrane showed a positive potential at low pH (< 7), which greatly decreased near pH 8, and finally showed negative potential at high pH. The acidic-type (PEG-C grafted) membrane gave a zero potential at very low pH, which greatly decreased near pH 4, and gave almost a constant value at pH > 5. The zeta potential for the MGC-type (mixed PEG-A/PEG-C grafted) amphoteric charged membrane showed an intermediate pH dependence behavior between the acidic-type and basic-type single charged membranes.

While the zeta potential of the *plateau* region in the ASC-type amphoteric charged membrane was expected to be zero, a negative zeta potential (about –15 mV) was obtained in this measurement. The basic-type membrane also had a negative zeta potential (about –15 mV) at high pH where the potential should be ideally zero. This negative value would be originated from the contribution of negative charge on the pore surface of PE membrane mentioned above. When the thickness of effective electrokinetic layer (approximately $3/\kappa$, where $1/\kappa$ is the Debye screening length) of charged substrate is grater than the thickness of grafted polymer chain on the substrate, it is known that the effect of charged substrate for electrokinetic phenomena is not negligible [4].

5.3.3 Theoretical analysis according to a site dissociation model

In order to explain the pH dependence of experimental results mentioned above, we simulated the apparent surface charge density/pore surface pH profiles using a site dissociation model as described in chapter 2. Apparent surface charge density/pH profiles at constant ionic strength are particularly useful, since they reflect the ionizable character of the pore surface. The experimental data of the zeta potential in 10 mmol/L KCl solution was used for the SDM analysis in this study, because the contribution of the pH regulator, HCl or KOH, was too large for the zeta potential measurements in 1 mmol/L KCl, and the contribution of the electrolyte ion adsorption was not negligible for the zeta potential in 100 mmol/L KCl [5]. When the effect of the specific adsorption of electrolyte ions is not considered, the equilibrium between charge groups and the solution at the interface is represented as:

$$AH \leftrightarrow A^- + H^+ \tag{5.4}$$

$$BH^+ \leftrightarrow B + H^+ \tag{5.5}$$

where AH and B are the acidic and basic groups, respectively. These equilibria have the following dissociation constants, K:

$$K_a = \frac{[A^-][H^+]_S}{[AH]} \tag{5.6}$$

$$K_b = \frac{[B][H^+]_S}{[BH^+]} \tag{5.7}$$

where the subscripts a and b stand for the acidic site and basic site, respectively. $[H^+]_S$ is the hydronium ion concentration at the pore surface, which is based on the hypothesis that the ion concentration in the electrolyte solution follows the Boltzmann distribution outside the plane where the zeta potential is generated, and is written in the form

$$[H^+]_S = [H^+]_0 \exp\left(\frac{-e\zeta}{kT}\right) \tag{5.8}$$

where $[H^+]_0$ is the hydronium ion concentration in the bulk solution. The total site density of the pore surface, N, is denoted by

$$N_a = [A^-] + [AH] \tag{5.9}$$

$$N_b = [BH^+] + [B] \tag{5.10}$$

Therefore, the apparent surface charge density, σ_S, can be expressed by combining eqs (5.6) and (5.7) with (5.9) and (5.10). For a multiple charged pore surface, σ_S is given by

$$\sigma_S = -e\sum_i [A^-]_i + e\sum_j [BH^+]_j$$

$$= \sum_i \left[\frac{-eN_a}{1+10^{(pK_a - pH_S)}} \right] + \sum_j \left[\frac{eN_b}{1+10^{(pH_S - pK_b)}} \right] \qquad (5.11)$$

where pK_a and pK_b are the equilibrium acidic dissociation constants of the acidic and basic sites, respectively, and pH_S is the surface pH.

The experimental value of the apparent surface charge density obtained by eq (5.11) is plotted as a function of surface pH in Figure 5-4. The solid line in Figure 5-4 represents the calculated value according to a nonlinear regression method based on a SDM. The *pK* values, pK_a and pK_b, which are in ref 6, and the fitting parameters, N_a and N_b, which were determined by implementing the nonlinear parameter estimation program UNCMIN [7], are summarized in Table 5-2. In this calculation, we added the effect of charge groups originated from a PE membrane to a SDM in order to consider the effect of the unexpected negative charge groups as mentioned above. The *pK* value of this negative charge group is 4.8, which was obtained from the fitting parameter on calculating with the SDM based on the assumption that there is one type of acidic group on the pore surface of a PE membrane. The fitting curve using this constant agreed well with the experimental data (Figure 5-4a).

The experimental results of the ASC-type amphoteric charged membrane could be explained by a SDM using the *pK* value of cysteine in ref 6, $pK_a = 1.9$ and $pK_b = 10.8$, which involved the effect of the dipolar ion structure (Figure 5-4b). Therefore, it is postulated that the *plateau* region over pH 6－11 in the zeta potential/pH profile would originate in the dipolar ion structure of the cysteine residues on the side chain of the grafted polymer chains. The *plateau* region disappears with an increase in the electrolyte concentration of the external solution (Figure 5-5). This would indicate that the ion pair between the amino group and carboxyl group via a proton was broken by the electrolyte ions in solution.

The experimental results of the pH dependence of the apparent surface charge density for the basic-type and the acidic-type membranes could be explained by the SDM using the *pK* values, which were $pK_b = 8.2$ (for aminoethanethiol) and $pK_a = 4.2$ (for mercaptopropionic acid) (Figure 5-4c). For the MGC-type amphoteric charged membrane, however, the distinct difference between the experimental result and the calculated one appears at pH > 5 (Figure 5-4c). For the experimental data, the rapid decrease in the apparent surface charge density was observed near pH 5. This behavior was observed

merely in the low-concentration electrolyte solution (1 mmol/L and 10 mmol/L KCl, see Figures 5-3c and 6a). In 100 mmol/L KCl solution, the zeta potential of the MGC-type membrane did not show this rapid decrease but showed a two-step decrease near pH 4 and pH 8 with the increase in pH (Figure 5-6b). The rapid decrease near pH 5 would be caused by the change in the surface states with pH, that is, the conformational change in the grafted polyelectrolyte chains by the electrostatic interaction between charge groups on the grafted chain and surface charge on original PE surface. A schematic representation of the charge state and polymer chain conformation on the pore surface of the MGC-type membrane is illustrated in Figure 5-7. The negatively charged chain is more extended by the electrostatic repulsion at pH > 5 and conversely, the positively charged chain is less extended by the attractive electrostatic interaction in the range of pH 4.8－8.2. Since the zeta potential is generated at the hydrodynamic slipping plane (see chapter 2), it is more sensitive for the polyelectrolyte chain highly extended into the solution [4]. In conclusion, our analysis demonstrated that the effect of conformation of grafted chain on interfacial charge structure was substantial for the MGC-type membrane. Therefore, it is impossible to explain the interfacial charge of the MGC-type membrane using the classical SDM only based on the dissociation of ionizable groups. We need to extend the SDM to the polyelectrolyte chain grafted surface where the effect of the conformation change with the change in the charge property is not negligible in the further step.

5.4 Conclusions

Two kinds of amphoteric charged membranes, which are the ASC and MGC type, were prepared by the radiation-induced graft copolymerization of amphoteric PEG derivatives and the mixture of cationic and anionic PEG derivatives onto PE porous membranes, respectively. For the ASC-type membrane, the zeta potential/pH profile showed a *plateau* in the range of pH 6－11. This behavior would originate in the dipolar ion structure of the cysteine residues on the grafted chain. This was also supported by the theoretical prediction by a SDM using the cysteine's *pK* value in the literature [6]. This *plateau* region disappears with the increase in the electrolyte concentration of the external solution. The MGC-type membrane, on the other hand, showed an intermediate pH dependence of the zeta potential between the basic-type and acidic-type membranes. The apparent surface charge density on the

membranes obtained from the zeta potential was analyzed by a SDM based on the dissociation of charge groups on the pore surface. The experimental results of the pH dependence of the apparent surface charge density for the basic-type and acidic-type, and the ASC-type membranes could be explained by a SDM using the *pK* values of the charge groups in the literature [6]. For the MGC-type membrane, however, the difference between the experimental result and calculated one appeared at pH > 5. This would be caused by the change in the surface states with pH, that is, the conformational change of the grafted polyelectrolyte chains with the change in the charge state.

5.5 References

1. Matsumoto, H.; Koyama, Y.; Tanioka, A. *J. Colloid Interface Sci.* **2001**, *239*, 467.
2. Stryer, L. *Biochemistry* 3rd. ed.; W. H. Freeman and Company: New York, 1988.
3. Jimbo, T.; Tanioka A.; Minoura, N. *Colloids Surfaces A* **1999**, *159*, 459.
4. Österberg, E.; Bergström, K.; Holmberg, K.; Schuman, T. P.; Riggs, J. A.; Burns, N. L.; Emoto, K.; Van Alstine, J. M.; Harris, J. M. *J. Biomed. Mater. Res.* **1995**, *29*, 741.
5. Jacobasch, H.-J.; Schurz, J. *Progress in Colloid & Polymer Sci.* **1988**, *77*, 40.
6. Martell, A. E.; Smith, R. M. *Critical Stability Constants*; Plenum Press: New York, 1974; Vol. 1; 1975; Vol. 2; 1977; Vol. 3. For the assignment of cysteine's pK, see also: Greenstein, J. P.; Winitz, M. *Chemistry of the Amino Acids*; John Willey & Sons: New York, 1961; Vol.1, p.494. Calvin, M. In *Glutathione*; Colowick, S. P. Ed., Academic Press: New York, 1954; p.8.
7. Kahaner, D.; Moler, C.; Nash, S. *Numerical Methods and Software*; Prentice Hall: Englewood Cliffs, NJ, 1989.

Table 5-1. Physicochemical properties of unmodified and grafted PE membranes

Membrane	DG [a]	Hydraulic permeability [b] ($mL/m^2 \cdot h \cdot cmH_2O$)	Contact angle [c] (degree)
ASC type	4.5	36	86
MGC type	4.5	47	85
Acidic type	2.7	52	85
Basic type	5.7	34	79
Unmodified PE	-	72 [d]	102

[a] DG: Degree of graft polymerization; DG = $(W_2 - W_1)/W_1$, where W_1 = the weight of dried membrane before graft copolymerization and W_2 = the weight of dried membrane after graft copolymerization.

[b] Measured in deionized water at pH 5.6. All hydraulic permeability values were reproducible within ± 2 $mL/m^2 \cdot h \cdot cmH_2O$

[c] Dynamic sessile drop method, Measured with distilled water at pH 5.6. All contact angle values were reproducible within ± 3 degree.

[d] Measured after immersion in MeOH.

Table 5-2. Characteristic parameters for the unmodified and grafted PE membranes derived from the Site Dissociation Model

Membrane	Grafted polymer chain				Unmodified PE	
	pK_a	pK_b	$10^3 N_a$ (nm^{-2})	$10^3 N_b$ (nm^{-2})	pK_a	$10^3 N_a$ (nm^{-2})
ASC type	1.9 *	10.8 *	41.4	41.4	4.8	16.5
MGC type	4.2 *	8.2 *	16.5	36.8	4.8	17.6
Acidic type	4.2 *	-	12.5	-	4.8	19.2
Basic type	-	8.2 *	-	31.5	4.8	18.3
Unmodified PE	-	-	-	-	4.8	25.0

* In ref 6.

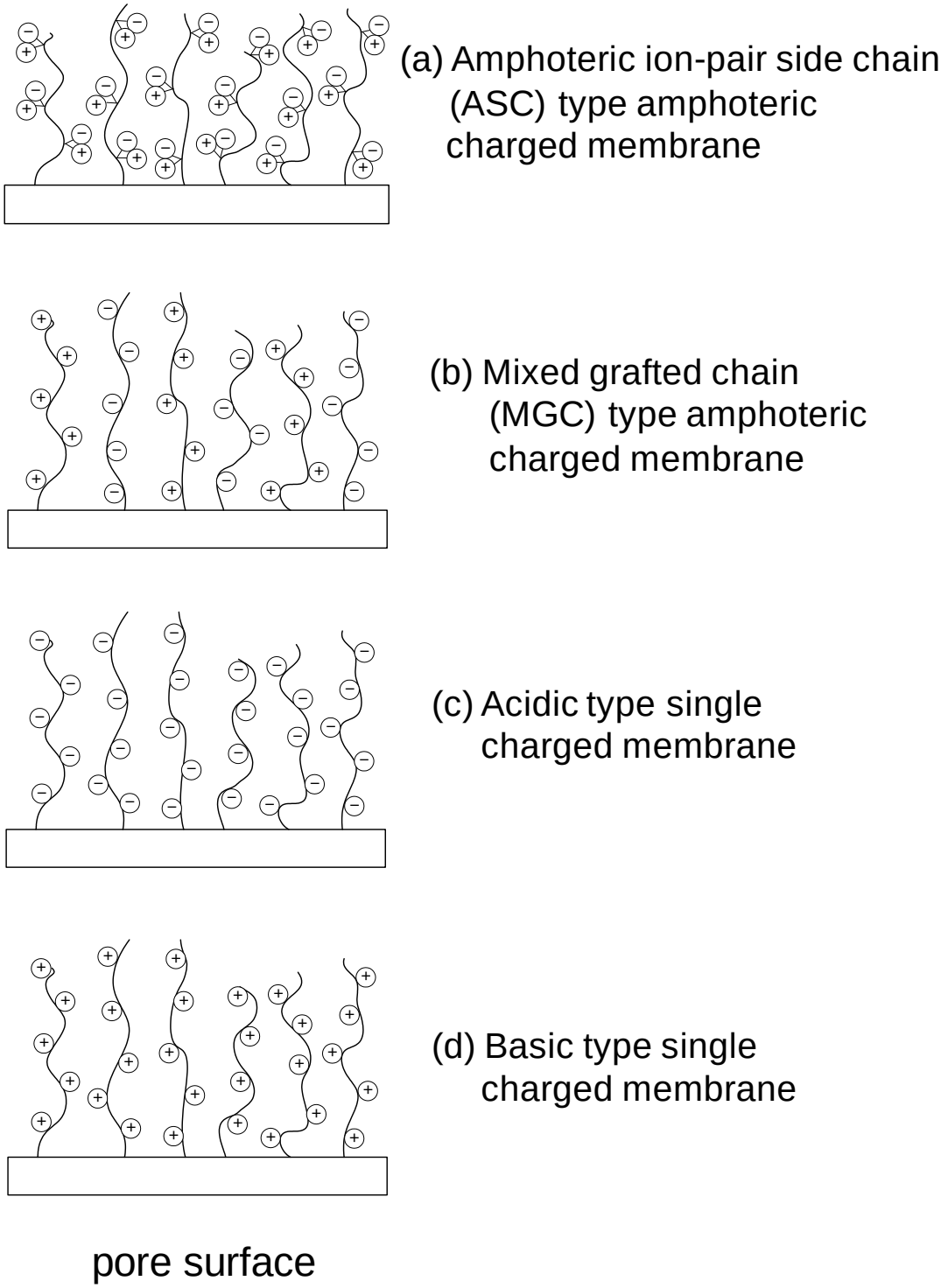

Figure 5-1. Schematic representation of the ideal morphological model for the grafted polymer chains on the pore surface of (a) ASC-type and (b) MGC-type amphoteric charged membranes, and (c) acidic-type and (d) basic-type single charged membranes, in ionized state.

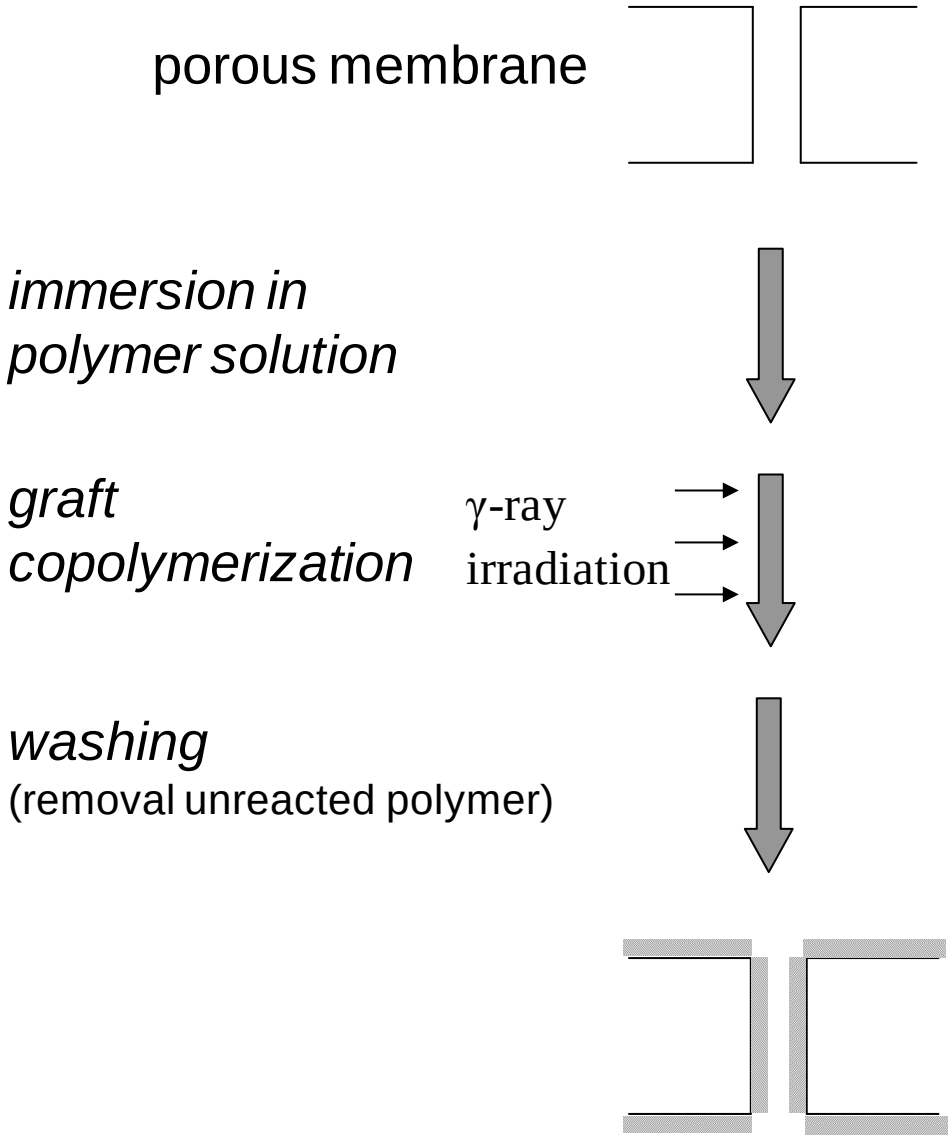

Figure 5-2. Graft copolymerization of ionic PEG derivatives on the pore surface of porous membranes by gamma-ray irradiation.

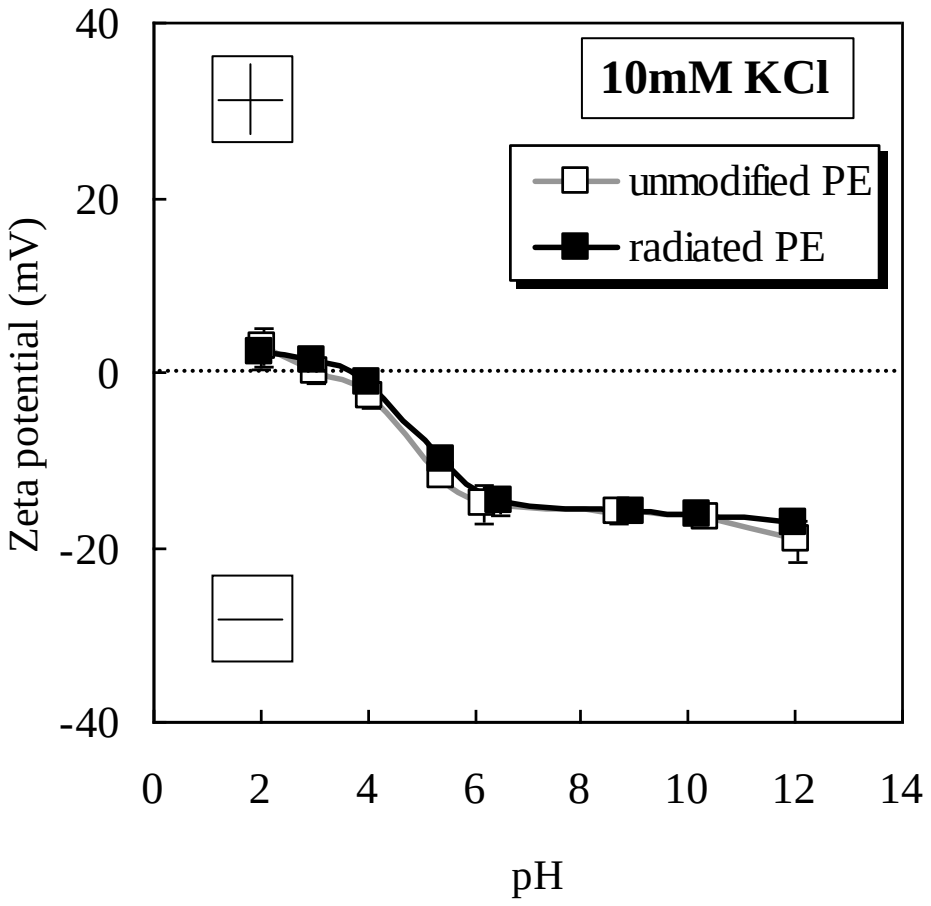

Figure 5-3a. The pH dependence of the zeta potential for unmodified and irradiated PE membranes.

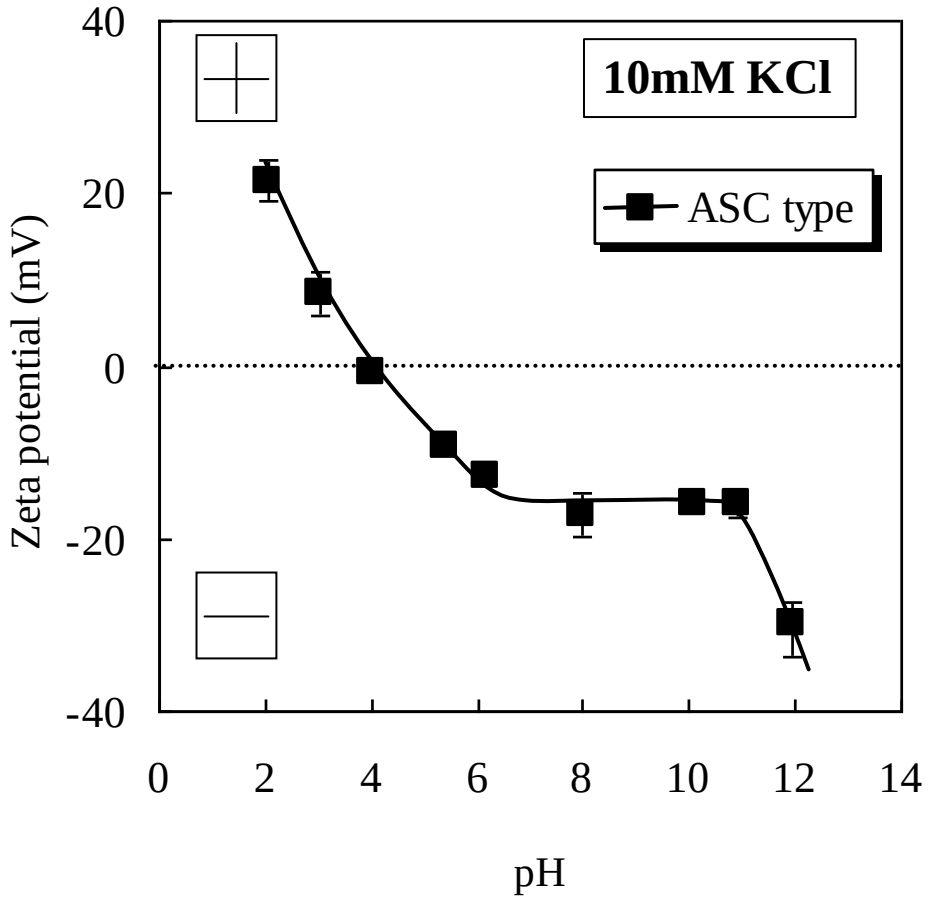

Figure 5-3b. The pH dependence of the zeta potential for the ASC-type (PEG-Cys grafted) amphoteric charged membrane.

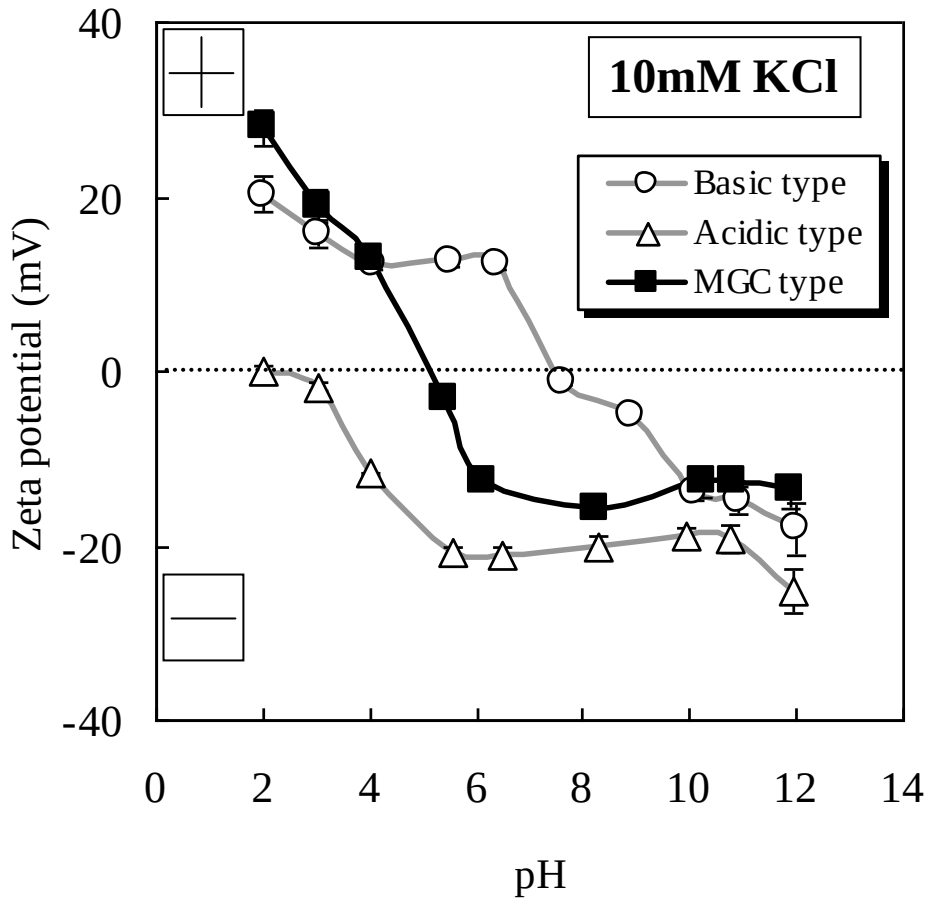

Figure 5-3c. The pH dependence of the zeta potential for the MGC-type (PEG-A/PEG-C grafted) amphoteric charged membrane.

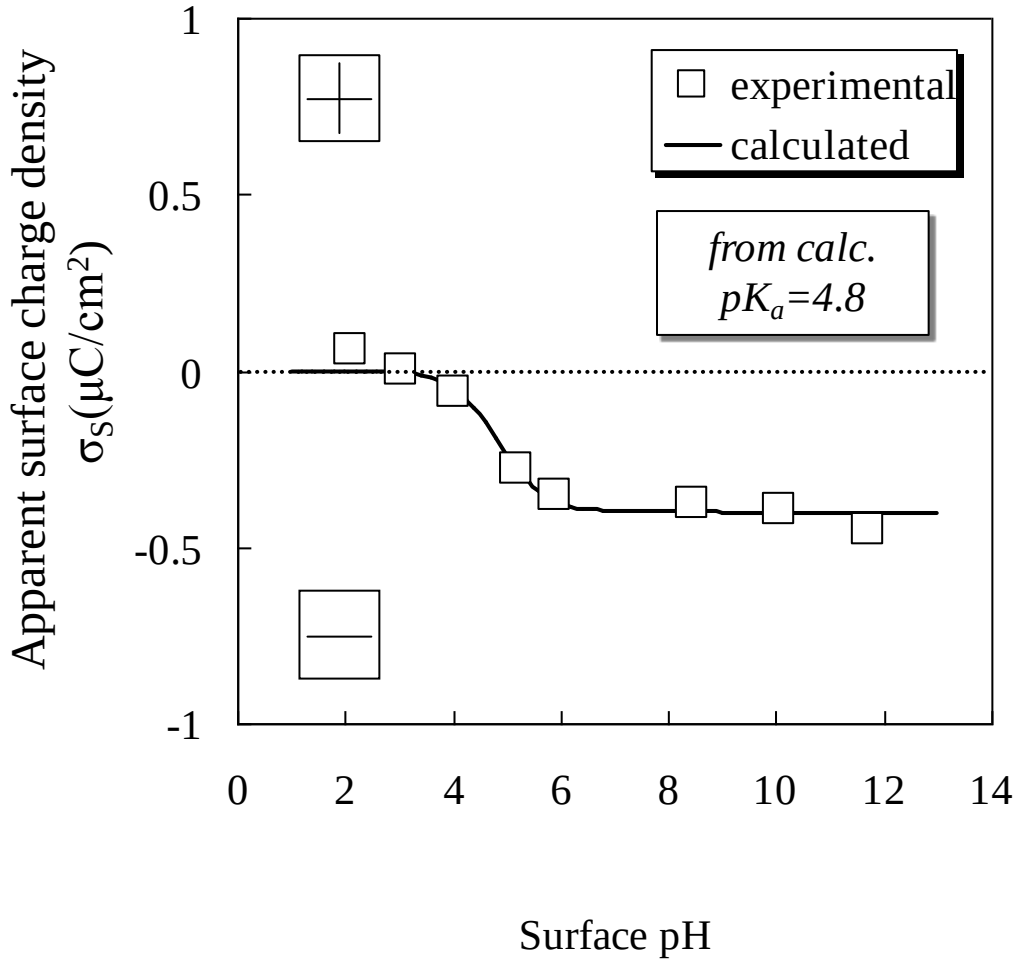

Figure 5-4a. The pH dependence of the apparent surface charge density for unmodified PE membrane (substrate). The solid line corresponds to the theoretical fits using the SDM.The characteristic parameters are listed in Table 5-2.

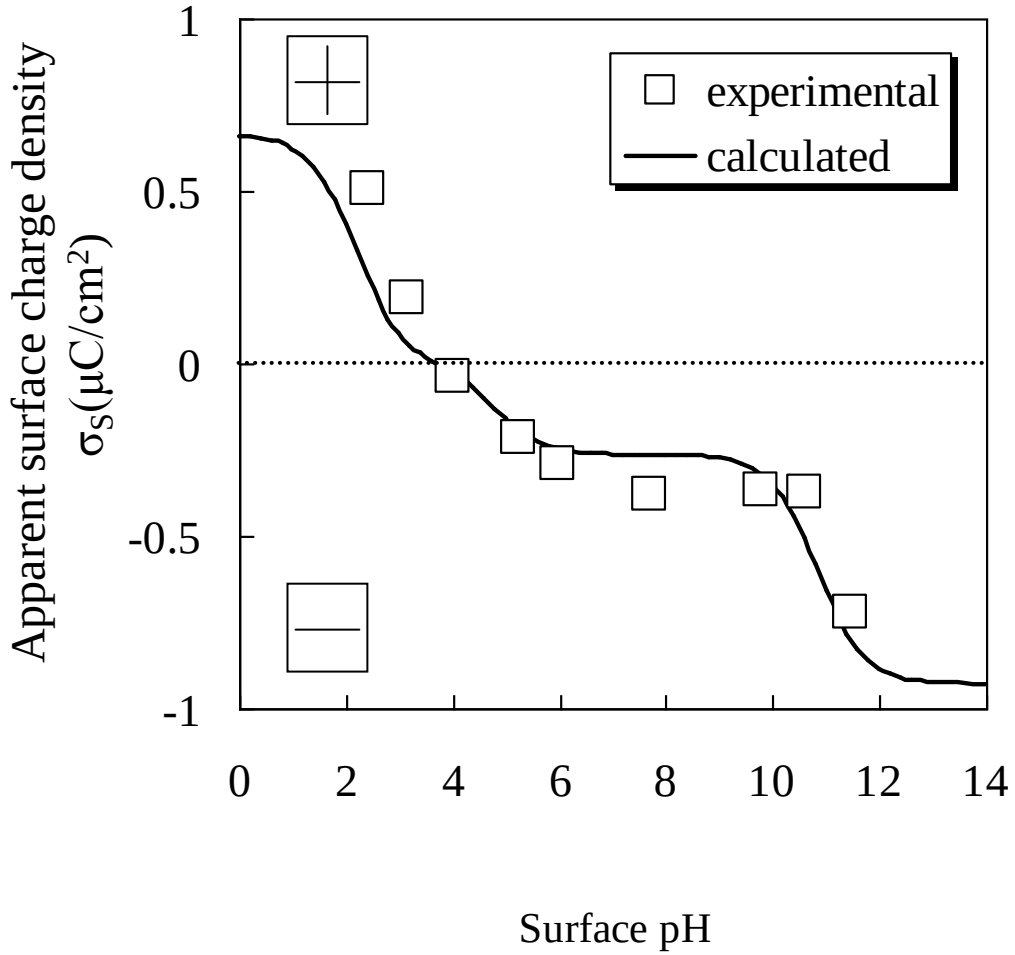

Figure 5-4b. The pH dependence of the apparent surface charge density for the ASC-type (PEG-Cys grafted) amphoteric charged membrane. The solid line corresponds to the theoretical fits using the SDM. The characteristic parameters are listed in Table 5-2.

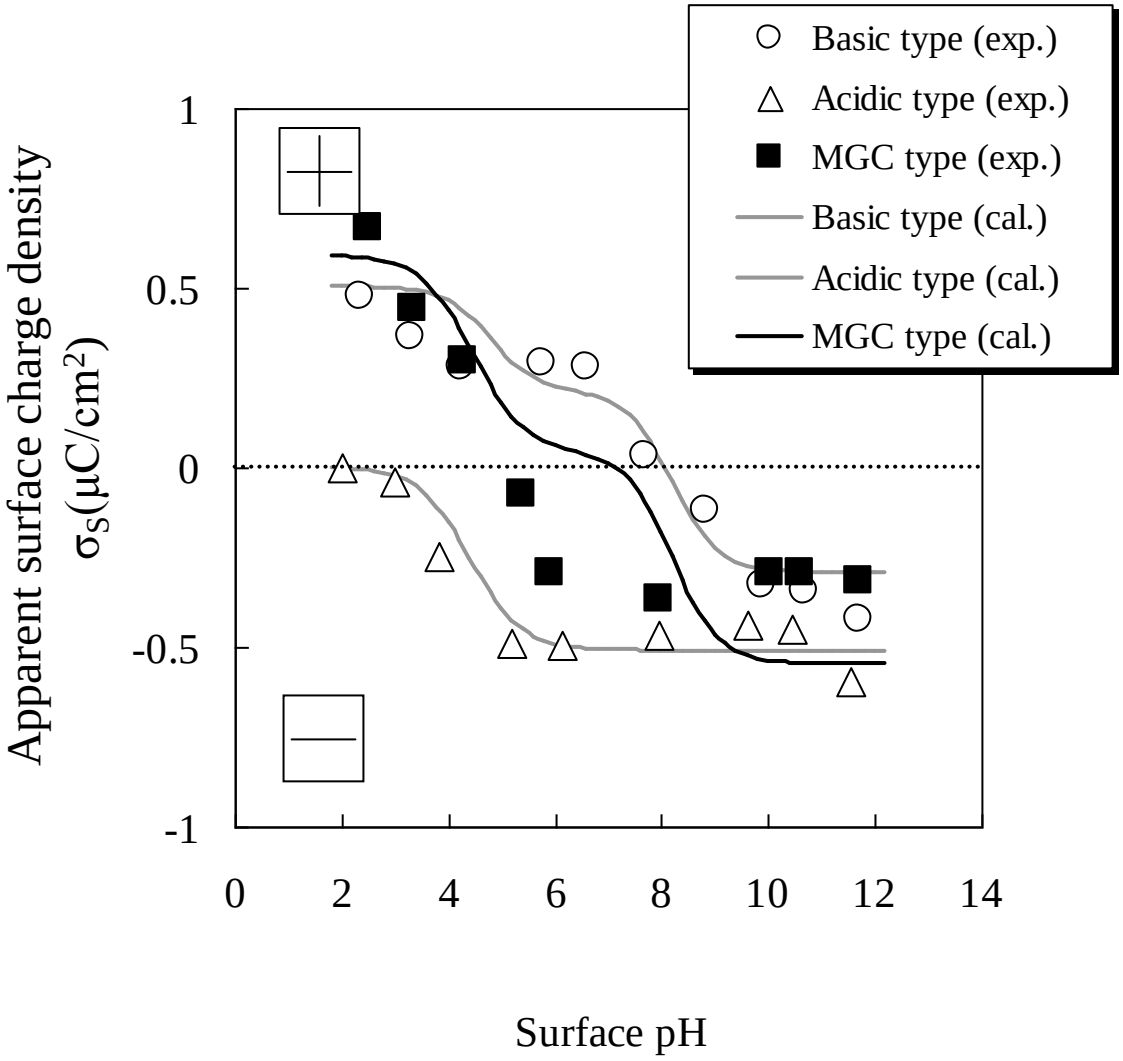

Figure 5-4c. The pH dependence of the apparent surface charge density for the MGC-type (PEG-A/PEG-C grafted) amphoteric charged membrane. The solid line corresponds to the theoretical fits using the SDM. The characteristic parameters are listed in Table 5-2.

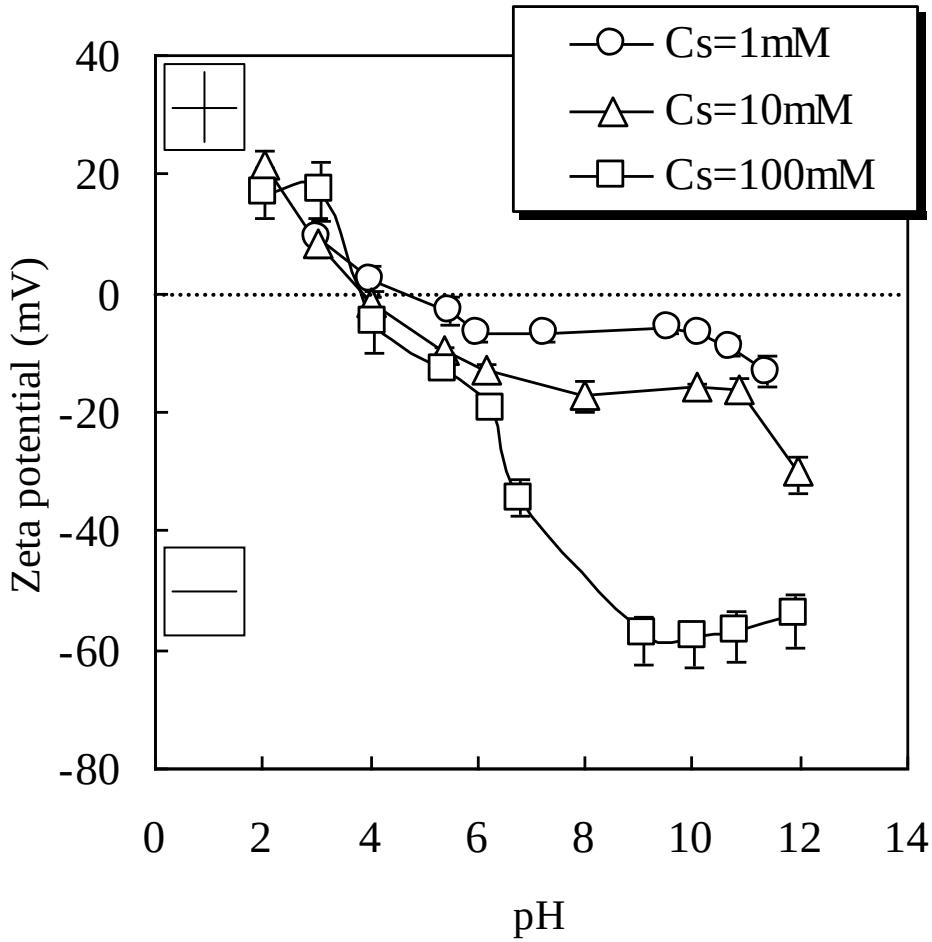

Figure 5-5. Effect of the concentration of the external solution on the pH dependence of the zeta potential for the ASC-type (PEG-Cys grafted) amphoteric charged membrane.

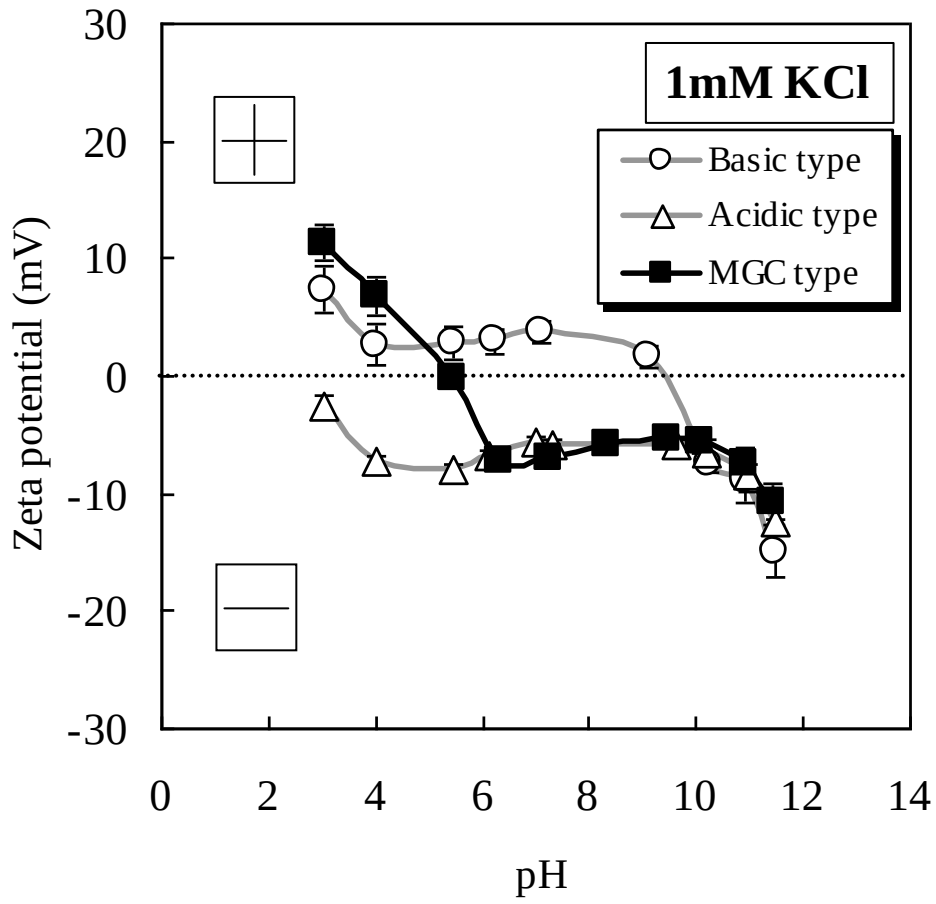

Figure 5-6a. Effect of the concentration of the external solution on the pH dependence of the zeta potential for the MGC-type (PEG-A/PEG-C grafted) amphoteric charged membrane, measured in 1mM KCl solution.

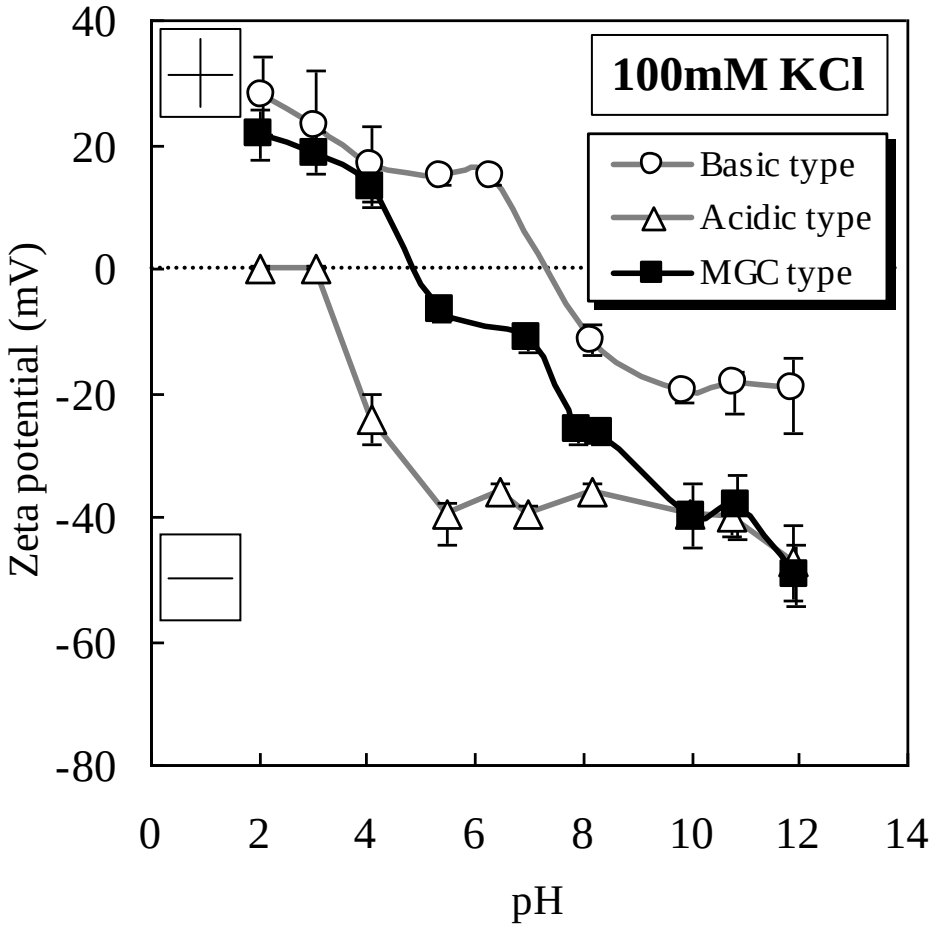

Figure 5-6b. Effect of the concentration of the external solution on the pH dependence of the zeta potential for the MGC-type (PEG-A/PEG-C grafted) amphoteric charged membrane, measured in 100mM KCl solution.

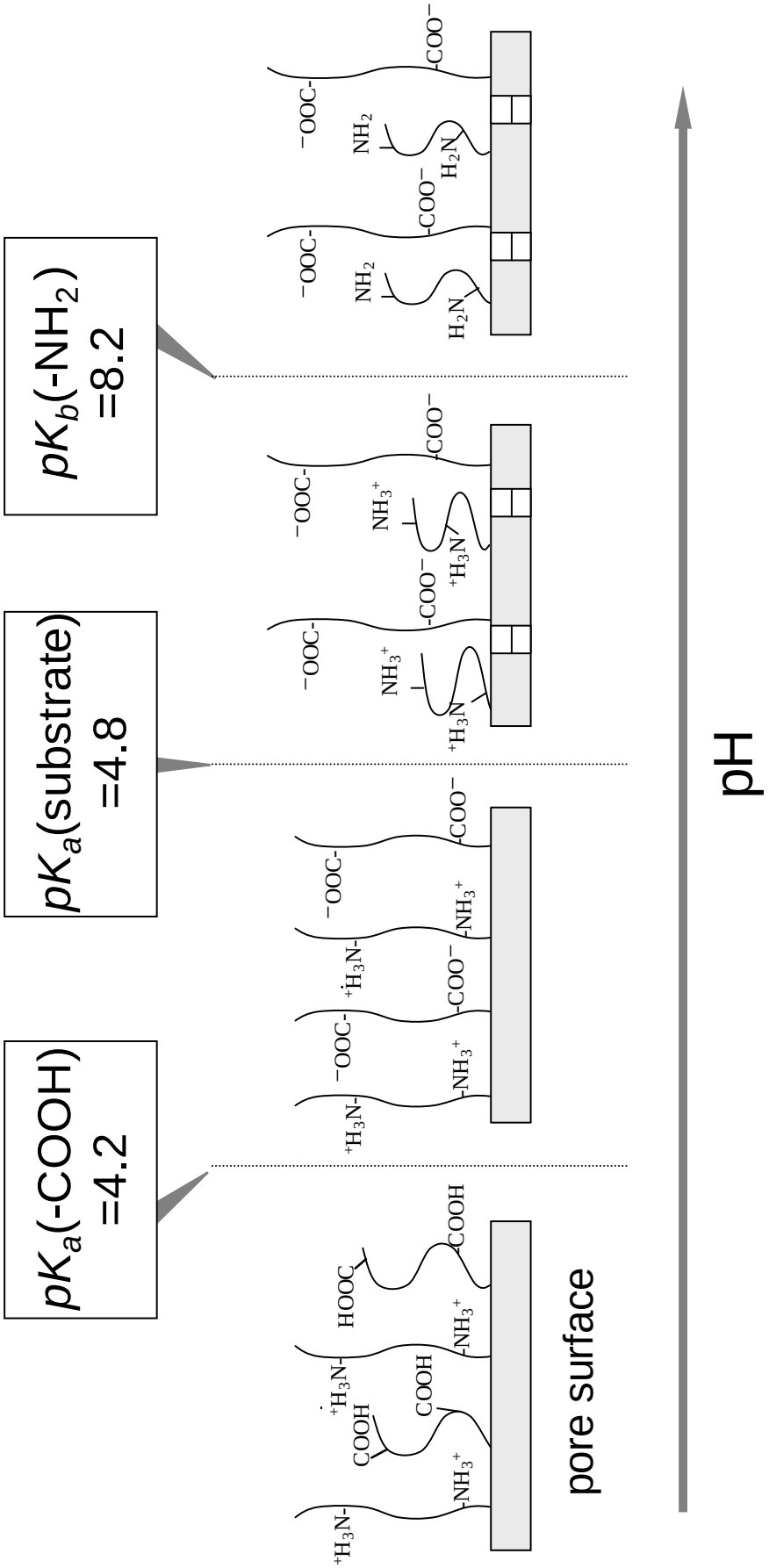

Figure 5-7. Charge state and possible coil conformation on the pore surface of the MGC-type (PEG-A/PEG-C grafted) amphoteric charged membranes as a function of pH.

Chapter 6

Interaction of Organic Molecules with Weak Amphoteric Charged Membranes

6.1 Introduction

The interfacial charge structure of weak amphoteric charged membranes, which contain both weak acidic groups and weak basic groups, is so complex that their interfacial properties have not been elucidated in detail. Particularly, there have been few physicochemical studies on the correlation between interfacial properties of weak amphoteric charged membranes and their interactions with organic molecules. In chapter 5, we have prepared two types of ionic PEG chain grafted weak amphoteric charged membranes. Their grafted polymer chains on the pore surface are expected to exclude hydrophobic interaction and to have a function based on electrostatic interaction. In order to identify characteristics of interactions between organic molecules and the ionic PEG chain grafted membrane surfaces (electrostatic interaction, hydrophobic interaction, or hydrogen bonding), we carefully selected four kinds of model organic molecules: pyrene (highly hydrophobic), 1-pyrenesulfonic acid (having an anionic group), 1-pyrenemethylamine (having a cationic group), and 1-aminopyrene (having a polar group). We chose pyrene and its derivatives for two reasons. First, the pyrene ring is highly hydrophobic. Second, their strong fluorescence allows accurate determination of the degree of adsorption at the membrane/solution interface, even at very low concentrations [2]. The time dependence of the adsorbed amount of these organic molecules onto the membranes was investigated with fluorescence spectroscopy. We present here the first findings of the interactions between the organic molecules and amphoteric charged membrane surfaces under the condition without electrolytes. The aims of this chapter are (1) to identify the characteristics of interactions between organic molecules and the ionic PEG chain grafted membranes, and (2) to examine the correlation between the interfacial charge properties of ionic PEG chain grafted

membranes and their interactions with charged molecules.

6.2 Experimental

6.2.1 Materials

Pyrene (extra-pure grade) and 1-pyrenesulfonic acid, sodium salt were purchased from Wako Pure Chemical, Japan and Molecular Probes, USA, respectively. 1-Aminopyrene (97% purity) and 1-pyrenemethylamine hydrochloride (95% purity) were purchased from Aldrich Chemical, USA. All reagents were used without further purification. The chemical structures are shown in Figure 6-1.

Two types of amphoteric charged membranes, the amphoteric ion-pair side chain (ASC) type and the mixed grafted chain (MGC) type, and two types of single charged membranes, the acidic type and the basic type (see chapter 5 [1]), were used. The interfacial properties of the unmodified and grafted PE membranes are listed in Table 6-1.

6.2.2 Adsorption experiments

Before the adsorption experiments, we developed calibration curves for the model adsorbents. The fluorescence agent (equivalent weight of 200 mL of 2.5 μmol/L solution) was first dissolved in 1 mL of acetone (for pyrene) or methanol (for other pyrene derivatives). The solution was spread on the wall of a pear-shaped flask, and then the solvent was evaporated for removal under reduced pressure. After 200 mL of deionized water was added to the flask, the solution was ultrasonicated for 15 min and heated in a thermostated bath at 60 ℃ for 30 min to give 2.5 μmol/L aqueous solution. We measured the fluorescence of these adsorbent solutions and confirmed the absence of excimer emission peak of pyrene derivatives near 470 nm [3]. The calibration curve was made at five measurement points from 2.5×10^{-8} to 2.5×10^{-7} mol/L: for pyrene, with 336 nm fluorescence excitation and 377 nm emission wavelength; for 1-pyrenesulfonic acid, with 347 nm fluorescence excitation and 379 nm emission wavelength; for 1-pyrenemethylamine, with 343 nm fluorescence excitation and 377 nm emission wavelength; and for 1-aminopyrene, with 355 nm fluorescence excitation and 442 nm emission wavelength. Fluorescence

spectra were measured with a spectrofluorometer (FP-750, JASCO, Japan), using a 1-cm^2 quartz cell (F10-UV-10, GL-Science, Japan). The emission and excitation slit widths were equaled to 5 and 5 nm, respectively.

The schematic diagram of the adsorption experiments is shown in Figure 6-2. A freeze-dried test membrane (1 × 1 cm^2) was immersed into 3 mL of 2.5×10^{-7} mol/L model adsorbent solution in the quartz cell. At the same time, fluorescence measurements were started and continued for 10－25 h. The concentration of the pyrene and its derivatives in solution was determined by the calibration curves. The adsorbed organic molecules on the membrane were estimated from the decreased amount of organic molecules in solution. The adsorbed amount on the quartz cell was also deduced as a blank. Pyrene and its derivative solutions were protected from light except for the fluorescence measurements, because their solutions are photolytic. All experiments were carried out in the pH 5.6 solution at 25 ± 1℃. The experiments were carried out three times for each membrane, and the mean value ($\pm$ standard deviation) of each membrane is indicated.

6.3 Results and Discussion

6.3.1 Fluorescence spectra and calibration curves of organic molecules

Fluorescence spectra and calibration curves of four kinds of organic molecules are shown in Figure 6-3. All calibration curves had good linearity (correlation factor R^2 nearly equals 0.999). The concentration of the organic molecules in the solutions can be determined from the maximum fluorescence intensity at 377 nm for pyrene, 379 nm for 1-pyrenesulfonic acid, 377 nm for 1-pyrenemethylamine, and 442 nm for 1-aminopyrene on the basis of each calibration curve.

6.3.2 Adsorption behavior of organic molecules

Figure 6-4 shows the adsorbed amount of organic molecules on unmodified and grafted PE membranes as a function of time. In this section, we try to estimate the characteristics of the interfacial interaction based on the properties from the pyrene ring and the functional group of the pyrene

derivatives.

(a) Pyrene: Pyrene has high hydrophobicity. Adsorption amounts of pyrene on the membranes were remarkably reduced by ionic PEG chain grafting in short time periods (< 3h, see Figure. 6-4a). For an unmodified PE membrane, the adsorption of pyrene will originate from hydrophobic interaction, because PE is also highly hydrophobic. The adsorption kinetics for ionic PEG chain grafted membranes suggested the following mechanism: because most of the pyrene molecules are excluded by the hydrophilic PEG chains on the pore surface [4], the diffusion of pyrene in the grafted PEG chain layer to the original PE membrane surface would be the rate-determining process for adsorption. These results indicated that ionic PEG chains were highly effective in reducing the adsorption of hydrophobic organic molecules, that is, in excluding the hydrophobic interaction as we expected.

(b) 1-Pyrenesulfonic acid and 1-Pyrenemethylamine: 1-Pyrenesulfonic acid, a strong acid, has a negative charge group. This organic molecule adsorbed only on the basic-type membrane, which has opposite (positive) charge groups (Table 6-1 and Figure 6-4b). On the other hand, 1-pyrenemethylamine is a cationic organic molecule at pH 5.6, because the pK_a of 1-pyrenemethylamine is 9.2 is from the fluorescence titration measurements. This organic molecule adsorbed on all the ionic PEG chain grafted membranes except the basic-type one having equal (positive) charge groups (Table 6-1 and Figure 6-4c). These results demonstrated that the contribution of attractive and repulsive electrostatic interaction was dominant for the adsorption of ionic organic molecules on ionic PEG chain grafted membranes. These adsorption experiments also revealed that the interfacial charge properties of ionic PEG chain grafted membranes played an important role in their interaction with ionic organic molecules: the sign of the interfacial charge from the zeta potential measurements correlated with the adsorption behavior of the ionic organic molecules. Here, we should note that the adsorption behavior on unmodified PE membrane was unique: the adsorption was not observed for the PE membrane having opposite (negative) charge property. We could not explain this result based on electrostatic interaction. This would originate from the contribution of the hydrophobic character of the PE membrane, because the adsorption of

1-pyrenemethylamine on the PE membrane was observed after immersion in MeOH.

(c) 1-Aminopyrene: 1-Aminopyrene is a nonionic organic molecule at pH5.6; because the pK_a of 1-aminopyrene is 3.4 [5]. Therefore, it behaves as an organic molecule with a polar group. As shown in Figure 6-4d, all ionic PEG chain grafted membranes showed uniform adsorption behavior, and their adsorbed amount at equilibrium was larger than that on the PE membrane. The aminopyrene adsorption behavior on ionic PEG chain grafted membranes showed no time lag in a short time period as shown for pyrene (Figure 6-4a), and therefore many aminopyrene molecules would interact with the grafted chains. 1-Aminopyrene is an amphiphilic molecule, which has both a hydrophobic pyrene ring and a polar group. This molecule could interact with the original PE membrane surface by the hydrophobic interaction between pyrene ring and PE, and with the grafted chain by the interaction between amino group and ionic PEG chain. The latter interaction would originate from the hydrogen bonding between the oxygen atom of the polyether backbone and the hydrogen atom of the amino group [6] as follows:

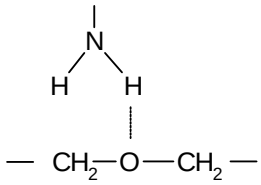

Here, chelating effect was thought as another interaction: each ionic PEG chain has 8.28 sulfur atoms from mercaptan per one polymer molecule (see chapter 3) and it may function as a chelate [7]. In order to identify clearly that the interaction between 1-aminopyrene and the ionic PEG chain is due to hydrogen bonding, adsorption experiments were carried out using pure poly(ethylene oxide) (PEO) gel without pendant ionizable groups and sulfur atoms. The PEO gel was prepared by irradiating 8 wt % PEO (M_w 5.0×10^5) aqueous solution with gamma-rays (total dose 100 kGy). Adsorption experiments were carried out in 3 mL of 2.5×10^{-7} mol/L adsorbent solution in the quartz cell mentioned above using rodlike PEO gel samples. Figure 6-5 shows the adsorbed amount of pyrene and 1-aminopyrene on PEO gel as a function of time. For pyrene, the adsorption was not observed. For 1-aminopyrene, on the other

hand, the adsorption was observed. These results supported that the amino group could interact with the polyether backbone. Consequently, the contribution of hydrogen bonding is substantial for the adsorption of organic molecules with polar groups on ionic PEG grafted membranes.

6.4 Conclusions

In this chapter, adsorption experiments were carried out using four kinds of model organic molecules, i.e. pyrene (highly hydrophobic) and its derivatives (having an anionic group, a cationic group, and a polar group). Our adsorption experiments have demonstrated the interaction characteristics of organic molecules with unmodified and ionic PEG chain grafted PE membranes. (1) It was suggested that the ionic PEG chain was effective in reducing the adsorption of hydrophobic organic molecules. (2) The interfacial charge properties of ionic PEG chain grafted membranes played an important role in their interaction with ionic organic molecules: the contribution of electrostatic interaction was dominant for the adsorption of ionic organic molecules on ionic PEG chain grafted membranes. (3) The contribution of hydrogen bonding was substantial for the adsorption of polar organic molecules on ionic PEG chain grafted membranes. These results provide fundamental information for the design by surface modification using ionic PEG derivatives to control multiple interactions between organic molecules and membrane surfaces.

6.5 References

1. Matsumoto, H.; Koyama, Y.; Tanioka, A. *Langmuir* **2001**, *17*, 3375.
2. Oya, T.; Enoki, T.; Grosberg, A. Y.; Masamune, S.; Sakiyama, T.; Takeoka, Y.; Tanaka, K.; Wang, G.; Yilmaz, Y.; Feld, M. S.; Dasari, R.; Tanaka, T. *Science* **1999**, *286*, 1543.
3. Galla, H.-J.; Sackmann, E. *Biochim. Biophys. Acta* **1974**, *339*, 103.
4. Llanos, G., R.; Sefton, M. V. *J. Biomater. Sci. Polymer Edn.* **1993**, *4*, 381.
5. Krasnansky, R.; Thomas, J. K. *Langmuir* **1994**, *10*, 4551.
6. Azegami, S.; Tsuboi, A.; Izumi, T.; Hirata, M.; Dubin, P. L.; Wang, B.; Kokufuta, E. *Langmuir* **1999**, *15*, 940.
7. Stryer, L. *Biochemistry*, 3rd. ed.; W. H. Freeman and Company: New York, 1988; p 407.

Table 6-1. Interfacial properties of unmodified and grafted PE membranes

Membrane	Contact angle [a] (deg)	Zeta potential [b] (mV)
ASC type	86	-5.4
MGC type	85	-0.2
Acidic type	85	-7.9
Basic type	79	+2.9
Unmodified PE	102	-4.8 [c]

[a] Dynamic sessile drop method, Measured with distilled water at pH 5.6. All contact angle values were reproducible within ± 3 degree.

[b] Measured in 1mM KCl at pH 5.6. All zeta potential values were reproducible within ± 1.2 mV.

[c] Measured after immersion in MeOH.

All data shown are cited from chapter 5.

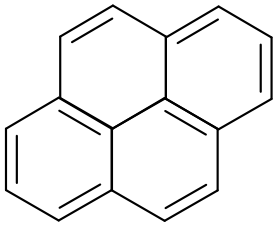

pyrene

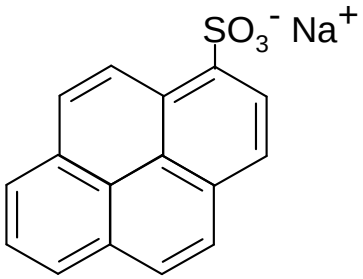

1-pyrenesulfonic acid

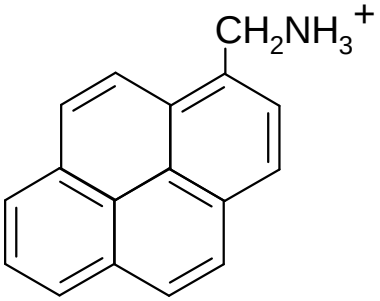

1-pyrenemethylamine

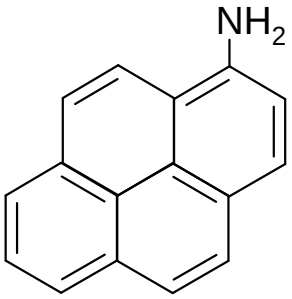

1-aminopyrene

Figure 6-1. Chemical structure of organic molecules at pH 5.6.

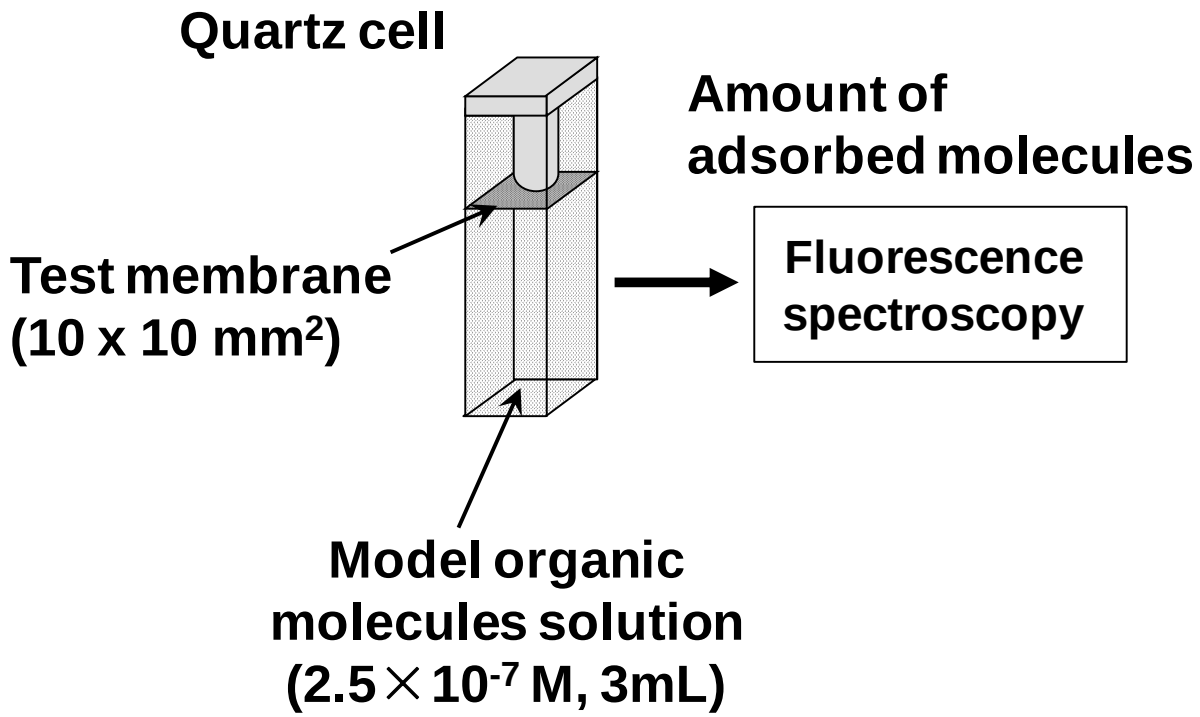

Figure 6-2. Schematic diagram of adsorption experiment.

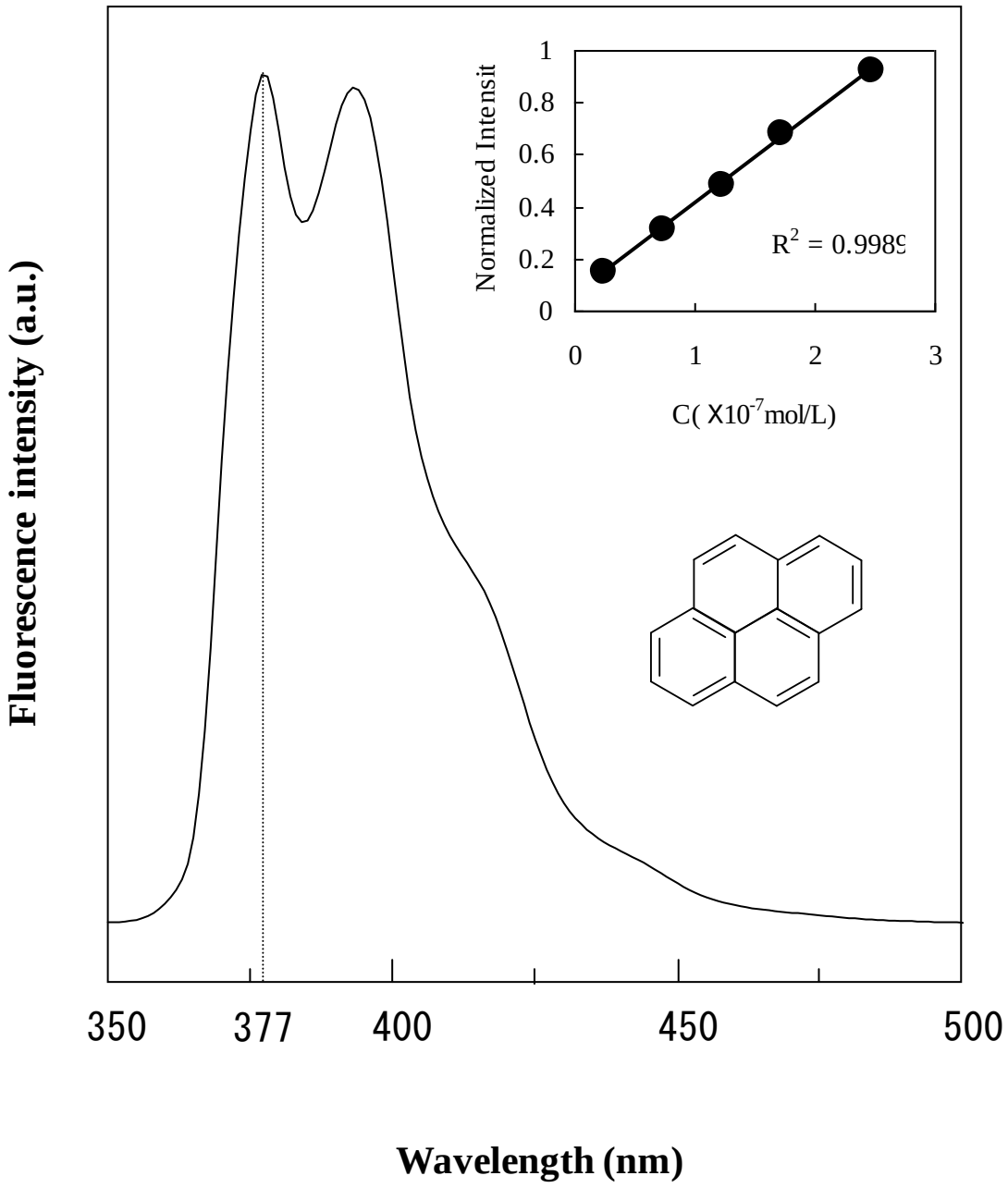

Figure 6-3a. Fluorescence spectrum of aqueous solution at pH 5.6 and its calibration curve of pyrene (λ_{ex}= 336 nm, λ_{em} = 377 nm).

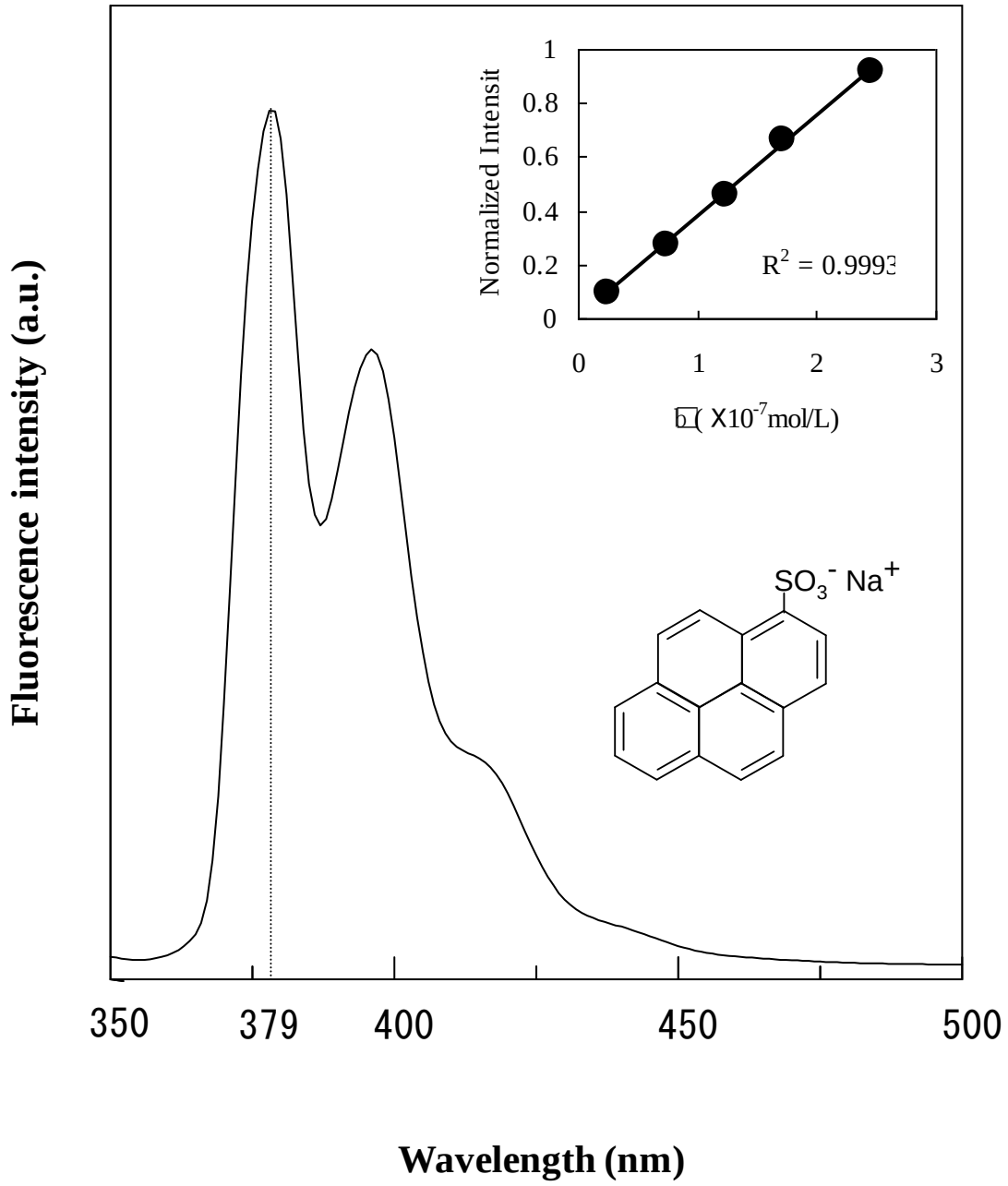

Figure 6-3b. Fluorescence spectrum of aqueous solution at pH 5.6 and its calibration curve of 1-pyrenesulfonic acid (λ_{ex}= 347 nm, λ_{em} = 379 nm).

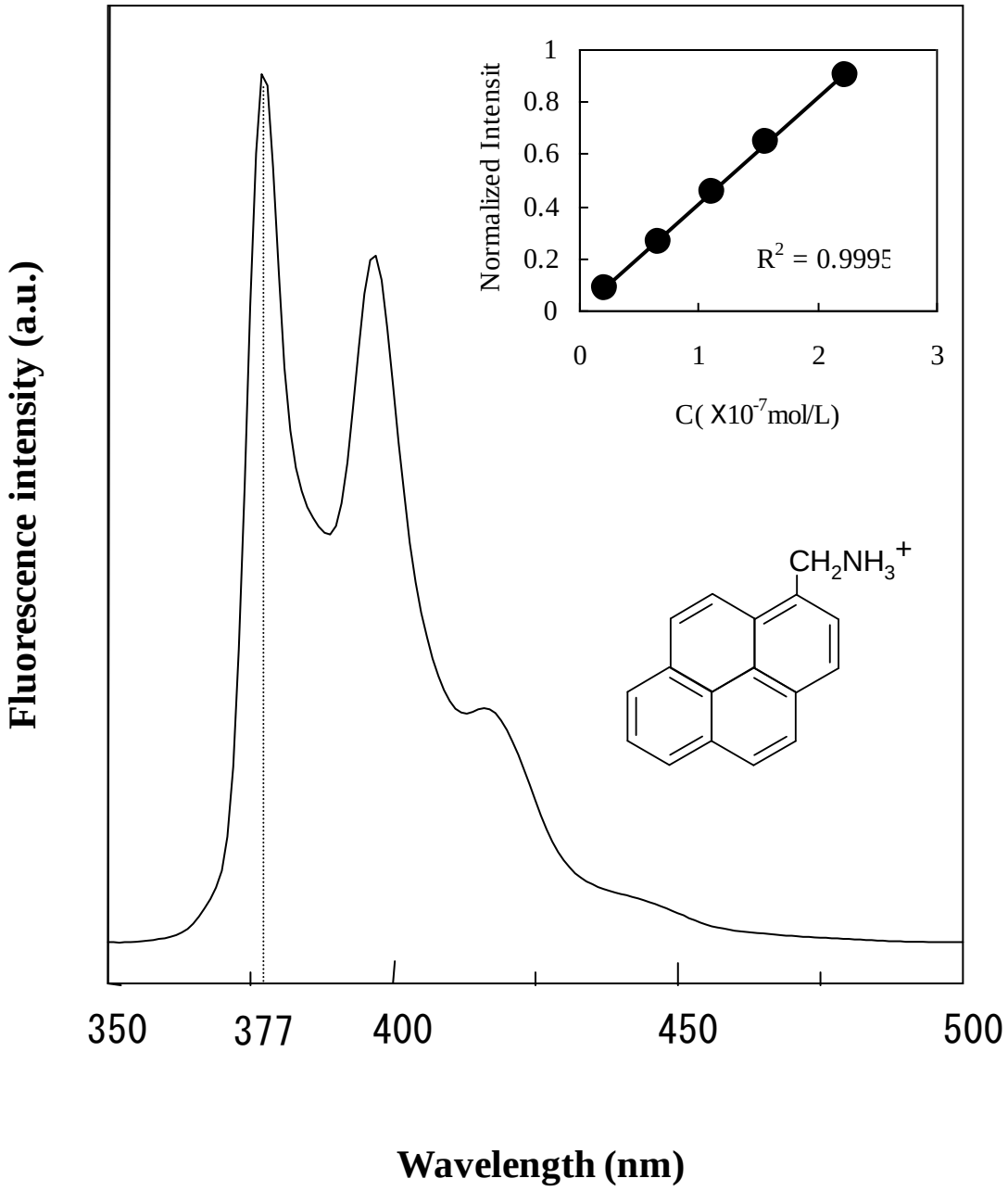

Figure 6-3c. Fluorescence spectrum of aqueous solution at pH 5.6 and its calibration curve of 1-pyrenemethylamine (λ_{ex}= 343 nm, λ_{em} = 377 nm).

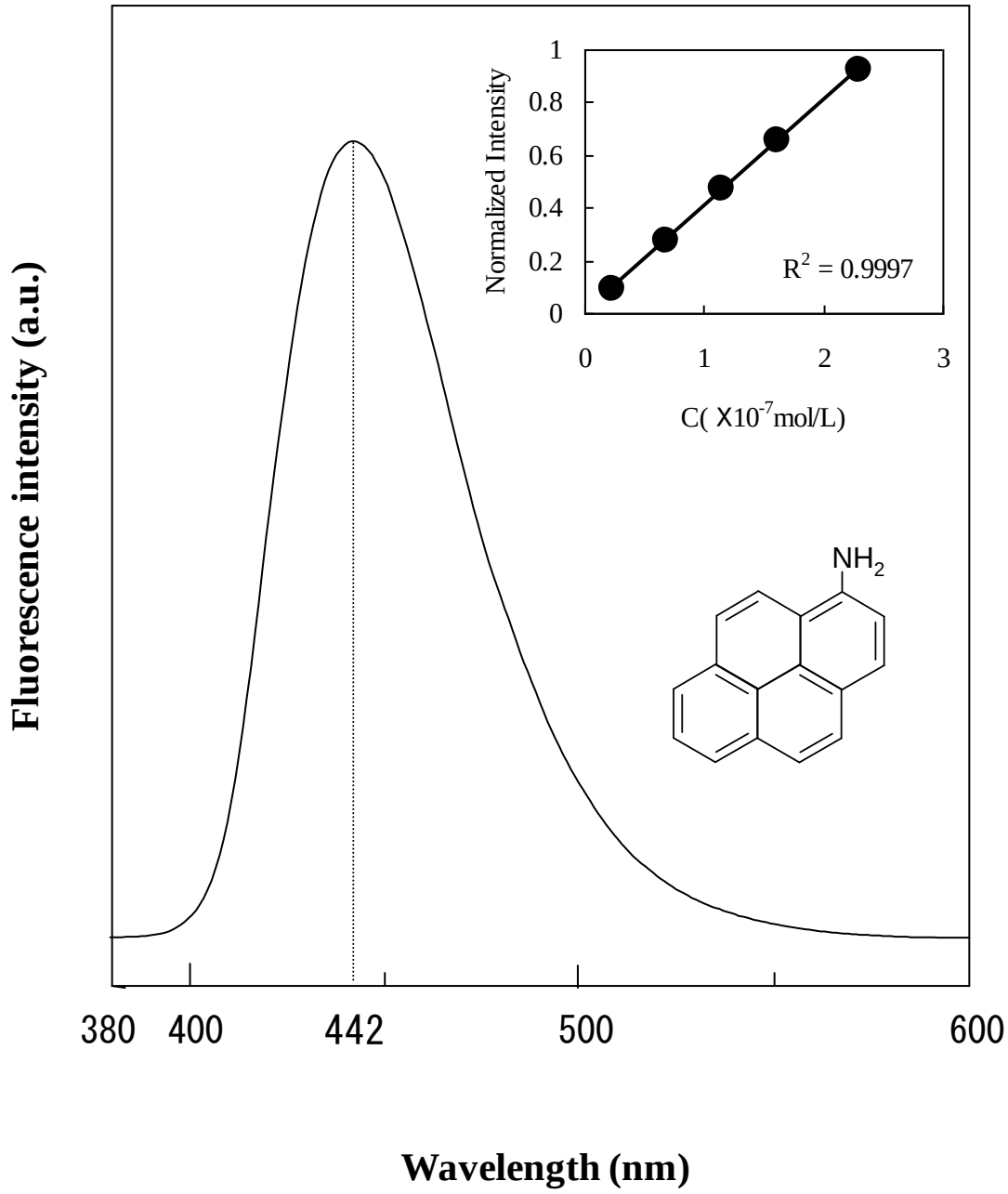

Figure 6-3d. Fluorescence spectrum of aqueous solution at pH 5.6 and its calibration curve of 1-aminopyrene (λ_{ex}= 355 nm, λ_{em} = 442 nm).

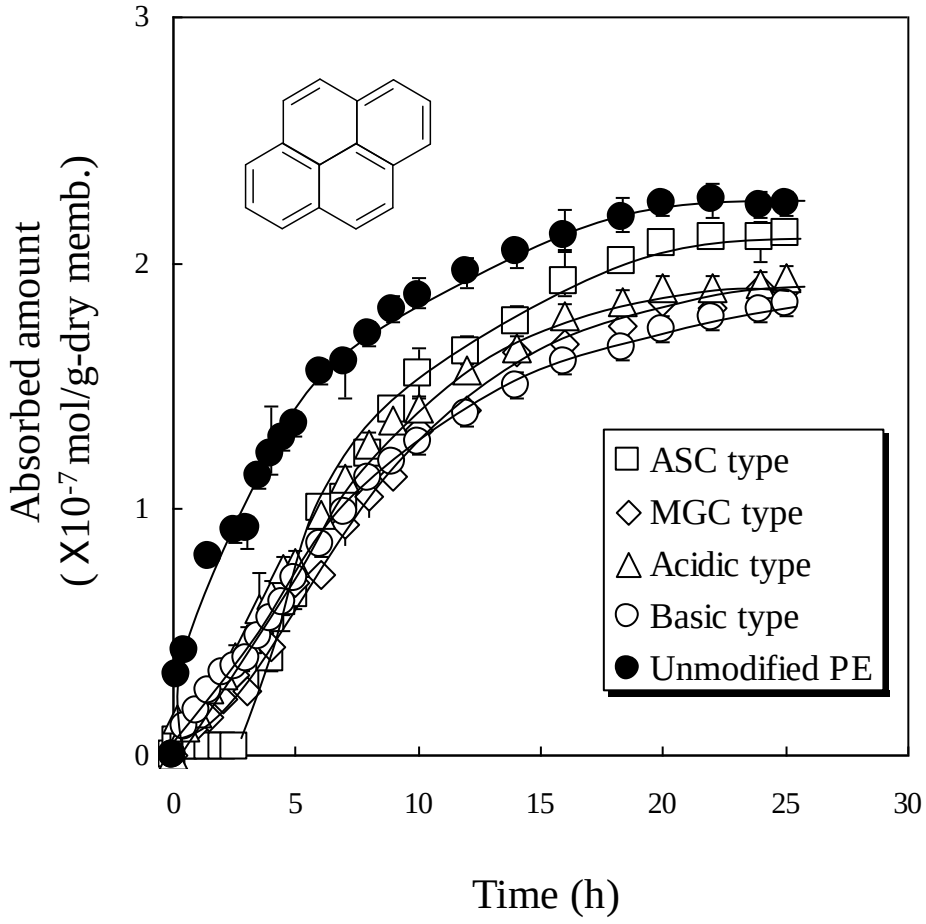

Figure 6-4a. Adsorbed amount of pyrene (λ_{ex}= 336 nm, λ_{em} = 377 nm) on unmodified and grafted PE membranes as a function of time at pH 5.6.

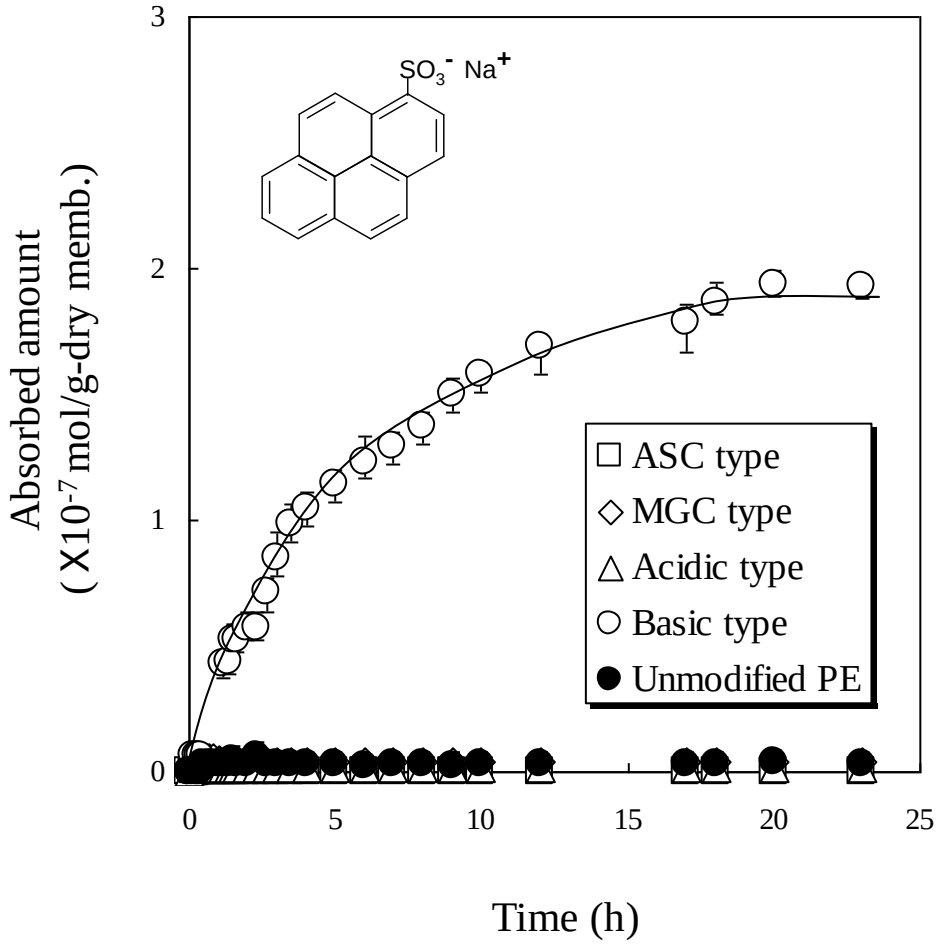

Figure 6-4b. Adsorbed amount of 1-pyrenesulfonic acid (λ_{ex}= 347 nm, λ_{em} = 379 nm) on unmodified and grafted PE membranes as a function of time at pH 5.6.

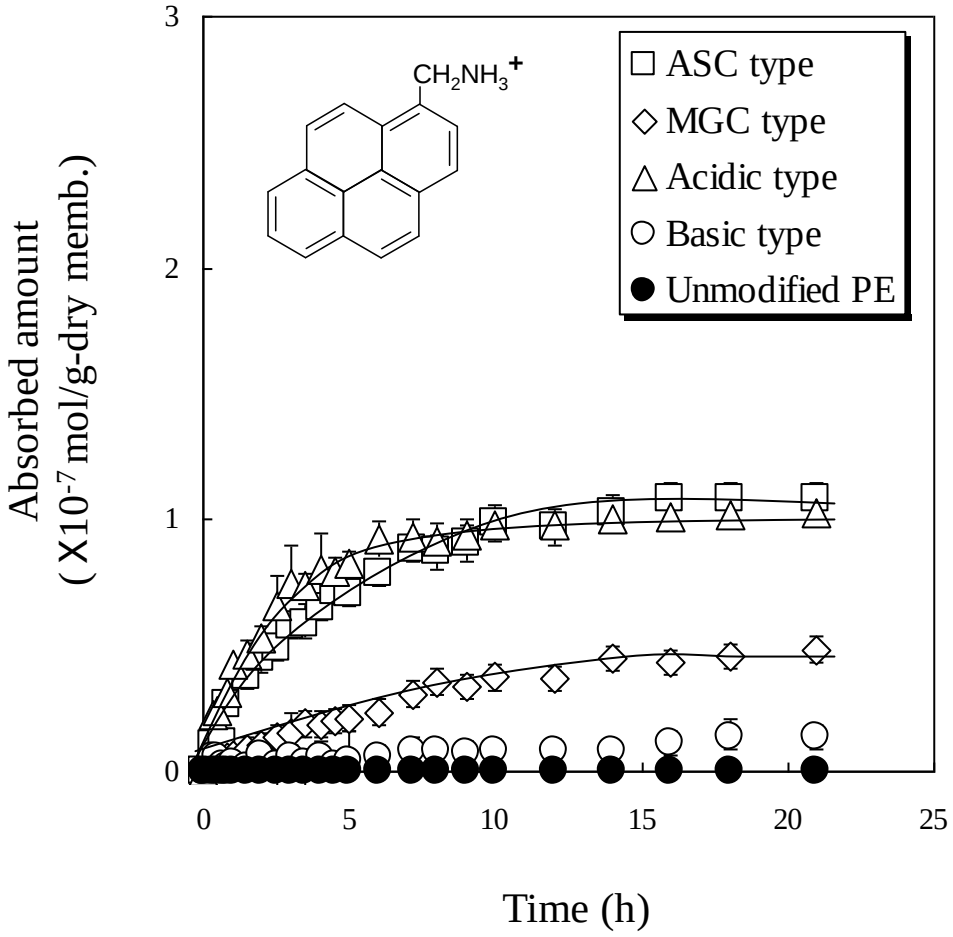

Figure 6-4c. Adsorbed amount of 1-pyrenemethylamine (λ_{ex}= 343 nm, λ_{em} = 377 nm) on unmodified and grafted PE membranes as a function of time at pH 5.6.

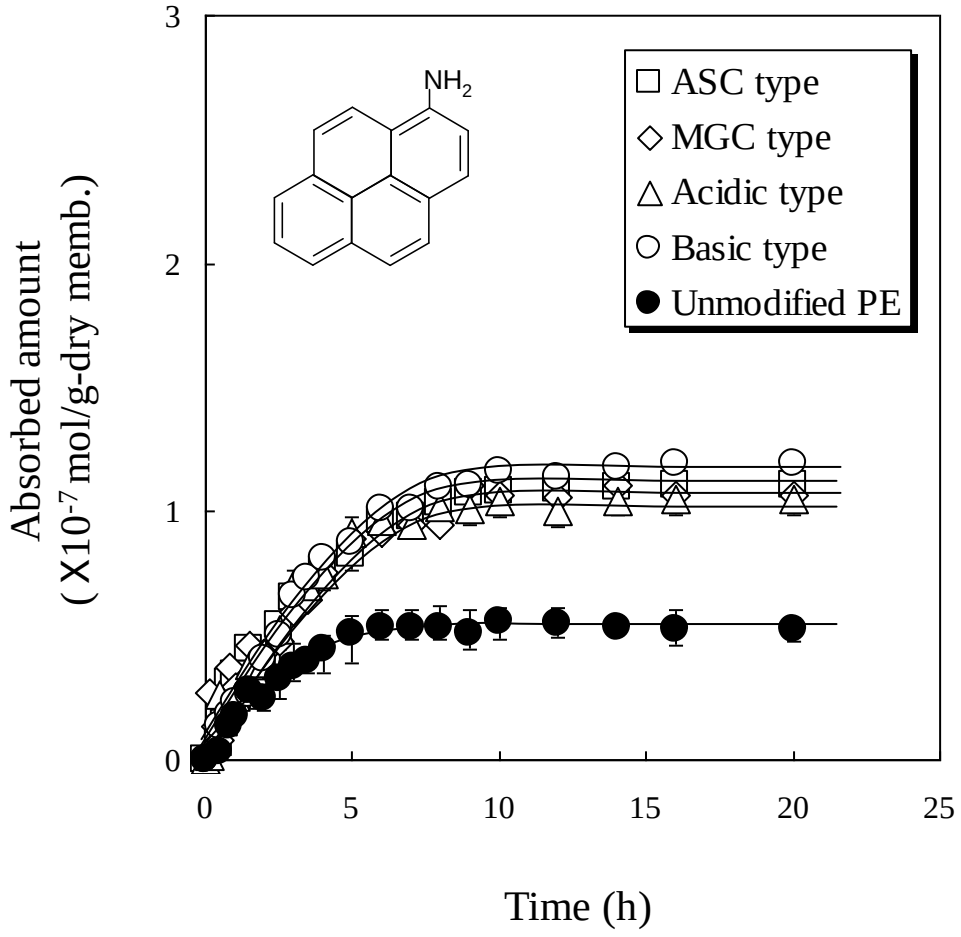

Figure 6-4d. Adsorbed amount of 1-aminopyrene (λ_{ex}= 355 nm, λ_{em} = 442 nm) on unmodified and grafted PE membranes as a function of time at pH 5.6.

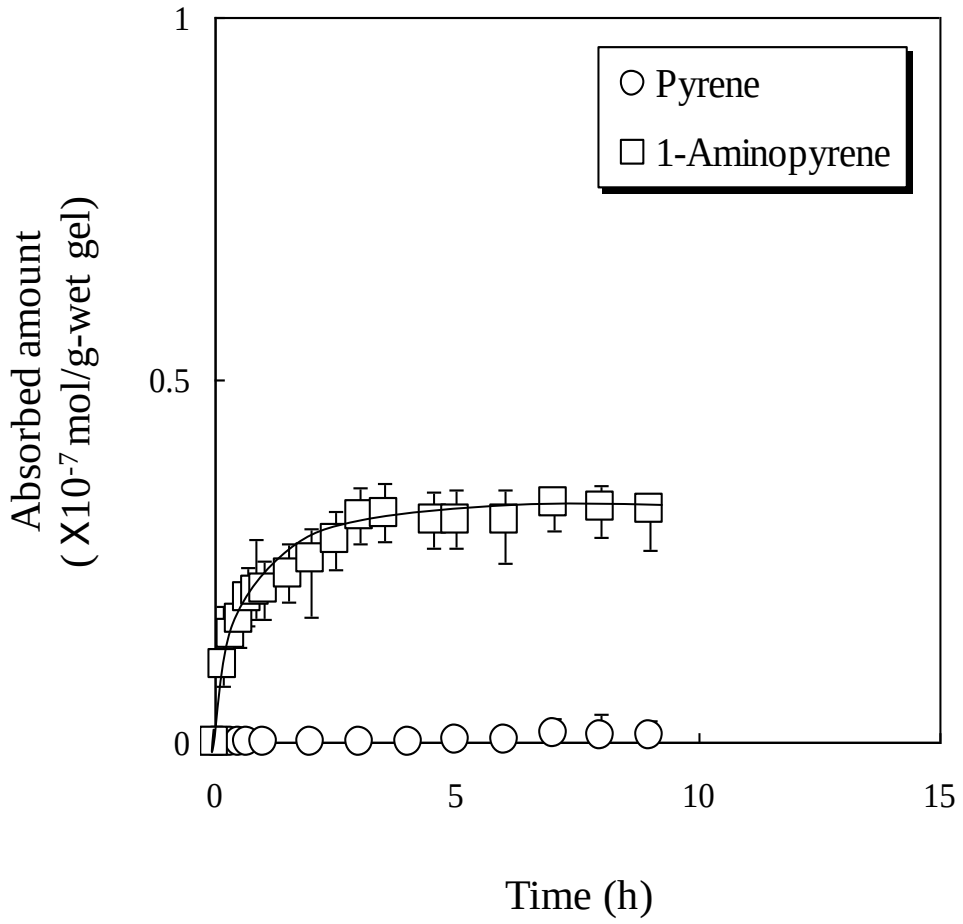

Figure 6-5. Adsorbed amount of pyrene (λ_{ex}= 336 nm, λ_{em} = 377 nm) and 1-aminopyrene (λ_{ex}= 355 nm, λ_{em} = 442 nm) on PEO gel as a function of time at pH 5.6.

Chapter 7

Interaction of Proteins with Weak Amphoteric Charged Membranes

7.1 Introduction

Protein adsorption on membrane surfaces is important in the fields related to separation science and biomedical research. Proteins are amphoteric and amphiphilic biological macromolecules which are built from a repertoire of 20 amino acids. These protein molecules can adsorb on almost all kinds of interfaces and their adsorption behavior has high complexity. It is now generally established that the interaction between proteins and solid surfaces is mainly determined by: (1) changes in the hydration of the surface and protein molecule, (2) electrostatic interaction between the surface and protein, and (3) structure rearrangements in the adsorbing protein molecules [1]. Of these contributions, the electrostatic interaction (attractive or repulsive) is a key factor for the control of the protein adsorption behavior onto the membrane surface. Most studies of the protein adsorption behavior onto polymer surfaces were carried out under physiological conditions for biomedical use [2-6]. The pH dependence of the protein adsorption behavior, however, is essential not only for application in protein or cell separation but also for fundamental studies on the interactions between proteins (amphoteric biological macromolecules) and amphoteric surfaces [7, 8]. Furthermore, the interactions of ionic PEG chain grafted membranes, which can exclude hydrophobic interactions and interact with polar groups by hydrogen bonding [9], with proteins are interesting for both the fundamental characteristics and the potential as a protein separator of ionic PEG derivatives.

In this chapter, the pH dependence of the adsorbed amount of protein, the fluorescein isothiocyanate-labeled bovine serum albumin (FITC-BSA), onto weak amphoteric charged membranes was investigated by fluorescence spectroscopy. The interfacial charge properties of the membranes and BSA were also characterized at different pH values by streaming potential and electrophoretic light scattering (ELS) measurements, respectively. The objectives of this chapter are (1) to demonstrate the pH dependence of the protein adsorption behavior onto the ionic PEG chain grafted membranes, and (2) to

examine the correlation between the interfacial charge properties of the ionic PEG chain grafted membranes and their interactions with proteins.

7.2 Experimental

7.2.1 Materials

Bovine serum albumin (BSA, crystallized and lyophilized, product no. A4378) and fluorescein isothiocyanate-labeled bovine serum albumin (FITC-BSA, product no. A9771, prepared from A4378) were purchased from Sigma, USA. The molecular weight of BSA is approximately 66,000 and the isoelectric point (IEP) is 4.7－4.8 [10]. Before the ELS measurements, 2 mg/mL of BSA buffer solution was filtered through a 0.1 μm filter unit (MILLEX®-VV, Millipore, USA). The FITC-BSA aqueous solution was centrifuged using an ultra-filtration membrane filter device (Ultrafree®-CL, 10,000 nominal molecular weight limit, Millipore, USA) for removal of the low-molecular-weight impurities, and then freeze-dried before use.

Acetic acid, potassium hydrogen phthalate, disodium hydrogen phosphate, potassium dihydrogen phosphate, sodium hydrogen carbonate, and sodium carbonate were purchased from Wako Pure Chemical, Japan. These reagents were of extra-pure grade. All reagents were used without further purification.

Two types of amphoteric charged membranes, the amphoteric ion-pair side chain (ASC) type and the mixed grafted chain (MGC) type, and two types of single charged membranes, the acidic type and the basic type (see chapter 5 [11]), were used.

7.2.2 Measurements

7.2.2.1 Adsorption experiments

A 0.1mg sample of FITC-BSA was dissolved in 100mL of 10 mM buffer to form a 1 μg/mL protein solution. Here, four kinds of buffers, i.e. 10 mM acetate buffer (10 mM acetic acid, pH 3.3), 10 mM phthalate buffer (10 mM potassium hydrogen phthalate, pH 4.1), 10 mM phosphate buffer (6 mM disodium hydrogen phosphate + 4 mM potassium dihydrogen phosphate, pH 7.2), and 10 mM carbonate buffer (5 mM sodium hydrogen carbonate + 5 mM sodium carbonate, pH 10.2), were used. The pH values of these buffers corresponded to the acidic pH lower than the IEP of BSA, the IEP range, the

physiological pH range, and the basic pH higher than the IEP, respectively. Before the adsorption experiments, a calibration curve for FITC-BSA was made at five measurement points from 0.1 to 1 μg/mL protein solution in each 10 mM buffer solution, with about 495 nm fluorescence excitation and about 520 nm emission wavelength. The fluorescence spectra were measured with a spectrofluorometer (FP-750, JASCO, Japan) using a 1-cm^2 quartz cell (F10-UV-10, GL-Science, Japan). The emission and excitation slit widths were equaled to 5 and 5 nm, respectively. The schematic diagram of the adsorption experiments is shown in Figure 7-1. A freeze-dried test membrane (1 $\times$ 1 cm^2) was immersed in 3 mL of 1 μg/mL protein solution in the quartz cell. At the same time, the fluorescence measurements were started and continued for 3－5 h. The concentration of proteins in the solution was determined by the calibration curves. The adsorbed proteins on the membrane were estimated from the decreased amount of proteins in solution. The adsorbed amount on the quartz cell was also deduced as a blank. All experiments were performed at 25 ± 1℃. The experiments were carried out five times for each experimental condition, and the mean value ($\pm$ standard deviation) of each experimental point is indicated.

7.2.4.2 Streaming potential measurements

The experimental setup is the same as that previously mentioned in chapter 2. By varying the applied pressure (ΔP) ranging from 15 to 120 cmH_2O, the streaming potential (ΔE), which had been generated by a flow of ions due to ΔP, was measured with a digital multimeter (HP3458A, Hewlett-Packard, USA) and the data recorded using a microcomputer. The zeta potential was obtained from the slope of a $\Delta E - \Delta P$ plot using the following Helmholtz－Smoluchowski equation:

$$\frac{\Delta E}{\Delta P} = \frac{\varepsilon \zeta}{\eta \lambda} \tag{7.1}$$

where η is the solution viscosity and ε and λ are the permittivity and electrical conductivity of the solution, respectively. The streaming potential measurements were conducted in the four kinds of buffers as mentioned above. Here, KCl was added to the buffers in order to improve the stability of the potential detected by the Ag/AgCl electrode. The final concentration of KCl was adjusted to 0.1 mM for each buffer condition. All measurements were performed five times at 25 ± 0.1℃. The experiments were

carried out five times for each experimental condition, and the mean value (± standard deviation) of each experimental point is indicated.

7.2.4.3 Electrophoretic light scattering (ELS) measurements [12]

The electrophoretic mobilities of BSA were measured with an electrophoretic light scattering spectrophotometer (ELS-6000, Otsuka Electronics Co., Ltd., Japan) in the four kinds of buffers as mentioned above. Laser light with a 632.8 nm wavelength from a 10 mW He－Ne laser was used as the incident beam. The measurements were performed at the scattering angle of 5° with an electric field of 32.5－34.4 V/cm. Because of the Doppler effect, the frequency of the scattered laser light is different from the frequency of the incident laser beam. This frequency shift is related to the particle velocity. The relationship between the frequency shift and electrophoretic mobility is expressed by the following equation:

$$u = (v_d \lambda)/[2En\sin(\theta/2)] \tag{7.2}$$

where v_d is the Doppler frequency, u is the electrophoretic mobility, E is the electrical field, n is the refractive index, λ is the wavelength of the incident laser beam, and θ is the scattering angle. From the obtained electrophoretic mobility, the zeta potential, ζ, was calculated using the Smoluchowski equation as follows:

$$\zeta = 4\pi\eta u/\varepsilon \tag{7.3}$$

where u is the electrophoretic mobility, and η and ε are the solution viscosity and electrical permittivity of the solution, respectively. All measurements were performed at 25±1℃. The experiments were carried out five times for each experimental condition, and the mean value (± standard deviation) of each membrane is indicated.

7.3 Results and Discussion

7.3.1 Adsorption experiments

A typical fluorescence spectrum and calibration curve of FITC-BSA in 10 mM buffer is shown in Figure 7-2. All the calibration curves had good linearity (correlation factor R^2 nearly equals 0.999) while the fluorescence intensity of FITC was known to be smaller at the lower pHs [13]. The concentration of FITC-BSA in each buffer was determined from the maximum fluorescence intensity at about 520 nm based on each calibration curve.

Figure 7-3a presents the adsorbed amount of BSA onto the unmodified and grafted PE membranes as a function of time in 10 mM phosphate buffer. It took about 40－60 min to reach the adsorption equilibrium for all membranes. The adsorption behaviors in other buffers showed the similar time dependence. The pH dependence of the adsorbed amount of BSA onto the membranes at equilibrium is shown in Figure 7-3b. The adsorbed amount onto each ionic PEG chain grafted membrane shows a maximum at pH 4.1 (near the IEP of BSA). Here, the electrostatic interaction between the membrane surface and BSA molecule was very weak and many BSA molecules would interact with the grafted chains; because there is no difference between each pendant ionizable groups for the adsorbed amount on the ionic PEG chain grafted membranes. It was also revealed that ionic PEG chain grafted membranes could exclude hydrophobic interactions and interact with polar group by hydrogen bonding in chapter 6. Therefore, the hydrogen bonding of the ether groups in the ionic PEG chain with the carboxyl group and phenolic OH groups in the protein would be substantial [14]. On both sides of the IEP of BSA, the electrostatic interaction contribution was dominant for the protein adsorption onto the ionic PEG chain grafted membranes. The effect of the electrostatic interaction on the adsorption behavior for each buffer condition will be discussed in detail (see section 7.3.3). The unmodified PE membrane, on the other hand, shows a maximum at pH 7.2. We could not explain this result on the electrostatic interaction between the membranes and BSA molecules. This could originate from the wettability of the PE membrane, from the hydrophobic character (see Table 6-1 in chapter 6) and the dissociation state of the charge groups on the PE membrane (chapter 5).

7.3.2 Zeta potential measurements of BSA and prepared membranes

In order to reexamine the electrostatic contribution to the interactions between the protein and

membrane surfaces, the zeta potential of BSA and the prepared membranes were measured in each buffer solution. Figure 7-4a shows the pH dependence of the zeta potential of BSA from the ELS measurements. The zeta potential for BSA changed from a positive to a negative value through the point of zero charge (PZC) at a pH of approximately 4.2, which compares with the reported IEP of 4.7－4.8 for BSA [10]. Figure 7-4b shows the pH dependence of the zeta potential for the unmodified and grafted PE membranes from the streaming potential measurements. Here, the PE membrane is so hydrophobic that the streaming potential measurements could be carried out after immersion in MeOH. The zeta potential/pH profile of each membrane showed similar pH dependence in 10 mM KCl as described in chapter 5. The zeta potential of the unmodified PE membrane had a near zero value near pH 3, but decreased with a pH increase, and had a constant negative value (about –25 mV) at pH > 7. This potential value would originate in the negatively charged groups on the pore surface of the PE membrane. The zeta potential of the ASC-type (PEG-Cys grafted) membrane had a positive potential at pH 3, but decreased with a pH increase, and showed a constant negative potential (about –15 mV) at pH > 4. The potential differences at pH > 4 between the unmodified PE and the ASC-type membranes would be explained by the position shift of hydrodynamic slipping plane due to the existence of a grafted PEG-Cys layer on the pore surface, because the neutral polymer layer shifts the position of the slipping plane away from the original PE surface, and weakened the contribution of the interfacial charge on the PE [16]. The basic-type (PEG-A grafted) membrane showed a positive potential at low and mid pHs, which significantly decreased near pH 8, and finally showed a negative value at pH 10. The acidic-type (PEG-C grafted) membrane gave a near zero potential at pH 3, but decreased with a pH increase, and gave almost a constant value (about –20 mV) at pH > 4. The potential differences at pH > 4 between the unmodified PE and the acidic-type membranes would originate from the position shift of the hydrodynamic slipping plane by the grafted layer mentioned above [16] and the negative charge in the grafted layer. Here, contributions of the negatively charged grafted chains on the zeta potential would be substantial (their charge density would be less than that of original PE surface). The zeta potential for the MGC type (PEG-A/PEG-C grafted) membrane showed an intermediate pH dependence behavior between the acidic-type and basic-type membranes.

7.3.3 Correlation between interfacial charge and protein adsorption

BSA adsorption amounts on the unmodified and grafted membranes in each buffer are summarized in Figure 7-5. The interfacial charge properties of the membranes and the protein are indicated by the zeta potential values. As a trend, the contribution of the electrostatic interaction between the BSA molecule and ionic PEG chain grafted membrane would be reflected in the adsorbed amount except in the case at pH 4.1 (near the IEP of BSA, Figure 7-5b) as discussed above. At pH 3.3 (Figure 7-5a), the acidic side of the IEP of BSA, the acidic-type membrane was negatively charged and the other grafted membranes and BSA were positively charged. BSA adsorbed on the oppositely (negatively) charged acidic-type membrane and equally (positively) charged MGC-type membrane. At pH 7.2 (Figure 7-5c), the range of the physiological pH condition, the basic-type membrane was positively charged, and the other grafted membranes and BSA were negatively charged. BSA adsorbed on the basic-type membrane having a counter (positive) charge and the MGC-type one having an equal (negative) charge. These results demonstrated that the contribution of the attractive and repulsive electrostatic interaction was dominant for the protein adsorption on the ionic PEG chain grafted membranes except for the MGC-type membrane. For the MGC-type membrane, on the other hand, the adsorption behavior would originate in the conformational difference between the PEG-A and PEG-C chains on the pore surface as described in chapter 5 (see Figure 5-7): the PEG-A chain would be more extended than the PEG-C chains on the pore surface at pH 3.3, and conversely, the PEG-C chain would be more extended than the PEG-A chain on the pore surface at pH 7.2. Therefore, the contribution of the more extended chain is superior to the less extended one for the electrokinetic charge property, but the contribution of the less extended chain (PEG-C at pH 3.3 and PEG-A at pH 7.2) was substantial for the protein adsorption. Interestingly, this unique adsorption behavior on the MGC-type membrane was observed only for BSA molecules but not for organic molecules (chapter 6). At pH 10.2 (Figure 7-5d), the basic side of the IEP of BSA, both all grafted membranes and BSA were negatively charged. A repulsive electrostatic interaction was expected to be dominant at this pH condition. The adsorbed amount for the basic-type and the MGC-type membrane was smaller than that at pH 7.2 (This would be from the contribution of the electrostatic repulsion), but the adsorbed amount for the acidic-type and the ASC-type membrane was larger than that at pH 7.2. Therefore, not only the contribution of the electrostatic interaction, but also the other

contributions (e.g., hydrogen bonding from the unfolding of BSA [17]) would be substantial at this condition.

7.4 Conclusions

Our protein adsorption experiments have demonstrated the pH dependence of the interaction characteristics of proteins with ionic PEG chain grafted PE membranes. (1) Each adsorbed amount/pH profile showed a bell-shaped behavior, which has a uniform maximum value near the IEP of the protein. Here, the contribution of the hydrogen bonding was substantial for the adsorption of proteins on the ionic PEG chain grafted membranes. (2) On both sides of the IEP, the interfacial charge properties of the ionic PEG chain grafted membranes and protein played an important role in their interaction with proteins: the contribution of the electrostatic interaction was dominant for the adsorption of proteins on the ionic PEG chain grafted membranes. This result also indicates the possibility of controlling the protein-ionic PEG chain interaction on the membrane surfaces by changing the pH of the outer solution.

7.5 References

1. Cohen Stuart, M. A; Fleer, G. J.; Lyklema, J.; Norde, W.; Scheutjens, J. M. H. M. *Adv. Colloid Interface Sci.* **1991**, *34*, 477.
2. Prime, K. L.; Whitesides, G.. M. *J. Am. Chem. Soc.* **1993**, *115*, 10714.
3. Bergström, K.; Holmberg, K.; Safranji, A.; Hoffman, A. S.; Edgell, M. J.; Kozlowski, A.; Hovanes, B. A.; Harris, J. M. *J. Biomed. Mater. Res.* **1992**, *26*, 779.
4. Österberg, E.; Bergström, K.; Holmberg, K.; Riggs, J. A.; Van Alstine, J. M.; Schuman, T. P.; Burns, N. L.; Harris, J. M. *Colloids Surfaces A* **1993**, *77*, 159.
5. Österberg, E.; Bergström, K.; Holmberg, K.; Schuman, T. P.; Riggs, J. A.; Burns, N. L.; Emoto, K.; Van Alstine, J. M.; Harris, J. M. *J. Biomed. Mater. Res.* **1995**, *29*, 741.
6. Yang, Z.; Galloway, J. A.; Yu, H. *Langmuir* **1999**, *15*, 8405.
7. Shirahama, H.; Ohno, H.; Suzawa, T. *Colloids Surfaces* **1991**, *60*, 1.
8. Burns, N. L.; Holmberg, K.; Brink, C. *J. Colloid Interface Sci.* **1996**, *178*, 116.
9. Matsumoto, H.; Koyama, Y.; Tanioka, A. *Langmuir* **2002**, *18*, 3698.
10. Peters, T. *Adv. Protein Chem.* **1985**, *37*, 161.
11. Matsumoto, H.; Koyama, Y.; Tanioka, A. *Langmuir* **2001**, *17*, 3375.
12. Harada, A.; Kataoka, K. *Macromolecules* **1998**, *31*, 288.
13. FlTC has a pH sensitivity very similar to that of the original compound fluorescein. For the pH dependence of fluorescein fluorescence, see: Munkholm, C.; Parkinson, D.-R.; Walt, D. R. *J. Am. Chem. Soc.* **1990**, *112*, 2608.
14. Azegami, S.; Tsuboi, A.; Izumi, T.; Hirata, M.; Dubin, P. L.; Wang, B.; Kokufuta, E. *Langmuir* **1999**, *15*, 940.
15. Holmes-Farley, S. R.; Bain, C. D.; Whitesides, G. M. *Langmuir* **1988**, *4*, 921.
16. Shirahama, H.; Suzawa, T. *J. Appl. Polym. Sci.* **1984**, *29*, 3651.
17. Shirahama, H.; Suzawa, T. *Colloid Polym. Sci.* **1985**, *263*, 141.

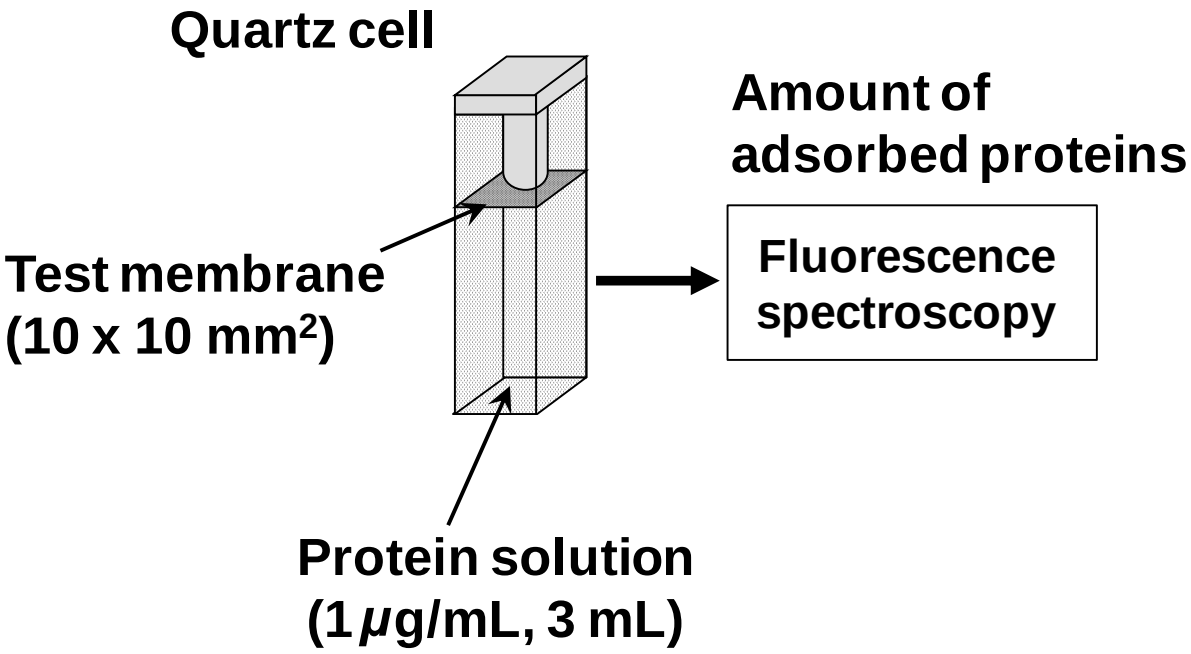

Figure 7-1. Schematic diagram of adsorption experiment.

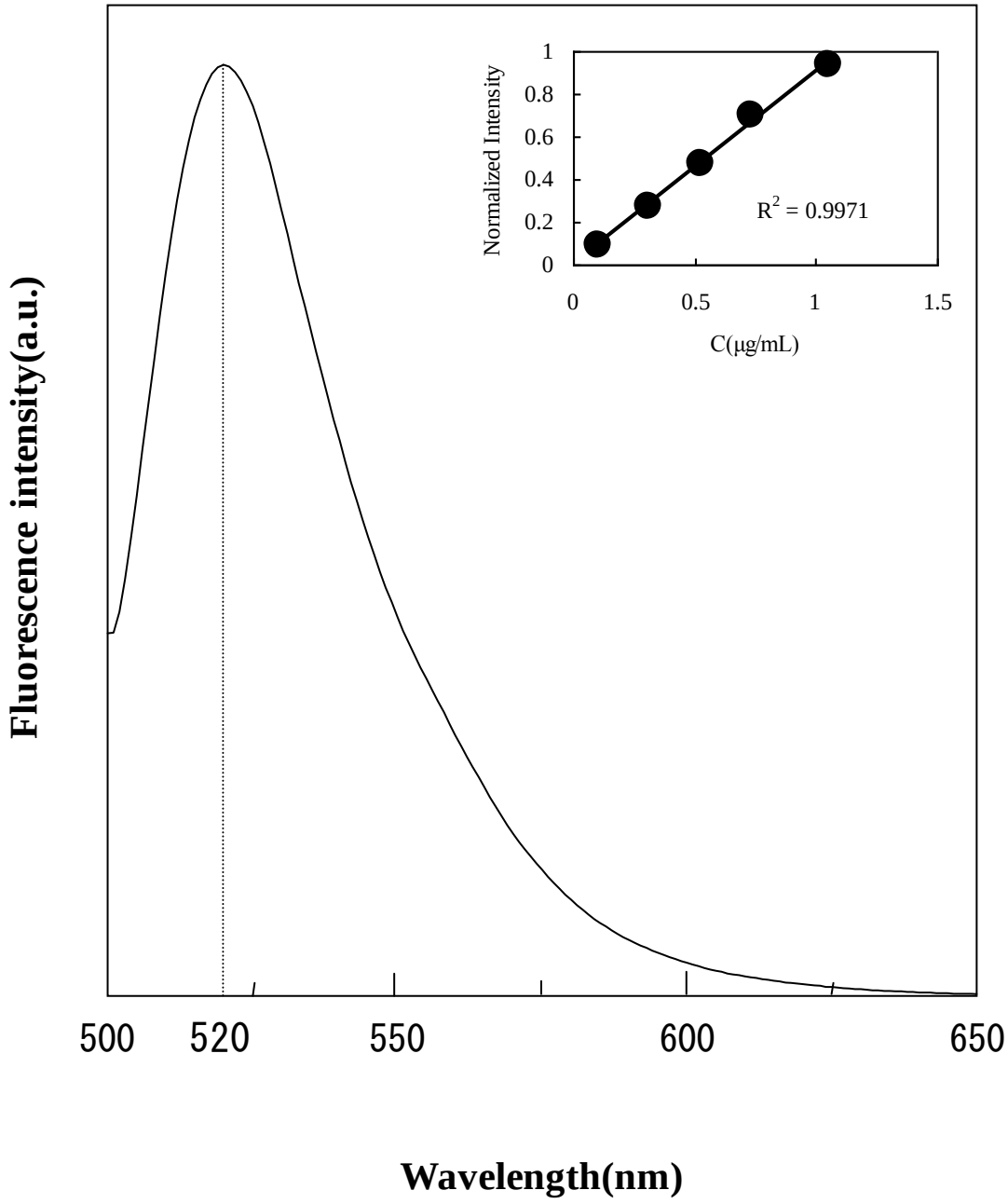

Figure 7-2. Fluorescence spectra of FITC-BSA and its calibration curve in 10 mM phosphate buffer (λ_{ex} = 493 nm, λ_{em} = 520 nm, pH 7.2), emission and excitation slit widths = 5 and 5 nm, respectively.

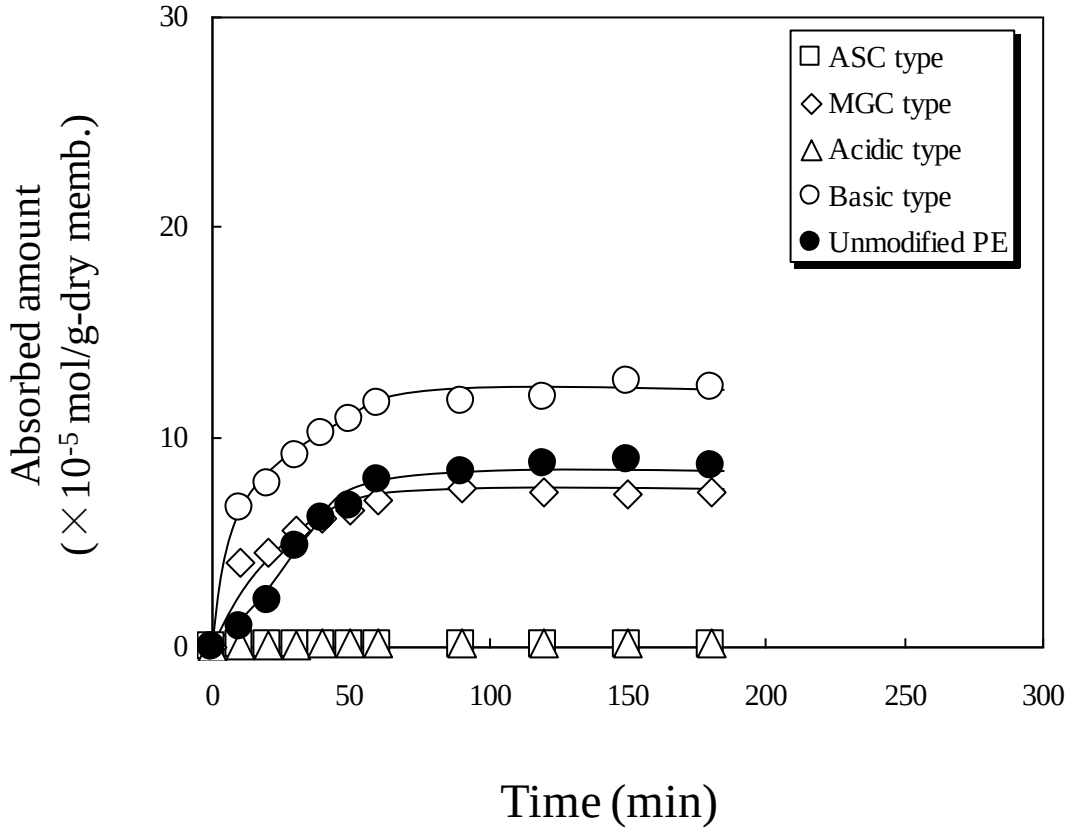

Figure 7-3a. Adsorbed amount of FITC-BSA on unmodified and grafted PE membranes in 10 mM phosphate buffer (λ_{ex}=493 nm, λ_{em}=520 nm, pH 7.2) as a function of time.

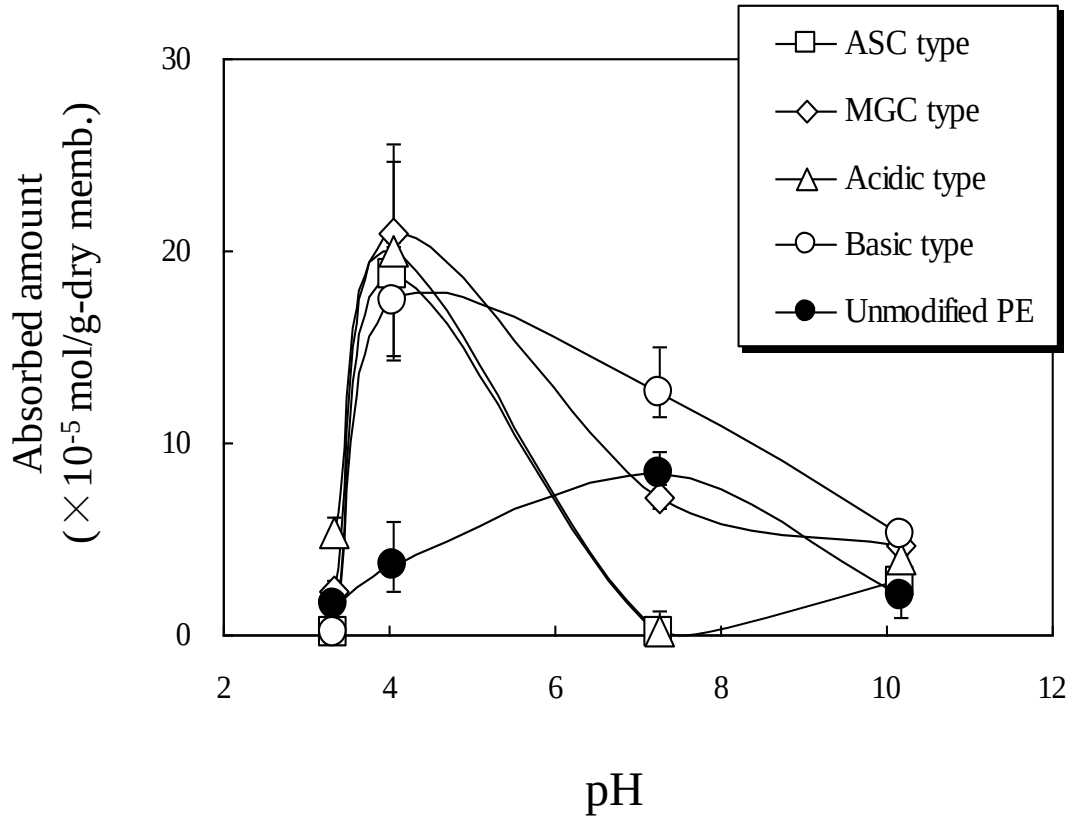

Figure 7-3b. The pH dependence of adsorbed amount of FITC-BSA on unmodified and grafted PE membranes.

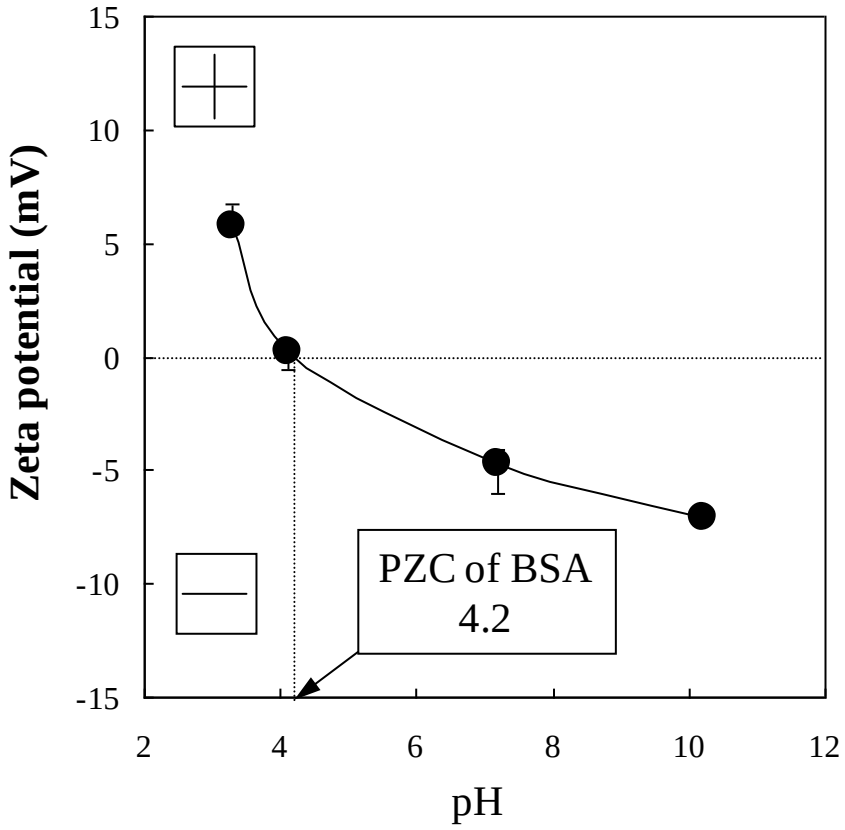

Figure 7-4a. The pH dependence of zeta potential for BSA.

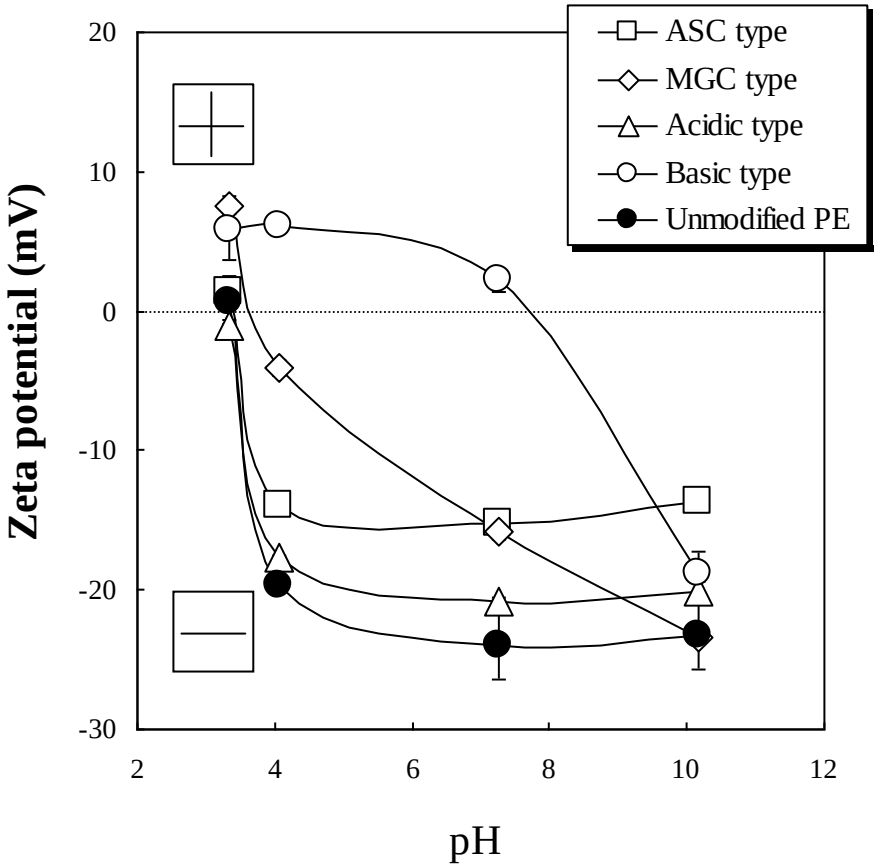

Figure 7-4b. The pH dependence of zeta potential for the unmodified and grafted PE membranes.

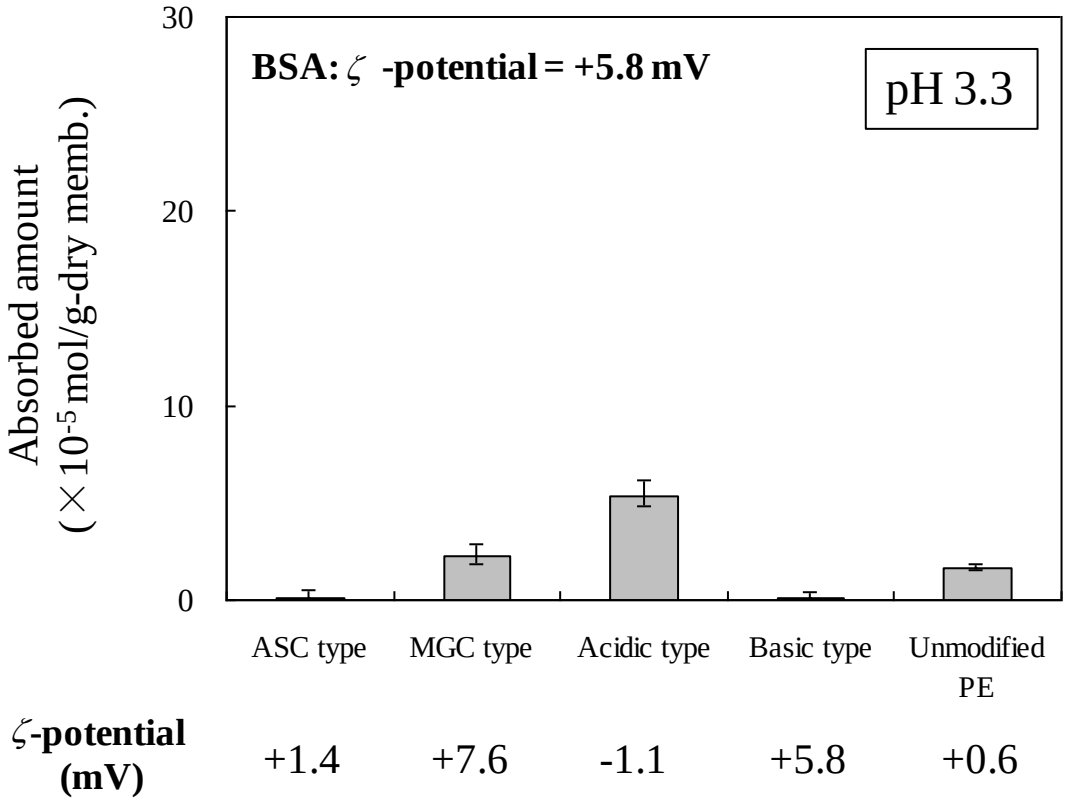

Figure 7-5a. Adsorbed amount of FITC-BSA on unmodified and grafted PE membranes in 10 mM acetate buffer (λ_{ex}= 499 nm, λ_{em}= 520 nm, pH 3.3).

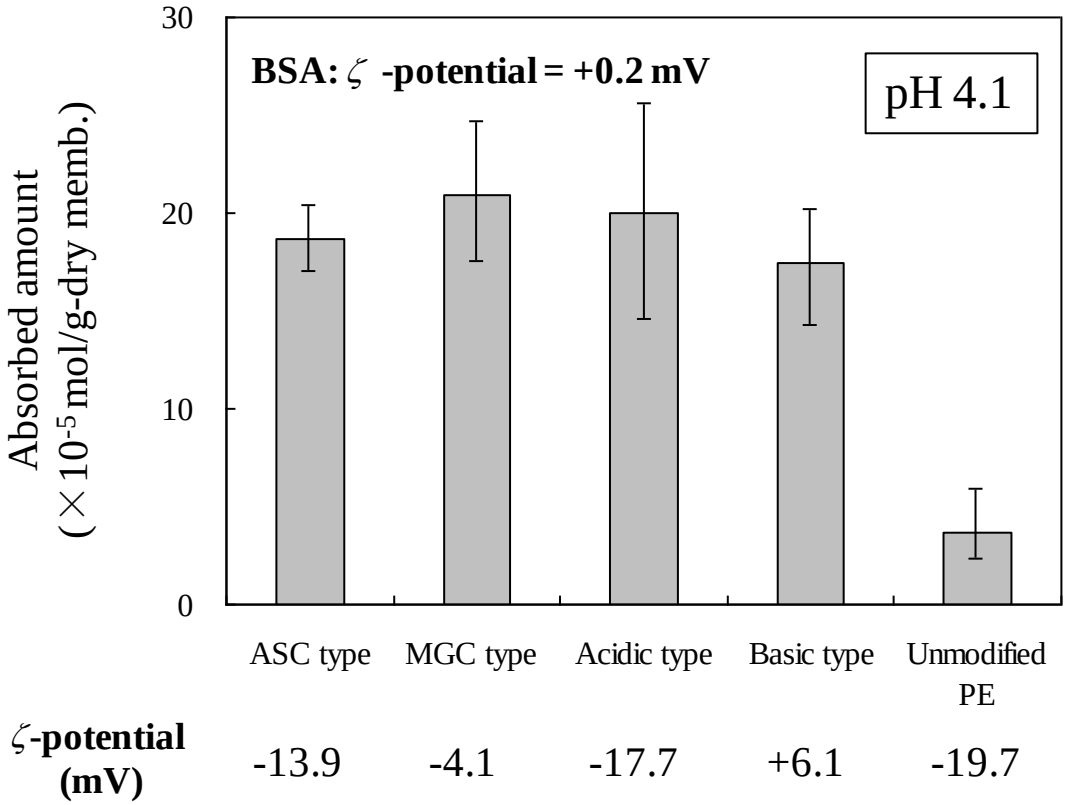

Figure 7-5b. Adsorbed amount of FITC-BSA on unmodified and grafted PE membranes in 10 mM phthalate buffer (λ_{ex} = 493 nm, λ_{em} = 520 nm, pH 4.1).

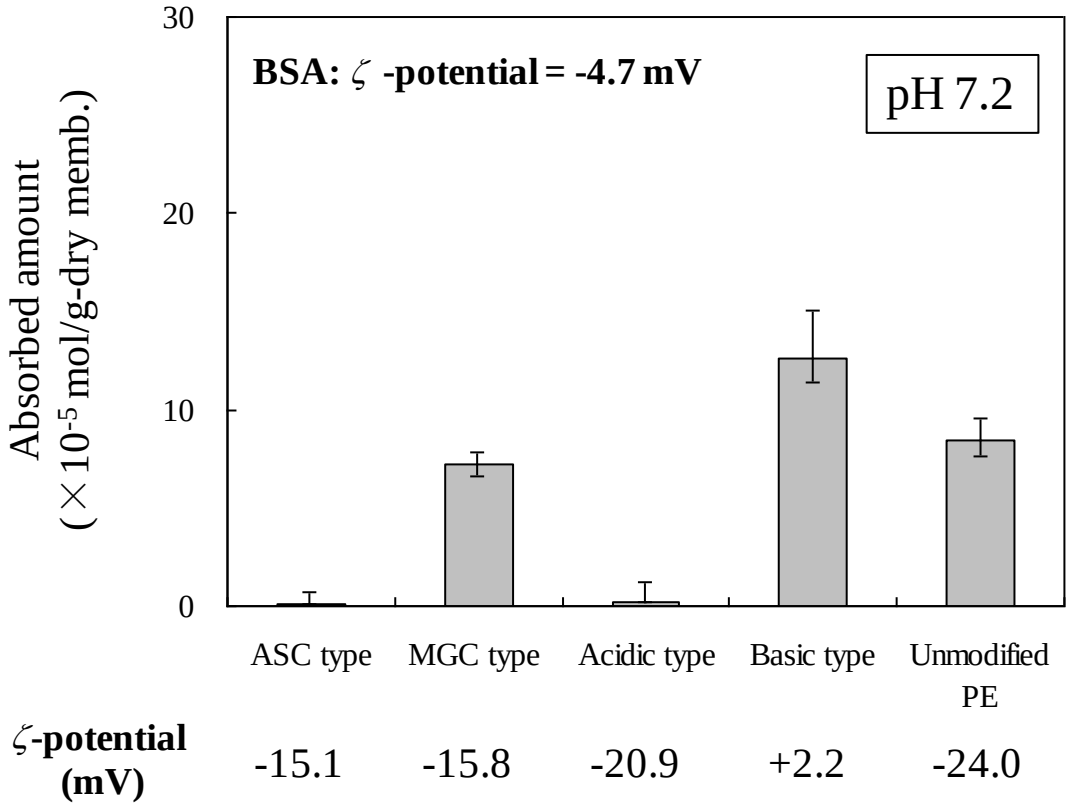

Figure 7-5c. Adsorbed amount of FITC-BSA on unmodified and grafted PE membranes in 10 mM phosphate buffer (λ_{ex} = 493 nm, λ_{em} = 520 nm, pH 7.2).

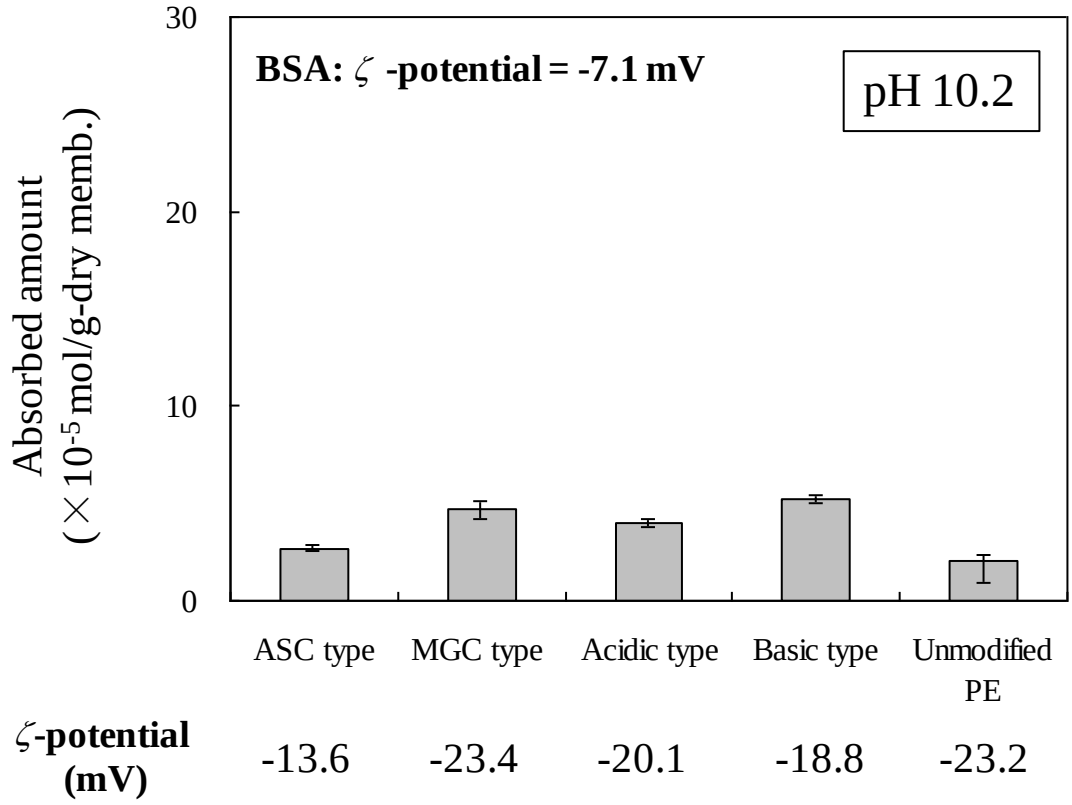

Figure 7-5d. Adsorbed amount of FITC-BSA on unmodified and grafted PE membranes in 10 mM carbonate buffer (λ_{ex} = 497 nm, λ_{em} = 520 nm, pH 10.2).

Chapter 8

Conclusions

Weak amphoteric charged membranes are expected as pH-responsive and antifouling material. The interfacial charge structure of these membranes, which contain both weak acidic groups and weak basic groups, is so complex that their interfacial properties have not clarified in detail. Particularly, there have been few physicochemical studies on the correlations between their interfacial properties and their interaction with organic molecules and proteins. This thesis aims to elucidate the interaction mechanism of solute molecules with weak amphoteric membranes based on electrokinetic properties of the membranes.

This dissertation consists of eight chapters and the following conclusions were obtained for each chapter:

Chapter 1

The significance of design and characterization of membrane interfaces from the viewpoints of solution for *fouling phenomena* was given and our concept of novel amphoteric charged membranes by surface modification using polyelectrolytes was presented.

Chapter 2

This chapter gave theoretical backgrounds and experimental details of streaming potential measurements, and described an analytical model of the pH dependence of the interfacial charge properties obtained from streaming potential for the characterization of weakly charged porous membranes.

Chapter 3

In this chapter, characteristics of membrane materials used in this study were shown. Two types of porous membranes were characterized by hydraulic permeability measurements and SEM observations. Three kinds of PEG derivatives with pendant ionizable groups were prepared by addition of mercaptans to the double bond pendants of coply(AGE/EO). ^{1}H NMR spectra revealed the completion of the reactions, and GPC profiles of these products showed their narrow molecular weight distributions. These cationic, anionic, and amphoteric PEG derivatives are expected for surface modification of porous membranes, especially for the preparation of novel amphoteric charged membranes.

Chapter 4

Novel weak amphoteric charged membranes having cysteine residues were prepared by graft polymerization of the amphoteric PEG derivatives onto CA porous membranes. The zeta potential/pH profiles of these membranes showed the peculiarity of a polyampholyte having amphoteric ion pairs. Since the original CA membrane has two types of charge groups, it is difficult to consider the total surface charge density on ionic PEG chain grafted CA membrane. We, however, can reach the conclusion that an analysis of the pore surface charge including the effect of not only amphoteric charge groups on the grafted polymer chains but also charge groups originated from the base membrane can be achieved by the SDM.

Chapter 5

Two kinds of amphoteric charged membranes, which are the ASC and MGC type, were prepared by the radiation-induced graft copolymerization of amphoteric PEG derivatives and the mixture of cationic and anionic PEG derivatives onto PE porous membranes, respectively. For the ASC-type membrane, the zeta potential/pH profile showed a *plateau* in the range of pH 6－11. This behavior would originate in the dipolar ion structure of the cysteine residues on the grafted chain. This was also supported by the theoretical prediction by a SDM using the cysteine's pK value in the literature [6]. This *plateau* region disappears with the increase in the electrolyte concentration of the external solution. On the other hand, the MGC-type membrane showed an intermediate pH dependence of the zeta potential between the

basic-type and acidic-type membranes. The apparent surface charge density on the membranes obtained from the zeta potential was analyzed by a SDM based on the dissociation of charge groups on the pore surface. The experimental results of the pH dependence of the apparent surface charge density for the basic-type and acidic-type, and the ASC-type membranes could be explained by a SDM using the pK values of the charge groups in the literature [6]. For the MGC-type membrane, however, the difference between the experimental result and calculated one appeared at pH > 5. This would be caused by the change in the surface states with pH, that is, the conformational change of the grafted polyelectrolyte chains with the change in the charge state.

Chapter 6

Adsorption experiments were carried out using four kinds of model organic molecules, i.e. pyrene (highly hydrophobic) and its derivatives (having an anionic group, a cationic group, and a polar group). The adsorption experiments have demonstrated the interaction characteristics of organic molecules with unmodified and ionic PEG chain grafted PE membranes. (1) It was suggested that the ionic PEG chain was effective in reducing the adsorption of hydrophobic organic molecules. (2) The interfacial charge properties of ionic PEG chain grafted membranes played an important role in their interaction with ionic organic molecules: the contribution of electrostatic interaction was dominant for the adsorption of ionic organic molecules on ionic PEG chain grafted membranes. (3) The contribution of hydrogen bonding was substantial for the adsorption of polar organic molecules on ionic PEG chain grafted membranes. These results provide fundamental information for the design by surface modification using ionic PEG derivatives to control multiple interactions between organic molecules and membranes.

Chapter 7

The protein adsorption experiments using BSA have demonstrated the pH dependence of the interaction characteristics of the proteins with ionic PEG chain grafted PE membranes. (1) Each adsorbed amount/pH profile showed a bell-shaped behavior, which has a uniform maximum value near the IEP of the protein. Here, the contributions of the hydrogen bonding would be substantial for the adsorption of proteins on the ionic PEG chain grafted membranes. (2) On both sides of the IEP, the interfacial charge

properties of the ionic PEG chain grafted membranes and protein played an important role in their interaction with proteins: the contribution of the electrostatic interaction was dominant for the adsorption of proteins on the ionic PEG chain grafted membranes. This result also indicates the possibility of controlling the protein-ionic PEG chain interaction on the membrane surfaces by changing the pH of the outer solution.

Chapter 8

Conclusions in each chapter are briefly summarized.

List of Publications

(1) Hidetoshi Matsumoto, Yoshiyuki Koyama, and Akihiko Tanioka; Preparation and Characterization of Novel Weak Amphoteric Charged Membrane Containing Cysteine Residues, *Journal of Colloid and Interface Science*, **239**, 467-474 (2001)

(2) Hidetoshi Matsumoto, Yoshiyuki Koyama, and Akihiko Tanioka; Characterization of Novel Weak Amphoteric Charged Membranes Using ζ-Potential Measurements: Effect of Dipolar Ion Structure, *Langmuir*, **17**, 3375-3381 (2001)

(3) Hidetoshi Matsumoto, Yoshiyuki Koyama, and Akihiko Tanioka; Interaction of Organic Molecules with Weak Amphoteric Charged Membrane Surfaces: Effect of Interfacial Charge Structure, *Langmuir*, **18**, 3698-3703 (2002)

(4) Hidetoshi Matsumoto, Yoshiyuki Koyama, and Akihiko Tanioka; Interaction of Proteins with Weak Amphoteric Charged Membrane Surfaces: Control of Electrostatic Effect by pH, *Journal of Colloid and Interface Science*, **264**, 82-88 (2003)

(5) Yoshiyuki Koyama, Tomoko Ito, Hidetoshi Matsumoto, Akihiko Tanioka, Tatsuya Okuda, Haruhiko Aoyagi, and Takuro Niidome; Novel Poly(ethylene glycol) Derivatives with Carboxylic Acid Pendant Groups: Synthesis and Their Protection and Enhancing Effect on Non-Viral Gene Transfection Systems, *Journal of Biomaterials Science. Polymer Edition*, **14**, 515-531 (2003)

(6) Hidetoshi Matsumoto, Yoshiyuki Koyama, and Akihiko Tanioka; Pore-Surface Characterization of Amphoteric Charged Membranes by Means of Zeta Potential Measurements, *Colloids and Surfaces A: Physicochemical and Engineering Aspects* (Symposium proceedings of "International Symposium on Electrokinetic Phenomena, ELKIN 2002", August 18-22, 2002, Cracow, Poland), **222**, 165-173 (2003)

Other Publications

(1) Hidetoshi Matsumoto, Akihiko Tanioka, Tatsuji Murata, Mitsuru Higa, and Ken Horiuchi; Effect of Proton on Potassium Ion in Countertransport across Fine Porous Charged Membranes, *The Journal of Physical Chemistry B*, **102**, 5011-5016 (1998)

(2) Hidetoshi Matsumoto, Akihiko Tanioka, and Susumu Kawauchi; Effect of Fixed Charged Groups and Counter Ions on the Transport Phenomena of Paraffin and Olefin across Anhydrous Negatively Charged Membranes, *Journal of Colloid and Interface Science*, **208**, 310-318 (1998)

(3) Kunihiro Adachi, Wei Hu, Hidetoshi Matsumoto, Kenji Ito, and Akihiko Tanioka; Permeation of n-Butane, 1-Butene, and 1,3-Butadiene through Anhydrated Ag^+-Doped Perfluorocarbon-Type Ion-Exchange Membranes, *Polymer*, **39**, 2315-2323 (1998)

(4) Wei Hu, Kunihiro Adachi, Hidetoshi Matsumoto, and Akihiko Tanioka; Transport and High-Selectivity Mechanisms of C_4 Hydrocarbons through Anhydrous Ag^+-Doped Perfluorocarbon-Type Ion-Exchange Membranes, *Journal of the Chemical Society. Faraday Transactions*, **94**, 665-671 (1998)

List of Conference Presentations

(1) Hidetoshi Matsumoto, Akihiko Tanioka, and Yoshiyuki Koyama; Characterization of Weak Amphoteric Charged Membranes Having Cysteine Residues. Koubunshi Gakkai, 37th Symposium on Polymer and Water, Tokyo, December 3, 1999.

(2) Yoshiyuki Koyama, Hidetoshi Matsumoto, and Akihiko Tanioka; Preparation and Characterization of Novel Weak Amphoteric-Charged Membrane I: Synthesis of Novel Polyethylene Glycol Derivative Having Amphoteric Ion-Pair Pendants and Graft Copolymerization onto Porous Membrane. 49th Koubunshi Gakkai Nenjitaikai, Nagoya, May 31, 2000.

(3) Hidetoshi Matsumoto, Akihiko Tanioka, and Yoshiyuki Koyama; Preparation and Characterization of Novel Weak Amphoteric-Charged Membrane II: Analysis of Dissociation Behavior at the Amphoteric-Charged Porous Membrane/Solution Interface. 49th Koubunshi Gakkai Nenjitaikai, Nagoya, May 31, 2000.

(4) Hidetoshi Matsumoto, Akihiko Tanioka, and Yoshiyuki Koyama; Characterization of Weak Amphoteric Charged Membranes Using Zeta Potential Measurements: Effect of Dipolar Ion Structure between Charge Groups. 49th Koubunshi Gakkai Touronkai, Sendai, September 29, 2000.

(5) Hidetoshi Matsumoto, Akihiko Tanioka, and Yoshiyuki Koyama; Electrochemical Properties and Interactions with Organic Molecules on Surfaces of Weak Amphoteric Charged Membranes. 50th Koubushi Gakkai Nenjitaikai, Osaka, May 23, 2001.

(6) Hidetoshi Matsumoto, Akihiko Tanioka, and Yoshiyuki Koyama; Characterization of Amphoteric Charged Membranes Using Zeta Potential Measurements. Sen-i Gakkai, International Symposium on Membrane Science and Technology, Hamamatsu, June 7, 2001.

(7) Hidetoshi Matsumoto and Akihiko Tanioka; Characterization of Amphoteric Charged Membranes Using Zeta Potential Measurements. Tokyo Institute of Technology (TIT)–Korea Advanced Institute of Science and Technology (KAIST) Young Scientists Exchange Symposium, Tokyo, July 23, 2001.

(8) Hidetoshi Matsumoto, Akihiko Tanioka, and Yoshiyuki Koyama; Adsorption Kinetics of Organic Molecules on Weak Amphoteric Charged Membrane: Effect of Interfacial Charge Structure. 50th Koubunshi Gakkai Touronkai, Tokyo, September 12, 2001.

(9) Hidetoshi Matsumoto, Akihiko Tanioka, and Yoshiyuki Koyama; Preparation of Weak Amphoteric Charged Membranes Using Ionic Poly(Ethylene Glycol) Derivatives and Their Interfacial Charge Properties. Nippon Maku Gakkai, Membrane Symposium 2001, Kyoto, November 30, 2001.

(10) Hidetoshi Matsumoto, Akihiko Tanioka, and Yoshiyuki Koyama; Adsorption Behavior of Organic Molecules on Ionic Poly(Ethylene Glycol) Derivative-Grafted Weak Amphoteric Charged Membranes. Nippon Maku Gakkai 24th Nenkai, Tokyo, May 16-17, 2002.

(11) Hidetoshi Matsumoto, Akihiko Tanioka, and Yoshiyuki Koyama; Charge Characteristics and Interactions with Proteins at Weak Amphoteric Charged Membrane/Solution Interface. 51th Koubunshi Gakkai Nenjitaikai, Yokohama, May 30, 2002.

Acknowledgements

The author first would like to express his sincere appreciation to Professor Akihiko Tanioka for valuable advice throughout this study.

The author also wishes to express his heartily gratitude to Professor Yoshiyuki Koyama, Department of Home Economics, Otsuma Women's University, for guidance and valuable discussions. Without their support this thesis would never have materialized.

The author would like to express deeply thankfulness to Dr. Toshihiko Jimbo, Nippon Zeon Co., Ltd., for helpful discussions and continuous encouragement.

The author expresses deep gratitude to Mrs. Mie Minagawa for heartily encouragement and support.

The author is indebted to Mr. Hamada and Mr. Kinoshita, Asahi Kasei Corporation, for kindly providing high-density polyethylene porous membrane; Associate Professor Tadashi Nakanishi, Ochanomizu University, for the radiation-induced graft polymerization and kindly providing the PEO gels; Mr. Isao Yoda, Research Laboratory for Nuclear Reactors, Tokyo Institute of Technology, for the gamma-ray irradiation; Professor Masa-aki Kakimoto, Department of Organic and Polymeric Materials, Tokyo Institute of Technology, for the NMR measurements; Associate Professor Yasuyuki Tezuka, Department of Organic and Polymeric Materials, Tokyo Institute of Technology, for the GPC measurements; Mr. Tuneo Chiba, Department of Organic and Polymeric Materials, Tokyo Institute of Technology, for the SEM observations; Dr. Makoto Natsuisaka, National Space Development Agency of Japan, for the ELS measurements; and Mr. Tetsuya Watanabe, Kyowa Interface Science Co., Ltd., for the DCA measurements.

Thanks are tendered to Dr. Kazuya Nitta, Dr. Toshihisa Osaki, Mr. Ryotaro Yamamoto, and all members of Tanioka Laboratory.

Finally, the author would like to express deeply thankfulness to his family for their continuous understanding and encouragement.

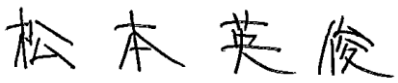

Hidetoshi Matsumoto

Department of Organic and Polymeric Materials
Graduate School of Science and Engineering
Tokyo Institute of Technology
Tokyo, Japan
June, 2002